UNIVERSITY OF ŽILINA

TRANSCOM 2009

8-th EUROPEAN CONFERENCE OF YOUNG RESEARCH AND SCIENTIFIC WORKERS

PROCEEDINGS

SECTION 4

ELECTRIC POWER SYSTEMS. ELECTRICAL AND ELECTRONIC ENGINEERING

ŽILINA June 22 - 24, 2009
SLOVAK REPUBLIC

UNIVERSITY OF ŽILINA

TRANSCOM 2009

8-th EUROPEAN CONFERENCE
OF YOUNG RESEARCH AND SCIENTIFIC WORKERS

under the auspices of

Prof. Ing. Ján Mikolaj, PhD.
Minister of Education, Slovak Republic

&

Prof. Ing. Ján Bujňák, PhD.
Rector of the University of Žilina

SECTION 4

ELECTRIC POWER SYSTEMS. ELECTRICAL AND ELECTRONIC ENGINEERING

ŽILINA June 22 - 24, 2009
SLOVAK REPUBLIC

Edited by Milan Smetana, Peter Braciník and Peter Brída

ISBN:….

TRANSCOM 2009
8-th European conference of young research and scientific workers

TRANSCOM 2009, the 8th international conference of young European researchers, scientists and educators, aims to establish and expand international contacts and co-operation. The main purpose of the conference is to provide young scientists with an encouraging and stimulating environment in which they present results of their research to the scientific community. TRANSCOM has been organised regularly every other year since 1995. Between 160 and 400 young researchers and scientists participate regularly in the event. The conference is organised for postgraduate students and young research workers up to the age of 35 and their tutors. Young workers are expected to present the results they had achieved.

The conference is organised by the University of Žilina. It is the university with about 13 000 graduate and postgraduate students. The university offers Bachelor, Master and PhD programmes in the fields of transport, telecommunications, forensic engineering, management operations, information systems, in mechanical, civil, electrical, special engineering and in social sciences.

SECTIONS AND SCIENTIFIC COMMITTEE

1. TRANSPORT AND COMMUNICATIONS TECHNOLOGY

Scientific committee: Baumann S. (D), Cenek P. (SK), Droździel P. (PL), Janáček J. (SK), Jánošíková Ľ. (SK), Kremeňová I. (SK), Novák A. (SK), Palúch S. (SK), Rievaj V. (SK), Řezáč M. (CZ), Schnieder E. (D), Surovec P. (SK), Žarnay P. (SK)

2. ECONOMICS AND MANAGEMENT

Scientific committee: Bartošová V. (SK), Blašková M. (SK), Březinová O. (CZ), Duncan F.H. (USA), Hittmár Š. (SK), Kos B. (PL), Kucharčíková A. (SK), Lyakin A. (RUS), Rostášová M. (SK), Rybakov F. (RUS), Strenitzerová M. (SK), Strišš J. (SK), Tomová A. (SK)

3. INFORMATION AND COMMUNICATION TECHNOLOGIES

Scientific committee: Bärwald W. (D), Dado M. (SK), Drozdová M. (SK), Hanuliak I. (SK), Keil R. (D), Klimo M. (SK), Kolev P. (BG), Kotsopoulos S. (GR), Madleňák R. (SK), Matiaško K. (SK), Spalek J. (SK), Vaculík J. (SK), Vaculík M. (SK), Vrček N. (HR)

4. ELECTRIC POWER SYSTEMS. ELECTRICAL AND ELECTRONIC ENGINEERING

Scientific committee: Altus J. (SK), Blažek V. (D), Čápová K. (SK), Dobrucký B. (SK), Dodds S.J. (GB), Santarius P. (CZ), Vittek J. (SK)

5. MATERIAL ENGINEERING. MECHANICAL ENGINEERING TECHNOLOGIES

Scientific committee: Adamczak S. (PL), Bokůvka O. (SK), Borkowski S. (PL), Dzimko M. (SK), Guagliano M. (I), Kunz L. (CZ), Meško J. (SK), Nicoletto G. (I), Palček P. (SK), Skočovský P. (SK), Takács J. (H)

6. MACHINES AND EQUIPMENTS. APPLIED MECHANICS

Scientific committee: Dekýš V. (SK), Gerlici J. (SK), Kalinčák D. (SK), Malenovský E. (CZ), Medvecký Š. (SK), Merkisz J. (PL), Nemček M. (CZ), Pawelczyk M. (PL), Sága M. (SK), Zapoměl J. (CZ), Žmindák M. (SK)

7. CIVIL ENGINEERING

Scientific committee: Bouchair H. (F), Dmitrovskaja L. (RUS), Garbuz A. (UA), Ižvolt L. (SK), Melcer J. (SK), Ivanov J. (BG), Teleman E.C. (RO), Vičan J. (SK), Zolotov M. (UA)

8. SOCIAL SCIENCES

Scientific committee: Banáry B. (SK), Baštinec J. (CZ), Cabanová V. (SK), Gulová L. (CZ), Kráľová Z. (SK), Růžičková M. (SK), Šindelářová J. (CZ), Vikoren V. (N)

9. SECURITY ENGINEERING. FORENSIC ENGINEERING

Scientific committee: Danihelka P. (SK), Horák R. (CZ), Navrátil L. (CZ), Poledňák P. (SK), Reitšpís J. (SK), Seidl M. (SK), Šenovský M. (CZ), Šimák L. (SK), Vasiliev D. (BG), Zamiar Z. (PL)

ORGANIZING COMMITTEE

CHAIRPERSON Bokůvka Otakar

EXECUTIVE SECRETARY Vráblová Helena

MEMBERS Bábel J., Belan J., Braciník P., Brída P., Brumerčík F., Dobrotková M., Dubcová Z., Frajtová-Michalíková K., Harušinec J., Hnátová Z., Houšková L., Imrišková E., Jánošíková G., Kačiaková B., Kardoš M., Kormancová M., Krasňan M., Kuzmová M., Ladovský T., Ližbetinová L., Mihalov K., Močková M., Mráz M., Murín M., Neslušan M., Ondrejka R., Pachová S., Pavelková I., Pilát P., Potkan T., Remek Ľ., Smetana M., Sršníková D., Stránska S., Štofková K., Tulejová L., Valentíková E., Varmus M., Vaško A., Vaško M., Záborský M.

SECTION 4 ELECTRICAL POWER ENGINEERING. ELECTRICAL AND ELECTRONIC ENGINEERING

REVIEWERS:

Altus Juraj
Braciník Peter
Čáp Ivo
Drábek Jiří
Gombárska Daniela
Hrabovcová Valéria
Hrbček Jozef
Janoušek Ladislav
Makyš Pavol
Muzikářová Ľudmila
Otčenášová Alena
Roch Marek
Tichá Dáša

Note:

Authors are responsible for language contents of their papers

CONTENTS

ALMAN, MARCEL, Žilina, Slovak Republic: Excitation System Influence on Eddy Currents Propagation in Process of Non-Destructive Material 9

BARABÁŠ, JÁN – PŠENÁKOVÁ, ZUZANA, Žilina, Slovak Republic: Numerical and Real-Life Phantoms Used in FDTD-Based Simulations-A Comparison 13

BAUER, JAN – LETTL, JIŘÍ – LINHART, LIBOR – BEDNÁŘ, MIROSLAV, Prague, Czech Republic: PWM Rectifier Control Algorithm 17

BEDNÁŘ, MIROSLAV – LETTL, JIŘÍ – FLÍGL, STANISLAV – LINHART, LIBOR, Prague, Czech Republic: Frequency Converter DC Link Voltage Oscillation Influence on the Induction Motor Shaft Torque 21

BRIŠ, PETER – KUREK, MICHAL – VITTEK, JÁN, Žilina, Slovak Republic: Servo-Position Forced Dynamic Control of PMSM 25

CHVÁLEK, ROMAN – HRADÍLEK, ZDENĚK, Ostrava, Czech Republic: Hydrogen Storage Energy Gained from Renewable Sources 29

CZIPPELOVÁ, BARBORA, Žilina, Slovak Republic: Modelling of Brain Vascular System Using Electromechanical Analogy 35

HEČKO, PETR, Žilina, Slovak Republic: Voltage Sag Problem and its Modeling by Using ATPDraw 39

KRAJČOVIČ, JÁN, Žilina, Slovak Republic: Overview of Voice Recognition Tools Based on HMM 43

KRAJČOVIČ, JÁN – HRNČÁR, MARTIN, Žilina, Slovak Republic: Parameterization and its Influence on Speech Recognition 47

KUBÁTKA, KAREL, Žilina, Slovak Republic: Train Performance Simulation 51

KUZMANOVIČ, DRAGAN – LETTL, JIŘÍ, Prague, Czech Republic: Induction Motor Drive Fed by Matrix Converter with Takahashi Direct Torque Control 55

LINHART, LIBOR – LETTL, JIŘÍ – BEDNÁŘ, MIROSLAV – BAUER, JAN, Prague, Czech Republic: Cosimulation of Two-Step Commutation Method of the Matrix Converter in Simulink/Modelsim 59

SMETANA, MILAN – STRAPÁČOVÁ, TATIANA, Žilina, Slovak Republic: Pulsed Eddy Currents as A New Approach in Nondestructive Evaluation of Conductive Materials 63

STACHO, BŘETISLAV – RUSEK, STANISLAV, Ostrava, Czech Republic: Determination of Limit Values of Maintenance Priority of 110 kV VMM Low-Oil-Content Breakers 67

STASIAK – BETLEJEWSKA, RENATA, Częstochowa, Poland: Costs of Improper Quality of Energy Services on the Context of Value Analysis 73

STRAPÁČOVÁ, TATIANA – SMETANA, MILAN, Žilina, Slovak Republic: Prosthetic Heart Valve Crack Signal Simulation in Eddy Current Testing 77

SZCZEŚNIAK, ADAM – SZCZEŚNIAK, ZBIGNIEW, Kielce, Poland: Signals of Optoelectronics Transducers Processed in Flip-Flop Circuits 81

ŠUŠOTA, MARTIN – RAFAJDUS, PAVOL, Žilina, Slovak Republic: Parameters Investigation of Switched Reluctance Motor 87

ZÁVADA, PETR – NOVÁK, TOMÁŠ – SOKANSKÝ KAREL, Ostrava, Czech Republic: Suggestion Methodology of Classification Luminaries Outside Lighting 91

ZELENKA, JÁN, Žilina, Slovak Republic: The Utilization of Software Tools for the Electronic Circuits Simulation by the Safety Analysis 97

ZRNÍK, JURAJ, Žilina, Slovak Republic: Models of Single Relaxation Processes in Biological Tissues Influenced by Electromagnetic Field 101

VYSLOUŽIL, MARTIN – HRADÍLEK, ZDENĚK, Ostrava - Poruba, Czech Republic: The Economic Aspects of Wind-power Plants 107

Transcom 2009, 22-24 June 2009
University of Žilina, Žilina, Slovak Republic

Excitation System Influence on Eddy Currents Propagation in Process of Non-Destructive Material Testing

[*]Marcel Alman
[*]University of Žilina, Faculty of Electrical Engineering, Department of Electromagnetic and Biomedical Engineering, Univerzitná 1, 010 26 Žilina, Slovakia, alman@fel.uniza.sk

Abstract. Excitation system plays an important role in eddy-current non-destructive testing as it determines detection capabilities of the method. The presented article describes some basic features of this system. Several parameters of the system like geometric shape, dimensions,, and its positioning are varied and influence of the parameters on eddy currents propagation are studied. The numerical results gained using the finite element method are presented.

Keywords: non-destructive testing, probe, excitation system, eddy currents, magnetic flux density, depth of penetration

1. Introduction

The process of non-destructive testing (NDT) determines the existence of surface and subsurface defects, discontinuities, leaks, contamination, thermal anomalies or imperfections in materials, components or assemblies without impairing the integrity or function of an inspected component. Eddy current testing (ECT) is a contact-less method for the inspection of metallic parts. Its principle comes out from the electromagnetic induction phenomena. When a probe is electromagnetically linked with a part under inspection, the alternating magnetic field created by the probe driven with alternating current induces eddy currents in the test part [1]. Discontinuities or property variations in the test part change the flow pattern of the eddy currents and this change can be detected by the probe.

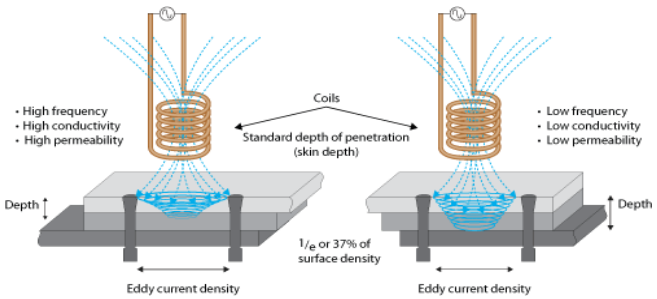

Fig.1 - Standard depth of penetration, influence frequency, conductivity and permeability

Eddy current density does not remain constant along the depth of a material. The density is largest at the surface and decreases exponentially with the depth due to the well known skin

effect. The *standard depth of penetration* that describes capability of eddy current testing is given by equation:

$$\delta = \frac{1}{\sqrt{\pi f \mu \sigma}} \tag{1}$$

where: δ - standard depth of penetration [m], f - frequency of driving electromagnetic field [Hz], μ - magnetic permeability [H/m], σ = electric conductivity [S/m].

As it can be seen from Fig. 1 the standard depth of penetration decreases with increasing frequency, conductivity, or permeability. To detect very shallow defects in a material, and also to measure the thickness of thin sheets, very high frequencies are used. Accordingly, in order to detect subsurface defects, and to test highly conductive, magnetic, or thick materials, lower frequencies should be used [1].

Conventional eddy current testing has traditionally used circular pancake coils. The recent needs of high sensitivity testing have prompted the researches to develop various kinds of test probes. The flaw detection characteristics in eddy current testing depend on the eddy current distribution induced in the material by the probe. Knowledge of the eddy current distribution in a test material is important because it determines the sensitivity level of the testing. Thus is it quite important to know the eddy current distribution in order to detect flaws in material under a given test conditions [2]. However, since there is significant variation in this distribution due to factors such as test frequency, material electromagnetic characteristics, and coil configurations, it is very difficult to estimate the distribution induced by the probe for a certain test condition.

Numerical investigations are performed to evaluate influence of the exciting system parameters on distribution of eddy currents in a tested object. The results are presented in the next section.

2. Numerical results

Numerical simulations using the Finite Element Method (FEM) are carried out to investigate influence of certain parameters of excitation system on eddy currents distribution. Two excitation coils are utilized to drive eddy currents. The first one is of the circular shape, so called pancake coil, and the second one has the rectangular shape. The coils are positioned in two basic positions – the normal one and the tangential position regarding the surface of a tested material. The configurations are shown in Fig. 2. Electromagnetic parameters of a plate specimen being tested are those ones of the Inconel 600; σ = 1.0 MS/m, μ_r=1. The plate is without any defect. The coils are situated 1 mm above the surface of the specimen.

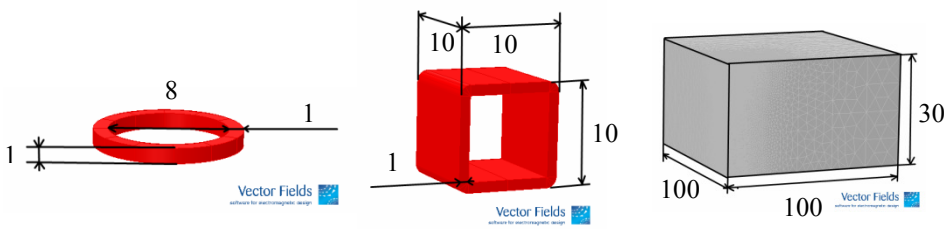

Fig. 2 – Numerical models pancake coil, normal coil, plate

Current density of the driving current is set to 1A/mm^2. Harmonic voltage supply with a frequency of 10 kHz is used for driving the coils. The simulations are performed for two coils in two different positions. To reduce size of the solved problem only ¼ of the plate is modelled with proper symmetry conditions.

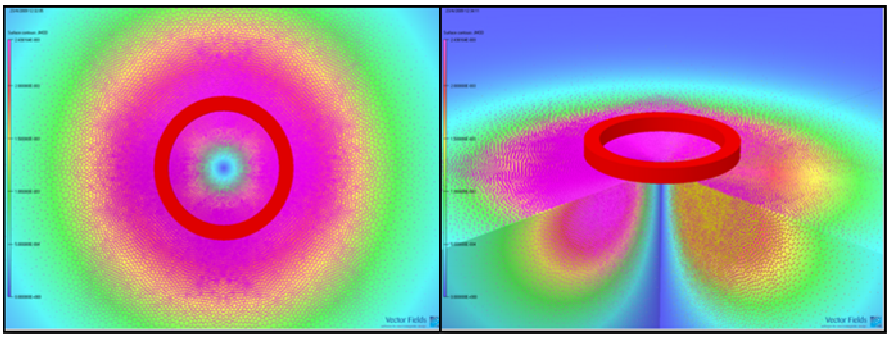

a) top view *b) cross-sectional view*

Fig. 3 – Eddy current density distribution for the circular coil in the normal position

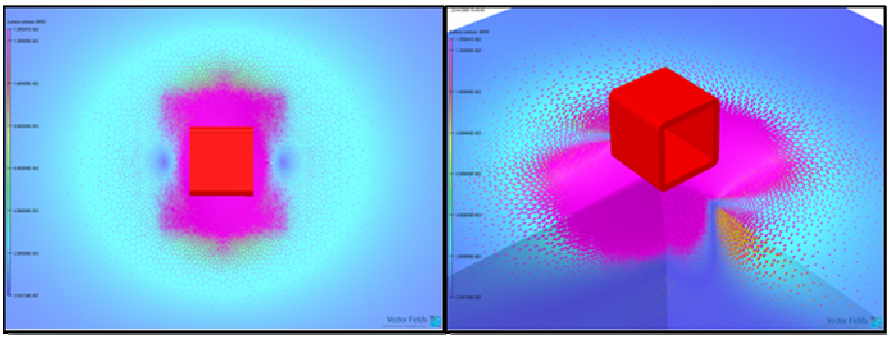

a) top view *b) cross-sectional view*

Fig. 4 – Eddy current density distribution for the rectangular coil in the tangential position

Figures 3 and 4 display particular results of eddy currents density distribution for the circular coil in the normal position and for the rectangular coil in the tangential position, respectively. As it can be seen, the coil in the normal position creates the circular pattern of eddy currents. In this case a defect of any orientation can be detected. On the other hand, uniformly distributed eddy currents are induced under the coil positioned tangentially regarding the surface of the plate. An ECT probe with such exiting coil has therefore directional detection properties.

Both coils are positioned in the normal and the tangential position. Distribution of eddy current density along the material depth is plotted in relative values in Fig. 5 for the circular and the rectangular coils, respectively. The figure shows that the exciting coil in the tangential position drives eddy currents more deeply comparing its normal position.

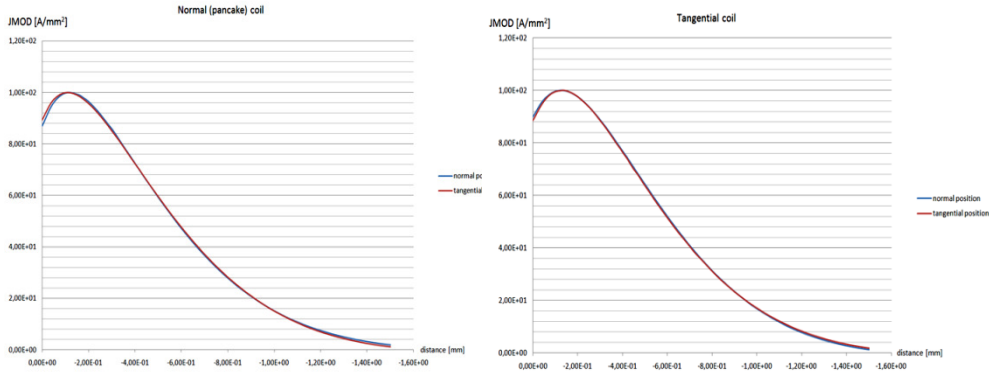

Fig. 5 – Eddy current density in relative values along the material depth

3. Conclusion

The paper focused on investigations of exciting system parameters on the eddy current density distribution in non-destructive testing. Two exciting coils were used to drive the eddy-currents in a plate specimen made of the Inconel 600; the first one had circular shape and the second coil was the rectangular one. Both coils were oriented normally and tangentially regarding the surface of the plate. It can be concluded that a coil in the normal position creates circular pattern of eddy currents in the test-piece and thus a defect of any direction can be detected. When the coil is positioned tangentially the uniform eddy current pattern is obtained under the coil. This pattern has directional properties and a defect oriented in parallel to the eddy current density vector can be hardly detected. However, eddy current density is less attenuated into the material depth for the tangential position as for the normal one.

Acknowledgement

This work was supported by the Slovak Research and Development Agency under the contract No. APVV-0194-07.
This work was also supported by the Ministry of Education of the Slovak Republic under the contract No. VEGA 1/0308/08

References

[1] JACK BLITZ: Electrical and Magnetic Method of Non-destructive Testing. Second Edition, ISBN 0-412-79150-1

[2] HOSHIKAWA HIROSHI, KOYAMA KIYOSHI: Eddy Current Distribution in Conductive Plate Normalized by Standard Penetration Depth. Journal of JSNDI, VOL.48, Pages.21-28, ISSN 0367-5866

Transcom 2009, 22-24 June 2009
University of Žilina, Žilina, Slovak Republic

Numerical and Real-Life Phantoms Used in FDTD-Based Simulations – A Comparison

[*]Jan Barabas, [*]Zuzana Psenakova
[*]University of Zilina, Faculty of Electrical Engineering, Department of Electromagnetic and Biomedical Engineering, Univerzitna 1, 01026 Zilina, Slovakia, {barabas, psenakova}@fel.uniza.sk

Abstract. The presented article gives basic insight into various numerical and real-life phantoms used predominantly in SAR and thermal evaluations. Both homogeneous and heterogeneous phantoms are mentioned and a comparison between a numerical and real-life human head phantom is presented based on conducted real-life measurements and simulations.

Keywords: phantom, homogeneous, heterogeneous, FDTD, SAR, thermal evaluation

1. Introduction

The importance of wireless technologies has grown substantially over the last decade. Continued advancements in this field resulted in widespread adoption of this technology which nowadays forms an essential part of our everyday life. However, many health studies covering the effects of these wireless devices on human beings are dubious at best, with conclusions ranging from no observed negative effects to possible or even confirmed ones, casting further uncertainty into the matter. Given the already extensive presence of these technologies and their expected further penetration over the coming years, unified methodology in both real-life experiments and simulation setups would be beneficial. To this end, FDTD-based simulations may be used to complement real-life experiments, assuring the goal specific absorption rate (SAR) and thermal levels are reached, thus allowing modern studies to concentrate prevalently on non-thermally induced biological effects.

2. FDTD basics

The finite difference time domain method (FDTD) has been proposed by Yee in 1966, at which time the available computing power was largely sub-optimal given the computation complexity of this numerical method. However, currently available computers, especially when coupled by dedicated hardware acceleration cards, are capable of solving common problems in acceptable time ranges.

The FTDT-method is based on a spatial and temporal discretization of Maxwell's equations. The electric and magnetic field components are allocated in space on a staggered mesh of a Cartesian coordinate system, such as the one originally proposed by Yee. These are then updated in a leap-frog scheme using the finite-difference form of the curl which surrounds the component. Calculation of transient fields is possible once the initial field, boundary and source conditions are known. The result is a uniquely stable method because the first two of Maxwell's equations are solved at the same time for the electric and magnetic field, [1].

In addition to the traditional staircasing model representation, a conforming model may also be used. This model incorporates curved and inclined surfaces without the need for resolving overly detailed meshes, which would usually result in greatly increased number of cells, incurring long computational times.

Additional enhancements, such as the Prony algorithm, allow simulation of high Q devices without the associated overall slow-down of the simulation. The mentioned algorithm is actually an approximation to the true solution – eliminating the otherwise necessary convergence of the complete solution.

Some popular electromagnetic software that is based on FDTD includes *SEMCAD X*, developed by SPEAG, Zürich or *Concerto FDTD* from Vector Fields, with each software package adding their own algorithm refinements.

3. RF and microwave measurements

The majority of measurements are performed at RF or microwave frequencies, both of which generally penetrate well into the human body. The penetrating wave causes dipole alignment and drift of free charged particles and the resulting friction thereof ultimately results in an increase of temperature in the affected area.

The above mentioned effect is closely tied with the term *specific absorption rate*, which represents the time-averaged absorbed power and is expressed in W/kg:

$$SAR = \frac{1}{2}\frac{\omega\varepsilon_0\varepsilon_r}{\rho}|E|^2$$

Where: ω is the angular frequency , ε_0 is the permittivity of free space, ε_r is the imaginary part of the relative complex permittivity, ρ is the tissue density and E is the peak value of the total electric intensity inside the tissue material. The term $(1/2)\omega\varepsilon_0\varepsilon_r = \sigma$ is called material conductivity and is frequency and tissue-dependent. [2]

4. Real life phantoms

Phantoms can be thought of as dielectric shells containing tissue simulating liquid. They are readily available in various shapes, ranging from simple cylindrical shapes to whole body models, accurately modeling typical body postures during a phone call.

As was previously mentioned, material conductivity is frequency and tissue-dependent, of which the latter can be adjusted via composition of the enclosing hull or tissue stimulating liquid. To this end, various ingredients, such as sugar, oil, DGBE (Diethylene Glycol Butyl Ether) and others can be used to adjust the phantom to the required frequencies.

Commonly used commercially available phantoms include those manufactured by SPEAG and may be coupled with the proprietary DASY5 dosimetric assessment system to evaluate SAR and thermal properties, amongst others, [1].

However, various dosimetric phantoms can also be constructed, such as in our case. Of course the standards compliance (IEEE/CENELEC) of these phantoms is questionable, however in view of the limited measurements and purely scientific outputs, should not be of concern.

In our case we opted for a human head model based on a 28 year old female model. The head was first scanned using a 3D non-contact scanner manufactured by Minolta and imported into Polyworks software package. The model was then printed using a 3D printer manufactured by Stratasys and used for the creation of the moulds which were subsequently

used in vacuum casting – a method where the liquid to be cast (in our case the skull simulating material) is driven into the mold by atmospheric pressure, while the vacuum removes trapped air that would otherwise impede the free flow of the liquid casting material. The composition of the skull simulating material can be seen in *table 1* along properties for selected frequencies, [3].

Material	f [GHz]	ε_r [-]	Loss tangent [-]	μ_r [-]
Bone tissue	10	8,1	0,47	1
Chosen material composition: 44,4% Al, 5% C 50,6% ABS – polyurethane	10	6,1	0,02	1

Table 1 - Properties of real-life and replacement skull material at microwave frequencies

5. Numerical phantoms

When compared to real-life phantoms, numerical phantoms allow for a wide degree of freedom – thus giving ample headroom for various combinations of tissue parameters and/or placement variations. Another advantage of numerical phantoms lies in the model complexity – no longer is the model limited to several tissue types, but as much many as 70 or more different tissue types can be included in the simulation.

Recently, high resolution whole body models have been published by the IT'IS foundation and are free for non-commercial and scientific use. Included in the enhanced Virtual Family are both adult and child male and female models in ACIS SAT format.

To even further enhance the usability of simulation outputs, automatic identification and labeling of the brain regions in human CAD models is possible using the Talairach tool. In SEMCAD X, the mentioned tool detects brain tissue in the anatomical model and locates nine reference points, denoted as Talairach landmarks that are used to map the brain data into the atlas normalized space (*fig.1*). Electromagnetic simulation results are then automatically processed along the average dissipated power, minimum/maximum SAR, mass and volume of every region within the 1105 sites identified in the model brain, [1].

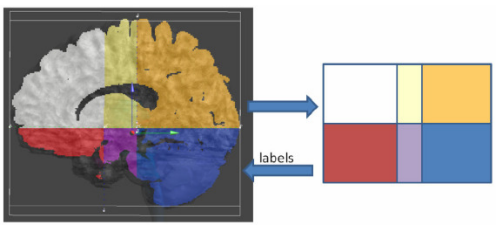

Figure 1 - Talairach brain mapping

However, for the scope of our investigation, the previously described two tissue phantom has been used. The CAD model that was acquired after 3D scanning was extruded to include a 2 mm skull shell alongside the inner volume representing the brain tissue, and both models were assigned tissue parameters identical to those used in the real-life measurements. Complementing the head model was a helix antenna based on the one used in the real-life experiment. Both simulation setups can be seen in *fig.2*.

Figure 2 – Real-life measurement setup (left) and simulation setup (right)

Results from the real-life measurements and the corresponding simulation are presented in *graph 1*. The numerical simulation also allowed for thermal evaluation, however thermal measurements were not conducted in the real-life setup.

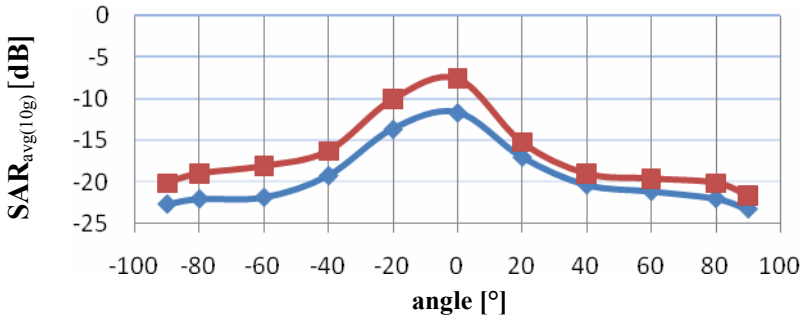

Graph 1 – Simulated (red, square) and real-life results (blue)
0dB = 1,397 W/kg

6. Conclusion

The results presented in *graph 1* show a very close correlation between the results obtained via real-life measurements and those from simulations, thus implying the usability thereof as a base for further investigation.

Thus, numerical methods present a viable alternative to costly real-life setups and non-thermal effects evaluation will benefit from the extra time gained for more thorough evaluation in this field, hopefully enlightening us on the long path of discovery of the true effects of electromagnetic fields on our health.

Acknowledgements

This article has been elaborated with support of the Slovak Grant Academy VEGA, filed under project number 1/0308/08.

References

[1] SCHMID & PARTNER ENGINEERING AG WEBSITE AND MANUALS, http://www.semcad.com/
[2] STAVROULAKIS P.: Biological effects of electromagnetic fields, Springer-Verlag Berlin Heidelberg 2003, ISBN 3-540-429891
[3] PŠENÁKOVÁ, Z.: *Vplyv elektromagnetického poľa na ľudský organizmus so zameraním na ľudskú hlavu, Dizertačná práca, Žilina 2007*

Transcom 2009, 22-24 June 2009
University of Žilina, Žilina, Slovak Republic

PWM Rectifier Control Algorithm

*Jan Bauer, *Jiří Lettl, *Libor Linhart, *Miroslav Bednář
*Czech Technical University in Prague, Faculty of Electrical Engineering,
Department of Electric Drives and Traction,
Technická 2, 166 27 Prague 6, Czech Republic, lettl@fel.cvut.cz

Abstract. The modern industrial production demands continuous and lossless conversion of electrical energy parameters. This need leads to wide spread of power semiconductor converters. The rapid development in power electronics and microprocessor technology enables to apply sophisticated control methods that eliminate negative side effects of the power converters on the supply network. The phase controlled thyristor rectifiers overload the supply network with higher harmonics and reactive power consumption. Utilization of PWM control in rectifiers eliminates the problems that were caused by phase controlled rectifiers operation. That is why the PWM rectifier is being examined. In comparison with the phase controlled rectifier it can be controlled to consume nearly sinusoidal current with power factor equal to unity. Another advantage of the PWM rectifier is its capability of energy recuperation.

Keywords: Active Front-End, PWM, Power Factor.

1. Introduction

Many modern electric devices need for its function DC voltage. For the conversion from AC to DC mostly diode or thyristor rectifiers are used. The phase control of these rectifiers generates harmonics to the supply network. This can cause damage or malfunction of other devices connected to the grid. There are many techniques which can be used for harmonics suppression. These techniques can be simply divided into two main groups, firstly devices for cancellation of existing harmonics and on the other side devices, which do not generate or generate limited number of harmonics.

The classical method of current harmonics reduction is to use passive LC filter. They are usually constructed as an inductor and capacitor connected to the grid. Each harmonics (5^{th}, 7^{th}, 11^{th} …) requires its own filter. This means that filters can not be designed in general way, but must be designed according to each application. Such a solution is simple but requires additional place and reduces reliability of the whole system.

The other possible technique is the application of PWM rectifier.

2. PWM Rectifier

In order to suppress these negative phenomena caused by the phase angle controlled rectifiers, are being used rectifiers with a more sophisticated control algorithm. Such rectifiers are realized by semiconductors that can be switched off such as IGBT transistors controlled by pulse width modulation. A rectifier controlled in this way consumes current of required shape, which is mostly sinusoidal. It works with a given phase displacement between the consumed current and the supply voltage. The power factor can also be controlled and there are minimal effects on the supply network.

PWM rectifiers can be divided into two groups according to power circuit connection – the current and the voltage type.

For proper function voltage type rectifiers require higher voltage on the DC side than the maximum value of the supply voltage. The rectified voltage on the output is smoother than the output voltage of the current type rectifier. But they require a more powerful microprocessor for their control.

2.1. Control Algorithm for PWM Rectifier

Basic scheme of the voltage type PWM Rectifier is shown in Figure 1.

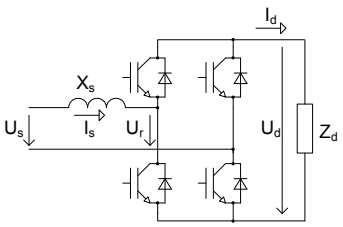

Fig. 1. Power part of the PWM Rectifier

Input voltage U_S and the voltage at the input of the rectifier U_r are two phasors separated by the input inductance X_S. Therefore the energy flow depends on the displacement angle between these two phasors.

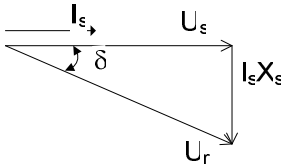

Fig. 2. Phasor diagram

The power transferred from the supply to the IGBT's

$$P_{SR} = (U_s U_r / X_s) \sin\delta = U_s I_s \cos\phi \tag{1}$$

In order to make rectified voltage constant, the output and input powers must be balanced. Also the rectifier is supposed to operate without reactive power consumption and with power factor near unity. That means that (1) can be adapted to:

$$I_s X_s = U_r \sin\delta \tag{2}$$

As was mentioned above the aim is the control of the rectifier to consume harmonic current, which is in phase with supply current. This can be achieved in many ways; on way is the pulse width modulation. Shapes of the voltage and the current under this control is shown in Fig. 3

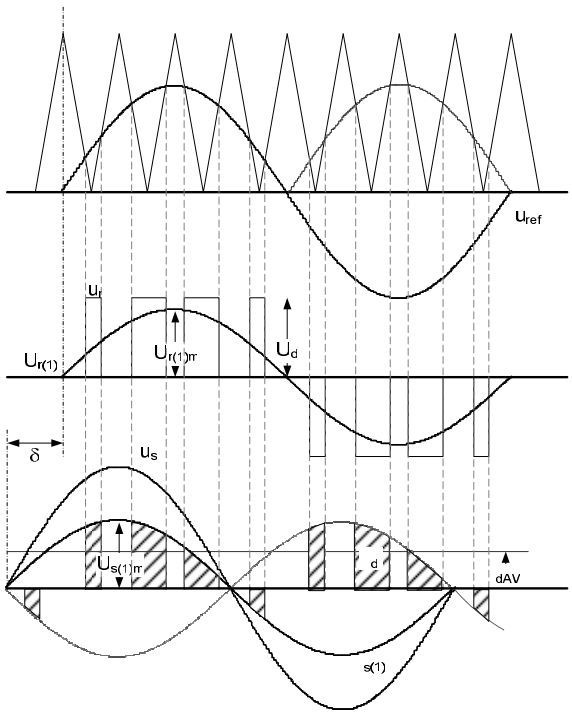

Fig. 3. Voltage and current waveforms by PWM control

From the Fig. 3 follows, that we can control the displacement angle δ, which describes the displacement between the generated voltage and between supply current and modulation index *z,* which is defined as

$$z = \frac{u_{ref}}{u_{saw}} = \frac{U_{r(1)m}}{U_{dAV}} \tag{3}$$

The i_d waveform can be derived from Fig. 3. If we consider as simplification instead of harmonic current i_s only its first harmonics $i_{s(1)}$

$$I_d = \frac{z \cdot I_{s(1)m}}{2} \cos\delta \tag{4}$$

The output voltage U_d is usually controlled to constant value, because it is then used by another converter e.g. an inverter. Therefore it is possible to assign for given output voltage U_d and current I_d a particular value of z and displacement angle δ as will be derived below.
If we consider the equality of input AC and output DC powers and the power factor equal to unity can be written

$$I_{s(1)m} = \frac{2U_{dAV} I_{dAV}}{U_{sm}} \tag{5}$$

From the phasor diagram in Fig. 2 and (4) and (5) follows

$$\delta = arctg \frac{2\omega L_s U_{dAV} I_{dAV}}{U_{sm}} \tag{6}$$

The control algorithm of the rectifier proceeds from above mentioned equations. The block scheme of the algorithm is in Fig.4.

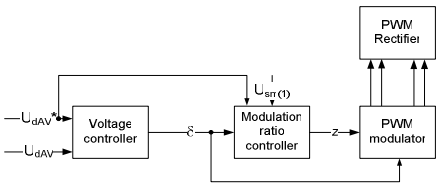

Fig. 4. Block scheme of the rectifier control

For proper rectifier function, it is also necessary to synchronize the control algorithm with the supply voltage. By detecting the zero crossing, the controller controls the displacement angle δ. The synchronization circuit must be very accurate and also fast and reliable.

Fig. 5 shows the measured waveforms taken by proposed PWM control of the rectifier. It can be seen, that consumed current (blue) is in phase with supply voltage (red) and the shape is nearly sinusoidal.

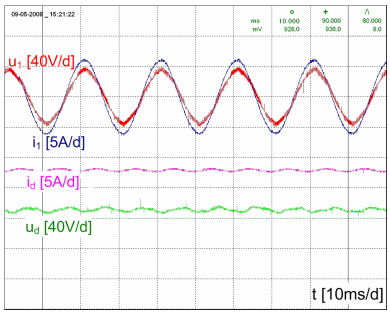

Fig. 5. Measured waveforms

3. Conclusion

The use of PWM control in rectifiers eliminates the problems caused by using phase controlled rectifiers. The PWM rectifier can perform well in many applications, for example as an active filter, or as an input rectifier for an indirect frequency converter. This application is useful mainly in traction, where the AC voltage from the trolley wire is first rectified, and the traction inverters and also other auxiliary converters are fed from the output of the rectifier. A traction vehicle equipped with a PWM rectifier does not consume reactive power, will not load the supply network with harmonics and can recuperate.

References

[1] WU, R., DEWAN S. B., SLEMON, G. R. *A PWM AC-to-DC converter with fixed switching frequency*. IEEE Transactions on Industry Applications, 1990, vol. 26, no. 5, pp. 880-885.

[2] LETTL, J. *Analysis of high-performance AC-DC PWM converter*. In Proceedings of International Conference on Electric Drives and Power Electronics. Štrbské Pleso (Slovakia), 1990, vol. 1, pp. 8-13.

[3] KÜNZEL, K., LETTL, J., ŽÁČEK, J. *Some problems of PWM rectifiers*. Proceedings of UEES´96, Szczecin, 1996.

Transcom 2009, 22-24 June 2009
University of Žilina, Žilina, Slovak Republic

Frequency Converter DC Link Voltage Oscillation Influence on the Induction Motor Shaft Torque

*Miroslav Bednář, *Jiří Lettl, *Stanislav Flígl, *Libor Linhart
*Czech Technical University in Prague, Faculty of Electrical Engineering,
Department of Electric Drives and Traction,
Technická 2, 166 27 Prague 6, Czech Republic, lettl@fel.cvut.cz

Abstract. This paper discusses the problem of high power traction drive working on AC supply system where rectifier and inverter are working together. It describes the DC link voltage oscillation caused by one phase supplying and its influence on the whole vehicle behaviour. The induction machine shaft torque oscillation can be taken as the view of the drive evaluation. The example of the torque oscillation observed on the locomotive SKODA 109E is given.

Keywords: Induction Machine, Vector Control, Torque Oscillation.

1. Introduction

At the beginning it is important to note that the only one phase wire supplies the traction converter. The torque oscillation is influenced by some factors. The first factor taking influence on the torque oscillation is the principle of the voltage inverter function. Pulse switching of IGBT´s implicates the current oscillation which implicates the oscillation of the shaft torque. The magnitude depends on the drive properties. This oscillation type can be influenced by the parameters setting at the drive design only. The oscillation magnitude depends on the leakage inductance of the machine windings, on IGBT's switching frequency, and on the rotational speed of the machine.

The fact, that the magnitude of the stator current oscillation is smaller at low speed, is employed by the traction effort graph design. It means that the converter overload can be higher at low speed. Although the locomotive drive has disadvantageous parameters from this view (small IGBT's switching frequency, small leakage inductance), this type of torque oscillation does not represent the problem.

The second negative factor influencing the drive properties is inverter input voltage oscillation. The full elimination of the subcircuit voltage oscillation is not possible in a converter supplied by AC voltage.

2. DC link voltage oscillation influence on the motor shaft torque

The total power factor of the vehicle is very important parameter and it should tend to unity. That implies the tendency to minimize the deformation power. This requirement can accomplish using of the pulse rectifier. The optimization criterion of the input current spectrum leads to containing of minimum of harmonics. The input power oscillation is the result of the demand on the sine wave input current waveform. The oscillation frequency is twice higher then the frequency of the supply system.

Concurrently, the minimization of the shaft torque oscillations is demanded, because of the driving properties optimization. When the supply frequency is 50 Hz, it is possible to look forward the shaft torque oscillation frequency being 100 Hz. The dumping down of this oscillation depends on the bogie properties. Generally and with the view of experiences, these oscillations are not satisfactory dumped down by the bogie. The higher straining of the bogie components is the first result of this oscillation. The second result is worse adhesion properties of the vehicle. The shaft torque oscillates around its wanted value and the immediate torque value is higher then the wanted value in every period. This short-time shaft torque increasing may lead to dropping the wheel from the rail. That implies the anti-wheel slide control intervention and decreasing of the wanted torque value.

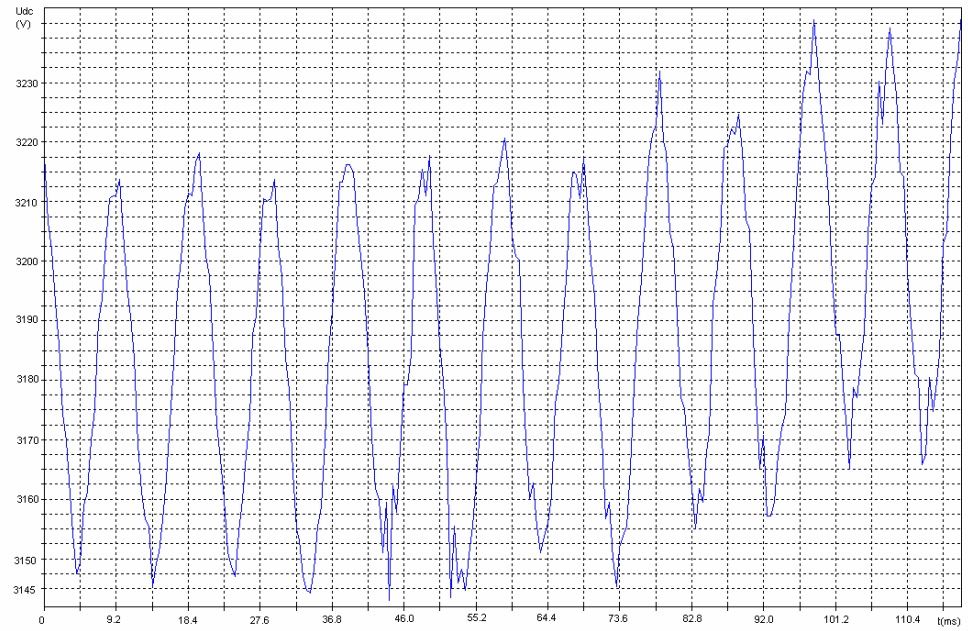

Fig. 1. The DC link voltage waveform in case of the locomotive SKODA 109E.

Let us take an example. The magnitude of DC link voltage oscillation is 100 V and the frequency is 100 Hz at the maximum load. The inverter output frequency is 100 Hz. This output frequency is typical for vehicle stable speed area, videlicet in the area of the maximum torque at the maximum speed. This is the most demanding working area from the view of the control. In the described situation, the inverter output frequency and DC link voltage oscillation frequency get to the synchronization. The machine winding unequal supplying can be observed. This leads to current offset that can be observed in the α, β axis system. The example of this situation is shown in Fig. 2. and Fig. 1. They were taken at the same time. The axis description is in relative computer units. The scale is 12800 computer units representing nominal current 720 A.

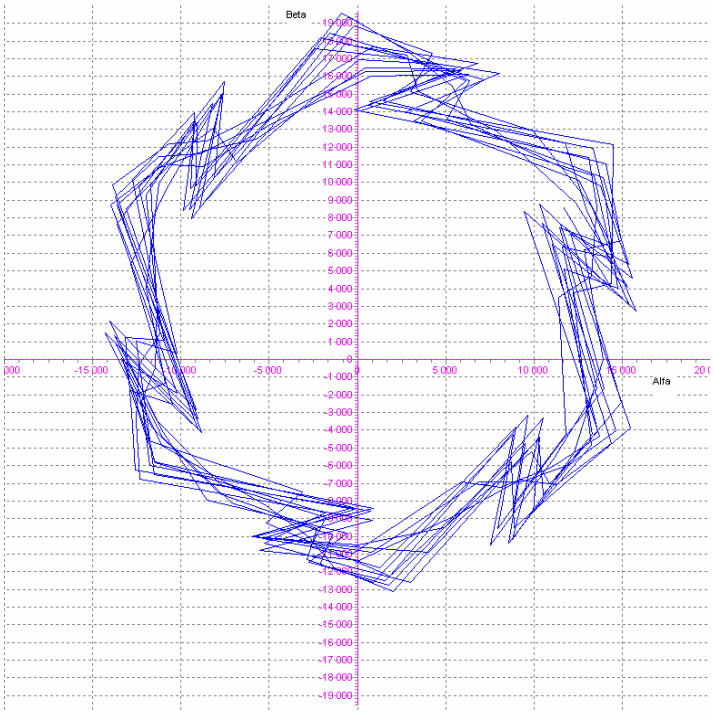

Fig. 2. Example of the stator current offset as the result of DC link voltage oscillation (12800~720A).

The stator current can be transformed into the axis system connected with rotor flux. The oscillations of torque and flux current components are evident in that axis system. This state can be seen in Fig. 3.

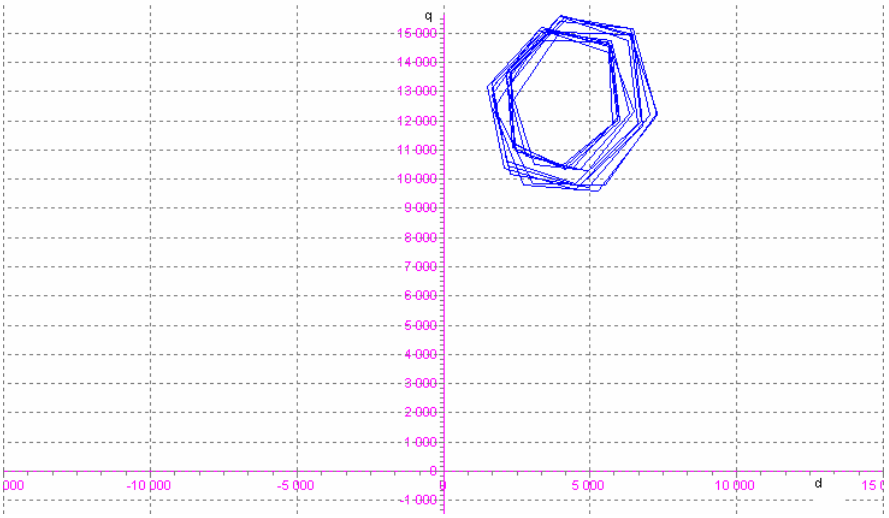

Fig. 3. DC link voltage's oscillation influence to stator current components in axis system connected to the rotor flux (12800 ~720A).

The change of the machine magnetic state during every electric revolution is the result of this imbalance. The effect of periodic changes in flux amplitude and speed is shaft torque oscillation. This can be seen in Fig. 4.

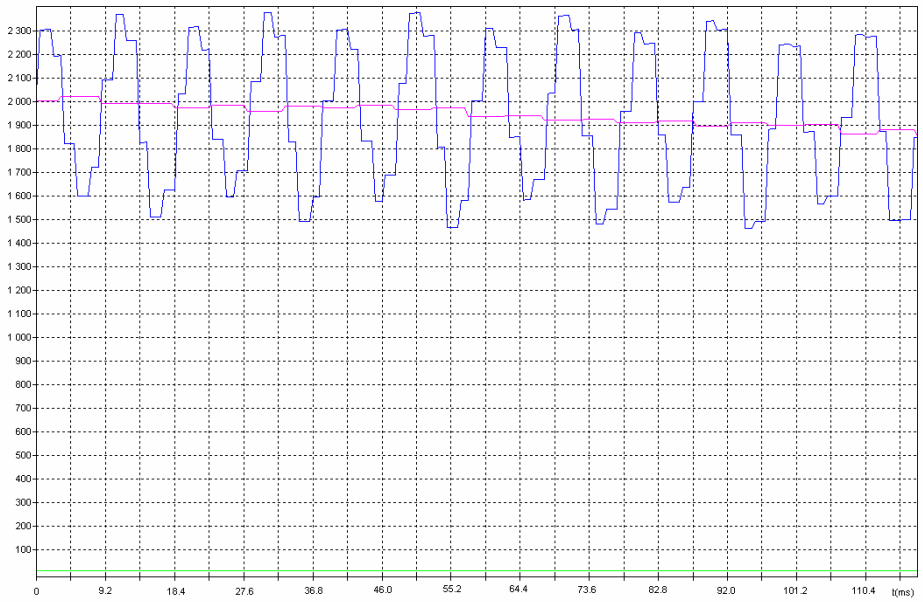

Fig. 4. Torque waveform (2000 ~ 8372 Nm).

The torque axis description in Fig. 4. is in relative computer units with the scale 2000 computer units responding to 8372 Nm.

3. Conclusion

The speed of changes is so fast that the control parameters are not able to compensate them. Only 8 control interferences can be applied during the oscillation period at the maximum IGBT's switching frequency of 800 Hz. It means that the control response cannot come earlier then delayed of 45°.

It ensues from the above that in case of the locomotive SKODA 109E inverter control algorithm design it is necessary to solve new problem that has not been observed on the other SKODA vehicles.

References

[1] JAVŮREK, J., KOPECKÝ, M. *Pulse rectifier – the input part of the three system locomotive*, AT&P Journal, no. 2, 2005 (in Czech).

[2] JAVŮREK, J. *Control of Modern Electric Drives*, Grada, 2003 (in Czech).

[3] BRANDŠTETTER, P. *AC Control Drives*, VŠB FEI, Ostrava, 1999 (in Czech).

[4] ŠIMÁNEK, J., NOVÁK, J., DOLEČEK, R., ČERNÝ, O. *Control algorithms for permanent magnet synchronous traction motor*, EUROCON 2007 Conference Proceedings, Warsaw, 2007.

[5] LETTL, J., DOLEČEK, R. *EMC increasing of PWM rectifier in comparison with classical rectifier*, Radioengineering, vol. 17, no. 4, pp. 93-100, December 2008.

[6] ZDĚNEK, J. *Traction vehicle distributed control computer system architecture with auto reconfiguration features and extended DMA support*, EPE-PEMC 2008 Conference Proceedings, pp. 139-145, Poznan, 2008.

Transcom 2009, 22-24 June 2009
University of Žilina, Žilina, Slovak Republic

Servo-Position Forced Dynamic Control of PMSM

[*]Peter Briš, [*]Michal Kurek, [*]Ján Vittek
[*]University of Žilina, Faculty of Electrical Engineering, Department of Power Electrical Systems,
Univerzitná 1, 01026 Žilina, Slovakia, {Peter.Bris, Michal.Kurek}@kves.uniza.sk.

Abstract. In this paper simulations of position control of permanent magnet synchronous motor for servo-drives are carried out. Position control is based on forced dynamic control, which exploit principles of feedback linearization and forces controlled variable to follow demanded position with prescribed closed loop dynamics. Position loop is complemented by a special computing algorithm, which ensure minimum energy maneuvers and eliminates peaks in demanded variables. Further advantage of this approach is variable time of rotor position change in demanded value without difference between real and computed prescribed demanded curve. Control law is formulated in the rotor flux fixed d_q frame respecting vector control principles. Dynamic lag which appears in position response as the difference between rotor and demanded positions can be compensated by complementary derivative feed-forward precompensator.

Keywords: Servo-position control, Forced dynamic control, Permanent magnet synchronous motor, Minimum energy manoeuvres, Dynamic lag precompensator.

1. Introduction

In this paper are carried out simulations of position control of permanent magnet synchronous motor (PMSM) for servo-drives. Control is based on forced dynamic control (FDC) applied to position response with zero overshoot [1]. Such response to step demand usually requires peaks in control variables, especially value of demanded current in q-axis. To eliminate peak demands position loop is complemented by computing algorithm, which ensures minimum energy maneuvers [2]. Further advantage of this approach is variable time of rotor position change as response on demanded value without difference between real and prescribed demanded position curve. Single FDC position loop follows demanded curve with a certain error by increasing of position loop settling time. Using outer minimum energy position loop this settling time can be set to the most suitable value. Control law is formulated in the rotor flux fixed d_q frame respecting vector control principles. As FDC position control loop shows dynamic lag of rotor position versus demanded position, this position loop is complemented by derivative feedforward precompensator to eliminate this effect. This way is ensured that rotor position follows the demanded position with minimal dynamic lag [3].

2. Design of control algorithm

2.1. Forced Dynamic Control of Rotor Angle

Principles of feedback linearization are applied to the rotor speed and then similar technique is used for rotor angle control loop, therefore the proposed controller is of the cascade structure. First, an inner rotor speed control loop is designed, which yields the first

order linear dynamics, where T_ω is the prescribed time constant and $\omega_{r\ dem}$ is the demanded rotor speed. Mechanical equations of used PMSM in the rotor flux fixed d_q frame is as:

$$\Gamma_{el} = c\left[\Psi_{PM} i_q + \left(L_d - L_q\right) i_d i_q\right], \quad \Gamma_d = \Gamma_{el} - \Gamma_L = J_r \varepsilon_r, \tag{1a,b}$$

$$\frac{d\omega_r}{dt} = \varepsilon_r, \quad \frac{d\theta_r}{dt} = \omega_r, \tag{2a,b}$$

where c=3p/2 and p is number of pole pairs, Γ_{el}, Γ_d and Γ_L are electrical, dynamical and load torque respectively.

Current controlled inverter is assumed in which the current control law switches the stator phase voltages to, in turn, vary the stator voltage components, u_d and u_q, so that i_d and i_q follow their respective demands, $i_{d\ dem}$ and $i_{q\ dem}$, with zero dynamic lag. Magnetizing current is set as i_d=0 for vector control and this way the reluctance component of motor torque in (1a) is eliminated. This then simplifies the design of speed FDC controller and load torque observer. The control system automatically counteracts load torques using of load torque estimate $\hat{\Gamma}_L$ from an observer with observer settling time, T_{so},. Observer beside estimate of load torque provides also filtered estimate of rotor speed, $\hat{\omega}_r$.

In case of position loop, the plant is formed by ideal first order transfer function block of FDC speed control loop and kinematic integrator, which produces the rotor angle, as shown in Fig. 1. If the control position system is designed to have a specified settling time, $T_{s\theta}$, for multiple real poles it can be determined with the aid of the Dodds settling time formula (3). This ensures response to the step demand with zero overshoot.

$$\frac{\theta_r(s)}{\theta_{r\ dem}(s)} = \left[\frac{1}{1 + s\dfrac{T_{s\theta}}{1{,}5(1+n)}}\right]^n\Bigg|_{n=2} = \frac{1}{s^2\dfrac{4T_{s\theta}^2}{81} + s\dfrac{4T_{s\theta}}{9} + 1}. \tag{3}$$

Differential equations of PMSM stator currents, and more detailed description of FDC including programmed equations for speed and position control and load torque observer can be found in [1].

2.2. Minimum Energy Position Controller

Principle of minimum energy position controller exploits maximal rotor acceleration, ε_r, to achieve certain rotor speed, ω_r, then movement with constant value of speed and again exploiting maximal deceleration to brake rotor at the demanded position $\theta_{r\ dem}$. Advantage of this controller is variable demanded time, T_m of rotor position change to the demanded value. Increasing demanded time, T_m is leading to energy reduction and in opposite setting the minimal possible demanded time T_m, ensure time-optimal position control for no load torque operation.

From left hand side of (1b) results the relationship between maximal values of individual torques (4a), where maximal value of electromagnetic motor torque is $\Gamma_{e\ max}$, which is given by (4b) derived from (1a), in which reluctance torque component was eliminated by vector control.

$$\Gamma_{e\max} = \Gamma_{d\max} + \Gamma_{L\max}, \qquad \Gamma_{e\max} = c\Psi_{PM} I_{q\max}. \tag{4a,b}$$

Torque $\Gamma_{e\ max}$ is given by a maximal prescribed value of q-axis current I_{q_max} and torque constant, $c\Psi_{PM}$. Maximal value of dynamic torque is $\Gamma_{d\ max}$ and is given by (5a), which is derived from right hand side of (1b). Torque, $\Gamma_{d\ max}$ is given in conjunction of moment of inertia J_r and maximal value of rotor acceleration ε_{max}. It can be seen from (5b) derived from

(4a,b), (5a), that value of $\varepsilon_{\max}$ is determined also with the value of load torque $\Gamma_{L\_\max}$, which appears during change of demanded rotor position.

$$\Gamma_{d\max} = J_r \varepsilon_{\max}, \qquad \varepsilon_{\max} = \frac{c\Psi_{PM} I_{q\max} - \Gamma_{L\max}}{J_r}. \tag{5a,b}$$

From the definition of prescribed time change of acceleration ε_S, see Fig.1, and corresponding responses of rotor speed, ω_S and rotor position, θ_S, shown also in simulation results of Fig.2 or Fig.3 respectively, are derived following equations:

$$T_m \geq \sqrt{\frac{4\theta_{r\,dem}}{\varepsilon_{\max}}}, \qquad T_\varepsilon = \left(T_m - \sqrt{T_m^2 - 4\frac{\theta_{r\,dem}}{\varepsilon_{\max}}} \right) \Big/ 2 \tag{6a,b}$$

Equation (6a) describes minimal possible demanded time, T_m and (6b) determines time, T_ε of duration $\varepsilon_{\max}$ and $-\varepsilon_{\max}$, needed for programming of demanded position curve, θ_S.

2.3. Dynamic Lag Precompensator

Equation of derivative feedforward precompensator for elimination of FDC position loop dynamic lag is derived from prescribed transfer function (3) as its reciprocal value as:

$$\frac{\theta'_{r\,dem}(s)}{\theta_S(s)} = s^2 \frac{4T_{s\theta}^2}{81} + s\frac{4T_{s\theta}}{9} + 1, \qquad \theta'_{r\,dem} = \theta_S + \frac{4T_{s\theta}}{9}\omega_S + \frac{4T_{s\theta}^2}{81}\varepsilon_S. \tag{7a,b}$$

In (7a) the first and second derivative of position θ_S are replaced directly by ω_S and ε_S, and thus for programming purpose (7b) is obtained, where θ'_{r_dem} is the new demanded position for FDC position loop. The resulting block diagram of the overall control structure described is shown in Fig. 1.

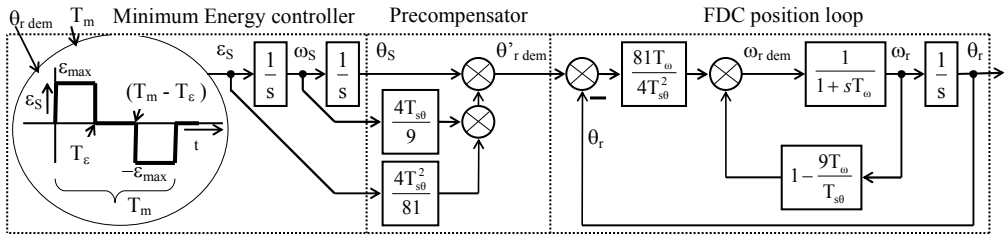

Fig. 1. Block diagram of overall control structure.

3. Simulations results

For all the simulation presented inverter dc supply voltage was U_{dc}=260 V. A step position demand, θ_{r_dem}=2π rad, with prescribed position loop settling time is $T_{s\theta}$ = 45 ms, prescribed time constant of speed control loop was $T_\omega = T_{s\theta}/9$ = 5ms to eliminate influence of speed feedback in position algorithm, and settling time of load torque observer was set to T_{so}=20 ms. Demanded time of rotor position, θ_r change was T_m=0,2 s. Rotor position, θ_r is quantized for more realistic results with quantization step $2\pi/2^{12}$ rad.

Maximal value of q-current $I_{q\,max}$ = 5 A which corresponds to the nominal effective value of phase current 3,6A results in maximal motor torque, $\Gamma_{e\,max}$ about 5 Nm. Two versions of simulation are carried out. The first version, which is shown in Fig.2, is for zero external load torque, Γ_L during position change, therefore value of $\Gamma_{L\,max}$ = 0 for (5b). Then for time

t>0.25 s is applied step change equal $\Gamma_{e\,max}$. In the second version, shown in Fig. 3, Γ_L is equal $\Gamma_{e\,max}/2$ and this is valid also for position change. Value $\Gamma_{e\,max}/2$ is also equal to $\Gamma_{L\,max}$ as input to (5b) for evaluating maximal acceleration ε_{max}, which is now half of the value if compared with the first version. All initial conditions of state variables are set to zero.

Parameters of PMSM are as follows: winding resistance, R_s=1,3 Ω, winding inductances, L_d=14,4 mH, L_q=16,3 mH, permanent magnet flux, Ψ_{PM}=0,13 Wb, number of pole pairs, p=5, moment of rotor inertia, J_r=0,0037 kgm^2 .

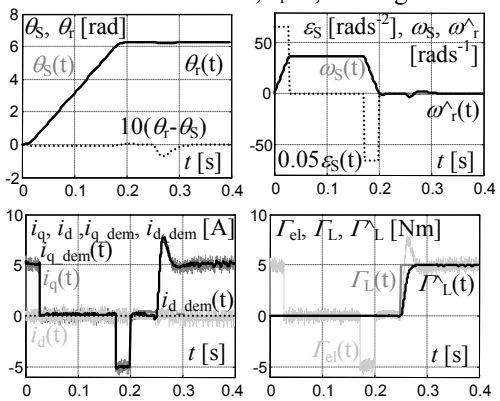

Fig. 2. Simulation results of first version.

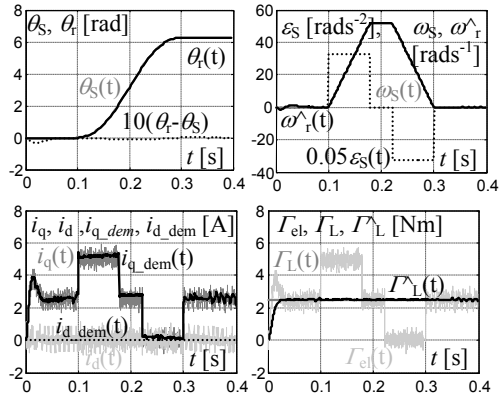

Fig. 3. Simulation results of second version.

4. Conclusion

The saddle in position response due to application of load torque can be minimized by shorter setting time constant of load torque observer. This can have effect not only in faster estimation of the value of load torque but also in lower estimation error in rotor speed during transients due to load torque application. In opposite, smaller settling time of observer is at the expense of its filtering effect. Further improvement of position saddle can be done in conjunction with model reference adaptive control.

For improvement of time-optimal position control under loaded motor it would be useful to prescribe higher value of deceleration during braking conditions, which will reflects also in higher i_q component demand. This way torque of the machine will be exploited more efficiently and the control can get closer to time-optimal conditions, where minimal possible time of demanded position change is prescribed. This is intention of further work over the minimum energy position controller.

Acknowledgement

The authors wish to thank Slovak Grant Agency VEGA for funding the project No.4087/07.

References

[1] VITTEK, J., BRIŠ, P., MAKYŠ, P., ŠTULRAJTER, M., VAVRÚŠ, V. *Control of Flexible Drive with PMSM employing Forced Dynamics*. IEEE / EPE - PEMC 2008 , Poznaň-Polsko, 2008, 09, 1.-3., p.: 2242-2249.

[2] DODDS, S. J., SOORIYAKUMAR, G., PERRYMAN, R. *Minimum Energy Forced Dynamic Position Control of PMSM Drives.* 3rd IASME/WSEAS Int. Conf. on Energy & Environment, University of Cambridge, UK, February 23-25, 2008, p.: 173-179.

[3] VITTEK, J., MAKYŠ, P., ŠTULRAJTER, M., DODDS, S. J., PERRYMAN, R. *Servo-Position Control with Dynamic Lag Precompensator for Pmsm Drives,* Journal of Electrical Engineering, Vol. 7/2007.

Transcom 2009, 22-24 June 2009
University of Žilina, Žilina, Slovak Republic

Hydrogen Storage Energy Gained from Renewable Sources

[*]Roman Chválek, [**]Zdeněk Hradílek
*Faculty of Electrical Engineering and Computer Science, Department of Electrical Power Engineering, 17. listopadu 15, 708 33 Ostrava {roman.chvalek}@vsb.cz
**Faculty of Electrical Engineering and Computer Science, Department of Electrical Power Engineering, 17. listopadu 15, 708 33 Ostrava {zdenek.hradilek}@vsb.cz

Abstract. This work deals with hydrogen made by electrolyser which is placed in hydrogen storage system. Electrolyser is fed by renewable energy (e.g. wind power) supplying the clean hydrogen to fuel cell transmuting hydrogen to electric energy. There is also described the equipment in VSB-TUO laboratory like an electrolyser HOGEN GC600 and fuel cell NEXA Power Module, etc.

Keywords: Hydrogen storage system, renewable energy sources.

1. Introduction

Hydrogen is often featured as a realistic solution of the world's power shortage because it offers clean boundless energy, in the period of climatic changes and limited sources of fossil fuels move the issue of energy supplies to consumers top focus. Hydrogen can be used in a connection with other alternative energetic forms and is able to retain their performance. Single alternative technologies are unreliable because they depend on environmental factors such as sunshine, wind, waves etc. Hydrogen can store energy of all different sources of renewable energy e.g. connection with a "smart" power grid which can be used for distribution of energy.

2. Accumulation of renewable energy

Accumulation is a process which enables to store energy at a right place and form to be ready for next usage in the required time, quality and quantity.

Most widespread are lead-acid accumulators, electrochemical and fly-wheel storage batteries, superconductive magnetic accumulators, heat accumulators, pumped storage hydro plants, etc.

Hydrogen storage system is fed by clean renewable energy (e.g. wind power). The disadvantage of renewable decentralized sources is the influence on transmission and distribution network (they influence the quality of the supplied electric power). It's possible to solve it by storing the energy in the hydrogen.

3. Hydrogen storage system

Diagram of storage system is displayed in Fig. 1. The hydrogen storage system is compounded of a rectifier, an electrolyser, a hydrogen storage tank, a water reservoir, a fuel cell and an inverter.

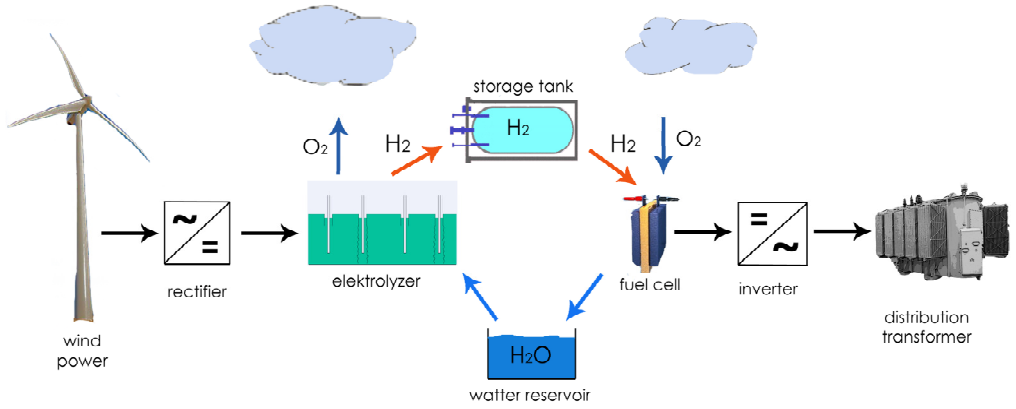

Fig. 1. Renewable energy transformation system

The function of the storage system with fuel cells is as follows. An alternating current (AC) generated in a wind power plant is converted to a direct current (DC) in a rectifier, the DC drives an electrolyser where water molecules are divided by this DC current into hydrogen and oxygen (see chapter 4). Hydrogen is then compressed and stored in a hydrogen tank (oxygen can also be stored in a special tank but not always has the electrolyser an accessible oxygen outlet). The stored hydrogen can then be used to drive the fuel cell together with the stored oxygen or with air as an oxidizer. The fuel cell generates DC which is then converted to AC in an inverter and this AC is supplied to grid [1].

4. Hydrogen production

High purity hydrogen can be produced through a direct chemical path using electrolysis. With a renewable electrical energy supply, electrolysis of water allows hydrogen to be made from water without pollution.

The quantity of hydrogen depends on the current density (A/m^2). Higher current density needs higher voltage supply (grows hydrogen power unit cost). Nevertheless, higher voltage will lower general size of electrolyser which will cost reduction. The most modern accessible electrolysers have energy efficiency somewhere between 65 - 80 % and operate with current densities about 2 000 A/m^2.

During the electrolysis, the quantity of the required electric power can be compensated by delivering the heat power into the reaction. Minimum voltage demand for water analysis at temperature 25°C is 1.23 V (needs heat delivery from an outside resource to be realized at all). At lower voltage with warm supply is a running electrolyser advantageous because thermal energy is usually cheaper than electrical energy and can be re-circulated. Electrolysis efficiency grows (no up) with growing temperature [2].

Other technologies of hydrogen productions are natural gas steam reforming, high-temperature electrolysis and termochemical cycles.

5. Hydrogen processing

The fundamental component of fuel cell consists of two electrodes, the anode and the cathode, separated by a polymer membrane electrolyte. Each of the electrodes is coated on one side with a thin platinum catalyst layer. The electrodes, catalyst and membrane together form the membrane electrode assembly. A single fuel cell consists of a membrane electrode assembly and two flow field plates.

Gases (hydrogen and air) are supplied to the electrodes on either side of the membrane through channels formed in the flow field plates. Hydrogen flows through the channels to the anode where the platinum catalyst promotes its separation into protons and electrons. The free electrons are conducted in the form of usable electric current through an external circuit, while the protons migrate through the membrane electrolyte to the cathode. At the cathode, oxygen from the air, electrons from the external circuit and protons combine to form pure water and heat.

Individual fuel cells are combined into a fuel cell stack to provide the required electric power. A single fuel cell produces about 1 volt at open circuit and about 0.6 volts at full load. Cells are stacked together in series to provide the required output voltage [3].

6. VSB-TUO hydrogen laboratory

The laboratory is equipped by full hydrogen economy. Hydrogen is stored in twelve standard pressure bottles (200 bars, 9m^3). Needed demineralised water (input electrolyser medium) is prepared in an osmotic filtration unit. A running fuel cell, an electrolyser and an arrangement are working in a security range hood which is equipped by metering of hydrogen concentration as well as anti-escape hydrogen ventilation [4].

6.1. Measuring technique

A measuring station includes a system formed by measuring sensors that convert and evaluate signals by a measuring card which is further executed by a computer.

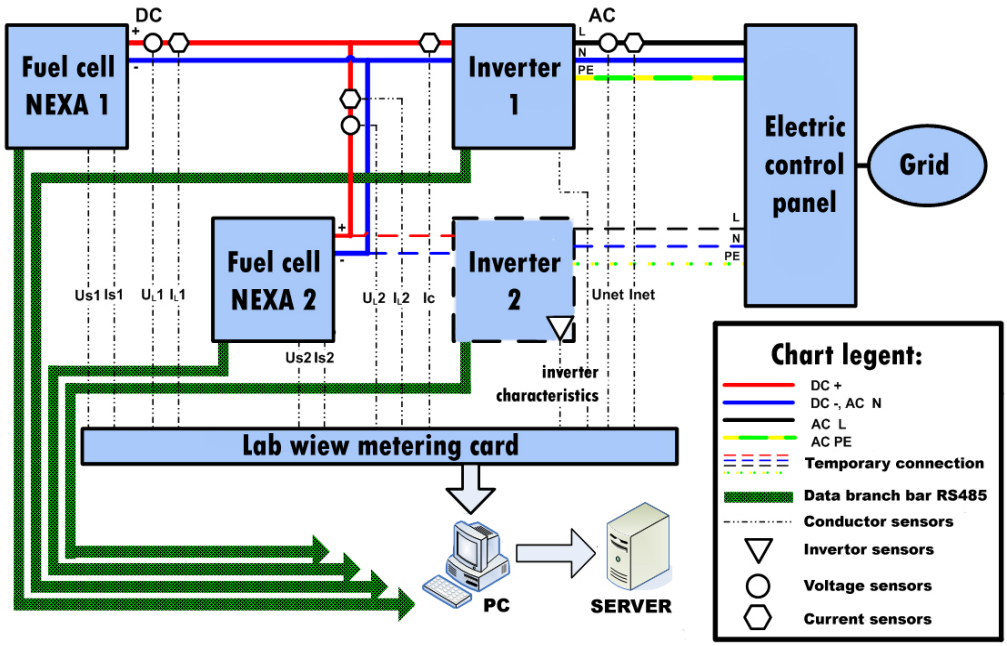

Fig. 2. Testing workplace scheme [3]

Sensors are realized by voltage and current detectors type LEM. There is a 16-bit metering card with USB interface handling its flexibility and mobility. The fuel cell stack voltage, its stack currents and output currents (without self-consumption), stack temperature, fuel pressure, fuel consumption, measuring time, etc. all belong among the measured values [4].

6.2. Fuel cell specifications

Fuel cells Nexa from Ballard Company shown in Figure 3. belong to a low–temperature fuel cells category. Electric power (of one fuel cell) is 1200 W and rated output voltage is about 26 V. It is a fully integrated system which supplies unregulated direct electric energy when hydrogen and oxygen are delivered. There are only two components that are emitted to the outside, and these are: the air (with lowered content oxygen like oxidant) and product water (which goes through damper before emitting) where it is partly changed into regenerative air and handling sufficient membranes humectation which is necessary for membrane functionality. Product is also warm in warmed cooling air form [4].

Fuel cell is composed of one main part called stack and several associated arrangement needed for its running. Ancillary subsystems include hydrogen delivery, oxidant air supply and cooling air supply. Onboard sensor monitor system performance and the control board and microprocessor fully automate operation. The Nexa System also incorporates operational safety systems for indoor operation [3].

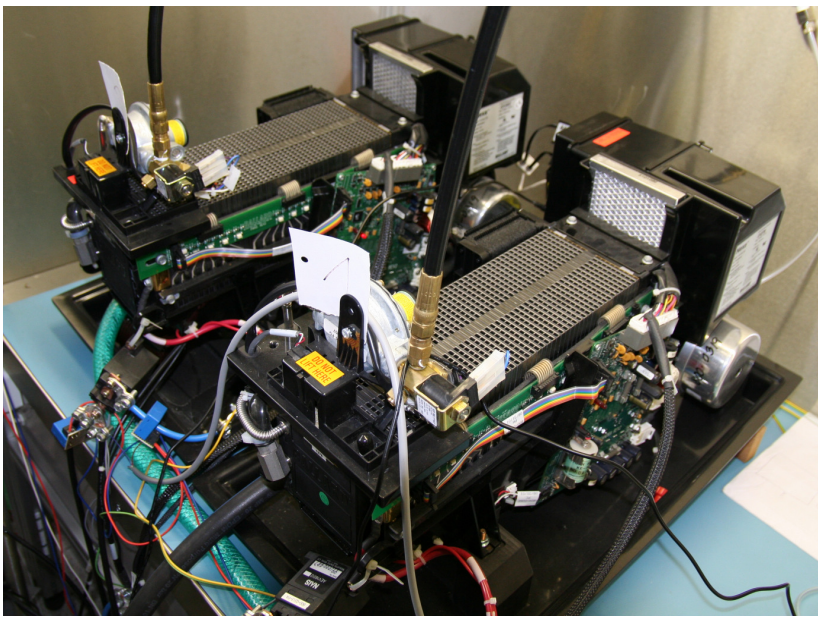

Fig. 3. Fuel cells NEXA

6.3. Electrolyser specifications

The HOGEN GC laboratory hydrogen generator (Fig. 4.), when connected to a suitable AC power source and fed with a suitable quality of DI water, produces a continuous stream of pressurized ultra high purity (UHP) hydrogen gas (99.9999%) and automatically maintains a user-selected downstream pressure(up to 1.38 Mpa). The HOGEN GC hydrogen generator, available in 600 cc/min hydrogen production capabilities, is suitable for use in laboratories and light industrial environments and is non-hazardous for transportation purposes [5].

Fig. 4. Electrolyser HOGEN GC600

7. Experiments

For better understanding of accumulation problems of renewable energy, it is necessary to perform a series of measurements. Is necessary to make measurements on renewable sources (wind power plant), electrolysers, as well as the fuel cells (which was already done by means of my paper).

Planned metering on electrolyser Hogen GC600 and its results will minister to the enlargement of knowledge about a single component and subsequently about the whole system. The obtained data (from cooperative colleagues) concerning wind power plants in connection with fuel cell and electrolyser values will be step by step processed and evaluated.

8. Conclusion

In the long-term view the hydrogen is the most probable porter of energy which is acceptable for "storing" energy from renewable sources. Distant equipments for renewable power sources usage (placed at areas with high windy potential, solar or geothermal energy) can be used for hydrogen production. Hydrogen could be transported to the places of usage where, with the aid of local fuel cells, can enable to use the energy from renewable sources in a form of electricity and warmth according to the demand. It means at the time and place when and where it is necessary for the energy to be used.

Hydrogen can also be used to store renewable electricity when it is not needed (like the wind blowing at night) and then the hydrogen can be used to meet power needs during the day or fuel vehicles.

Acknowledgement

This work is devoted to experimental intention MSM 6198910007.

References

[1] Šebesta R., Hradílek Z.: *Fuell cells for storage systems of electric energy compared by MCA*, ELNET December 2008, Ostrava Czech Republic, pp.2-3

[2] Educational materials of Ballard company: http://www.ballard.com/

[3] User's manual shipped with fuel cell Nexa Power Module from Ballard Company

[4] Minařík D., Sokanský K.: *Provozní charakteristiky palivového článku typu PEM a jeho laboratorní připojení do sítě*, HT-FCA 2008, ISBN 978-80-248-1753-8

[5] Educational material from Proton Energy company supplied to electrolyzer Hogen GC600

[6] Česká vodíková technologická platforma: http://www.hytep.cz/?loc=article&id=6

Transcom 2009, 22-24 June 2009
University of Žilina, Žilina, Slovak Republic

Modelling of Brain Vascular System Using Electromechanical Analogy

[*]Barbora Czippelová
[*]University of Žilina, Faculty of Electrical Engineering, Department of Electromagnetic and Biomedical Engineering, Univerzitná 1, 01026 Žilina, Slovakia, {Czippelova}@fel.uniza.sk

Abstract. The contribution deals with the investigation of haemodynamics in human brain arteries by means of electrical modelling and simulations. The electromechanical analogy of blood flow in vessel and electromagnetic wave propagating along an electric transmission line is used to create a complex computer model. Simulation examples of the healthy cerebral system arteries in comparison with the pathologically changed ones are presented and discussed.

Keywords: brain arteries, haemodynamics, arterial stenosis, electromechanical analogy, electrical modelling and simulation

1. Introduction

The cerebral arterial circle (also called Circle of Willis) is a circle of arteries that supply blood to the brain. The arrangement of the brain's arteries into the Circle of Willis creates redundancies in the cerebral circulation. If one part of the circle becomes blocked or narrowed (stenosed) or one of the arteries supplying the circle is blocked or narrowed, blood flow from the other blood vessels can often preserve the cerebral perfusion well enough to avoid the symptoms of ischemia.

Computer models of cerebral arteries enable us to investigate compensation effects of Circle of Willis under different pathological conditions without invasive intervention to organism or without necessity of presence of these pathologies in organism. The computer-aided non-invasive methods represent a helpful tool to facilitate the understanding of the biofluid mechanics in cardiovascular systems [1, 2].

2. Formulation of model

Very efficient method of the solution of hydrodynamic problems of blood flow in cardiovascular system is application of electromechanical analogy.

The blood flow is formally similar to propagation of electric current along electric lines. Differential equations of hydrodynamic processes in a vessel are similar to those describing transmission of electric charge in an electric line. Based on this, each particular vessel can be represented by serial connection of four-poles (vessel segments) characterized by transfer parameters of long wire. Analogy of mechanical and electric quantities should be documented by Tab. 1. Analogy of hydrodynamic (mechanical) process in a tube and transmission of electric current can be demonstrated by schematic drawing in Fig. 1. [3, 4]

	MECHANICAL QUANTITIES		ELECTRIC QUANTITIES
P	pressure	P	potential
P_t	transmural pressure	U	voltage
I	volume flow	I	current
V	volume	Q	charge
W_k	kinetic energy of blood flow	W_m	energy of magnetic field
W_e	energy of blood vessel wall elastic deformation	W_e	energy of electric field

Tab. 1. Analogical electric and mechanic quantities

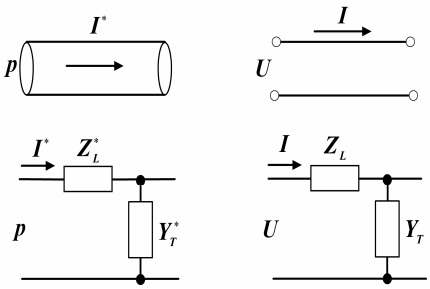

Fig. 1. Analogy of a vessel and an electric line

Longitudinal impedances $\boldsymbol{Z}_{\mathrm{L}}^{*}$ (mechanical) and $\boldsymbol{Z}_{\mathrm{L}}$ (electric) represent conservative and dissipative components, transversal admittances $\boldsymbol{Y}_{\mathrm{T}}^{*}$ and $\boldsymbol{Y}_{\mathrm{T}}$ describe cross elasticity and inter-wire capacity and cross losses [1, 2]. The main question of the analogy based methodology consists in derivation of relationships for parameters $\boldsymbol{Z}_{\mathrm{L}}$ and $\boldsymbol{Y}_{\mathrm{T}}$.

The base of modelling and simulations of blood flow in vessels constitutes mathematical description of haemodynamics:

1. Mechanical interaction between blood flow and vessel wall can be described by Navier-Stokes equation

$$\frac{\mathrm{d}(\rho \boldsymbol{v})}{\mathrm{d}t} = -\mathrm{grad}\, p + \eta \Delta \boldsymbol{v} + \boldsymbol{f} \tag{1}$$

where ρ is the liquid density, $\boldsymbol{v}$ – local flow velocity, p – pressure, η - dynamic viscosity , $\boldsymbol{f}$ – external force density.

2. The blood is considered as Newtonian fluid – incompressible and with constant density.
3. The vascular system is a closed system where the volume of blood inside the vessel can not increase - vascular system is considered as the system without sources. Therefore, for the vascular system description the continuity equation is valid.

$$div\, \boldsymbol{v} = 0 \tag{2}$$

Equations (1) and (2) along with the time variant boundary conditions on the vessels' walls form the system of partial differential equations describing the haemodynamics of blood flow.

We shall describe a flow of liquid in a cylindrical elastic tube and due to axial symmetry there is $v_\varphi = 0$. The eq. (1) can be broken into only two components

$$\rho \frac{\partial v_r}{\partial t} = -\frac{\partial p}{\partial r} + \eta \left(\frac{\partial^2 v_r}{\partial r^2} + \frac{1}{r}\frac{\partial v_r}{\partial r} - \frac{v_r}{r^2} + \frac{\partial^2 v_r}{\partial z^2} \right) \tag{3}$$

$$\rho \frac{\partial v_z}{\partial t} = -\frac{\partial p}{\partial z} + \eta \left(\frac{\partial^2 v_z}{\partial r^2} + \frac{1}{r}\frac{\partial v_z}{\partial r} + \frac{\partial^2 v_z}{\partial z^2} \right) \tag{4}$$

Eq. (2) obtains a form

$$\frac{\partial v_r}{\partial r} + \frac{1}{r} v_r + \frac{\partial v_z}{\partial z} = 0\,. \tag{5}$$

By deriving from these equations we can get the relation between pressure gradient and volume flow in blood vessels.

$$\dot{I}(z,t) = \int_0^{r_0} \dot{V}_z(r,z,t)\, 2\pi\, r\, dr = -\,\mathrm{j}\, \frac{\pi r_0^2}{\omega \rho} \frac{J_2(a r_0)}{J_0(a r_0)} \frac{\partial\, \dot{p}(z,t)}{\partial z} \tag{6}$$

By deriving from equations describing haemodynamics and by using electromechanic analogy we can get elements of equivalent circuit of blood vessel.

$$\boldsymbol{Z}_{\mathrm{L}}: \quad R_n = \frac{8\eta}{\pi r_0^{\,4}} n \qquad L_n = \frac{\rho}{\pi r_0^{\,2}} \frac{1}{2n-1} \qquad \boldsymbol{Y}_{\mathrm{T}}: \quad C = \frac{2\pi r_0}{\kappa K_w} \qquad G = \frac{2\pi r_0}{\kappa \eta_w} \tag{7}$$

r_0 - radius of the vessel wall, K_w is the volume stiffness of the tube wall and η_w – coefficient of internal friction (cause of deformation losses), κ - geometrical factor
The final equivalent circuit of vessel segment shows Fig. 2a.

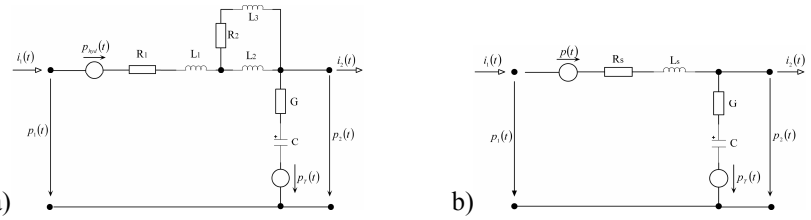

Fig. 2. Electric model of a) homogeneous vessel segment and b) stenosed vessel segment

When the pathological deformation of a vessel segment occurs, the equivalent electromagnetic model will differ from the homogeneous one at Fig. 2a. In the case of an arterial stenosis (a local narrowing of a vessel) the equivalent electric model is shown at Fig. 2b. In comparison with Fig. 2a the elements $R_1 \rightarrow R_s$, $L_1 \rightarrow L_s$ and $R_2 = 0$, $L_2 = L_3 = 0$. These components are based on empiric findings. [3, 4, 5]

3. Model of cerebral vascular system

A part of cerebral circulation – vessels on the base of the brain were chosen for modelling and simulations under physiological and different pathological conditions.

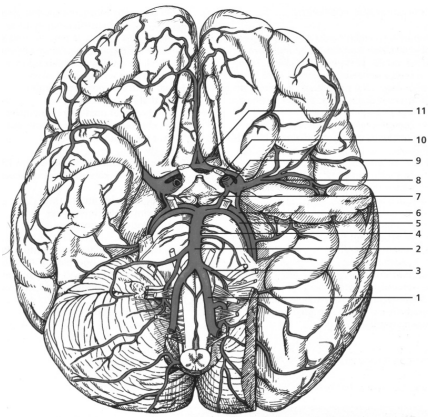

1 - a. vertebralis, 2 – a. basilaris, 3 – a. inferior anterior cerebelli, 4 – aa. pontis, 5 – a. superior cerebelli, 6 – a. cerebri posterior, 7 – a. communicans posterior, 8 – a. cerebri media, 9 – a. carotis interna, 10 - a. cerebri anterior, 11 – a. communicans anterior.

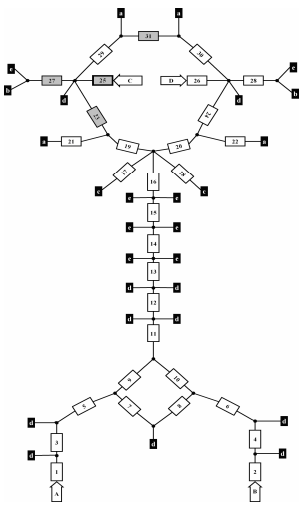

Fig. 3. Human brain arterial system and its topology (segmented into 31 parts)

Circulatory system on the base of the brain was separated into 31 homogenous segments. Modeled pathological state was the single side stenosis of a. carotis interna (segment 25) for stenosis degree values 50%, 70% and 90%. The shape of curves of blood pressure and blood flow was observed through segments 23 (a. communicans posterior), 27 (a. cerebri media) and 31 (a. communicans anterior) to evaluate the compensation effect of Circle of Willisi (CW). The simulation results of blood flow and pressure under physiological and pathological states are shown at Fig. 4.

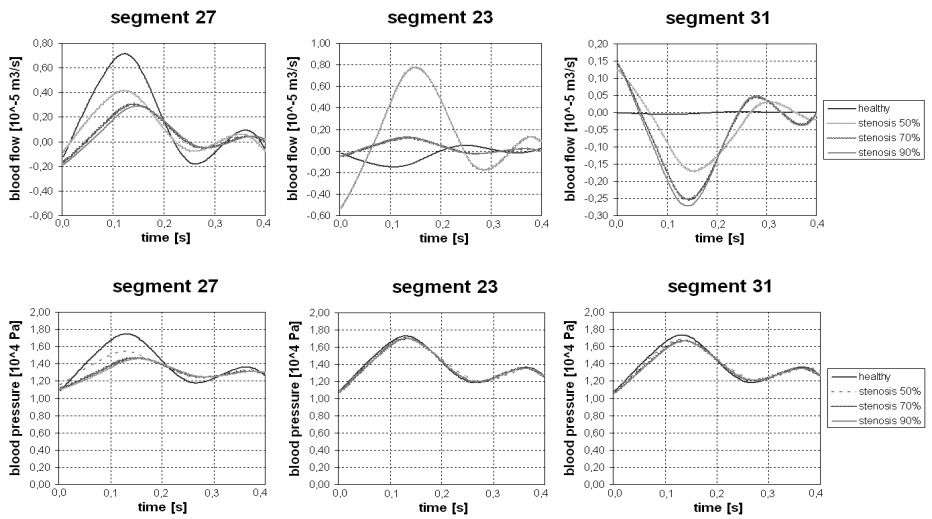

Fig. 4. Blood flow and blood pressure measured on: a. cerebri media (27), a. communicans posterior (23), a. communicans anterior (31)

Obtained simulation results show that with increasing degree of stenosis blood flow decreased through the segment 27 and increased through the segments 23 and 31 to supplement blood from other sources to affected parts of the brain. Consequently, thanks compensation role of CW, increases the blood flow through a. communicans posterior (segment 23) approximately 6 times and trough a. communicans anterior (segment 31) approximately 25 times. Due to this, the blood pressure and flow drop on the side of the segment 27 for the worst case - 90% stenosis of the segment 25 is about 50% in case of blood flow and about 70% in case of blood pressure compared to healthy state. [1]

4. Conclusion

A comprehensive computer model of the cerebral circulation, based on electromechanical analogy and electrical network analysis, was used to investigate the influences of stenoses for stenosis degree values 50%, 70% and 90% on regional cerebral haemodynamics. The obtained simulation results for the blood pressure and mainly for the blood flow show the compensation possibilities of CW in case of one brain arterial diameter reduction.

Knowledge of blood flow and blood pressure throughout the circulatory system, especially in the arterial system, is crucial to a complete understanding of the negative affects of various cardiovascular diseases. The results of the simulations suggest that our model may be a useful tool to study haemodynamic problems of the cerebral circulation.

References

[1] **CZIPPELOVÁ B.** *Modelling and simulation of cerebral vascular system using electromechanical analogy*, **Meditech - Innovative program of modern biomedical technologies, Bratislava 2008 (Proccedings of the ESF project conference with international participation), ISBN978-80-227-2881-2, Str. 8-13**

[2] **ČÁPOVÁ K., BLAŽEK V., ČÁP I.** *Investigation of Brain Arterial Circle Malformations Using Electrical Modelling and Simulation,* **AEEE, vol. 5 (2006), No. 1-2, p. 212-217. ISSN 1336-1376**

[3] **GAELINGS E. W.** *Numerische Simulation Haemodynamischer Processe in vascularen Netzen*, **Shaker Verlag Aachen, 1996, ISBN-3-8265-1509-9, Germany**

[4] **ČÁPOVÁ K., BLAŽEK V., ČÁP I.:** *Pathological Deformation of Brain Vascular System Modelling using Analogous Electromagnetic Systems,* **AEEE, vol. 3 (2004), No. 2, p. 213-216. ISSN 1336-1376**

[5] **ČÁP I., CZIPPELOVÁ B.** *Electromechanical model of blood flow in vessels,* **Advances in electrical and electronic engineering, vol.7/2008, pp. 338 – 341, ISSN 1336 – 1376**

Transcom 2009, 22-24 June 2009
University of Žilina, Žilina, Slovak Republic

Voltage Sag Problem and Its Modeling by Using ATPDraw

[*]Petr Hečko
[*]University of Žilina, Faculty of Electrical Engineering, Department of Power Electrical Systems, Univerzitna 1, 01026 Žilina, Slovakia, Petr.Hecko@kves.uniza.sk

Abstract. The problem of voltage sags and interruptions and its severe impact on sensitive loads is well known. To solve this problem, custom power devices are used. One of those devices is the Dynamic Voltage Restorer (DVR), which is one of the most efficient and effective modern custom power devices used in power distribution network. This paper describes voltage sags and interruptions problem, DVR operation principle and it also describes ATP-EMTP program, which is good for power network modeling. In conclusion of this paper is shown a model of one part of Slovak power network modeled in ATP-EMTP. In this model voltage sags caused by connection of big load is modeled.

Keywords: Voltage sags, Dynamic Voltage Restorer, ATP-EMTP, compensation, power network.

1. Voltage sags and interruptions problem

Voltage sags and interruptions are the most common types of power quality disturbances. A lot of money is lost in productivity each year in all over the world and it's a reason, why we must compensate this disturbances.

1.1. Definition of voltage sags and interruptions

Voltage sag is not complete interruption of power supply, it is a temporary drop below 90 percent of the nominal voltage level. Most voltage sags do not go below 50 percent of the nominal voltage and they normally last from 3 to 10 cycles, or 50 to 200 milliseconds. Voltage sags are probably the most significant power quality problem for industrial customers today, and they can be a significant problem for large commercial customers as well.

There are two sources of voltage sags: external and internal. Storms are the most common cause of external sags and momentary interruptions in most areas all over the world. Other common causes of external sags are ice storms, animals, and the start-up of large loads at neighboring facilities. Internal causes of voltage sags can include starting major loads and grounding or wirings problem. A course of voltage sag is depicted in Fig.1 [1].

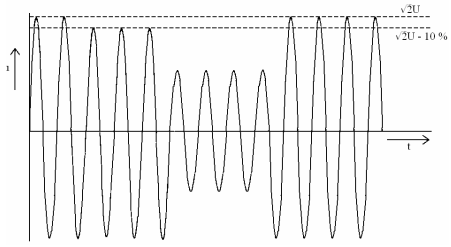

Fig. 1. Shape of the voltage curve during voltage sag [1]

2. Dynamic Voltage Restorer

Dynamic Voltage Restorer (DVR) is a series compensator which is able to protect a sensitive load from the distortion in the supply side during fault or overloaded in power network. The basic principle of a series compensator is simple, by inserting a voltage of required magnitude and frequency, the series compensator can restore the load side voltage to the desired amplitude and waveform even when the source voltage is unbalanced or distorted. This DVR device employs gate turn off thyristor (GTO) solid state power electronic switches in a pulse width modulated (PWM) inverter structure.

The DVR can generate or absorb independently controllable real and reactive power converter that injects a set of three phase AC output voltages in series and synchronism with the distribution feeder voltages. The amplitude and phase angle of the injected voltages are variable thereby allowing control of the real and reactive power exchange between the DVR and the distribution system. The DC input terminal of a DVR is connected to an energy source or an energy storage device of appropriate capacity. The reactive power exchanged between the DVR and the distribution system is internally generated by the DVR without AC passive reactive components. The real power exchanged at the DVR output AC terminals is provided by the DVR input DC terminal by an external energy source or energy storage system.

DVR structure comprises rectifier, inverter, filter and coupling transformer (Fig.2). Besides, pulse width modulated (PWM) technique is used to control variable voltage. Filter is used for elimination harmonics generated from high switching frequency in PWM technique [2].

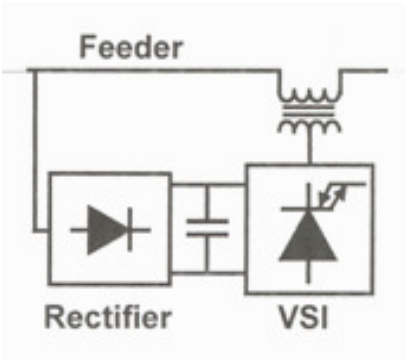

Fig. 2. The DVR structure [2]

2.1. The principle operation of DVR system

In normal situation, without short circuit in power system, a capacitor between rectifier and inverter (Fig. 2) will be charging. When voltage sag happened, this capacitor will discharge to maintain load voltage supply. Nominal voltage will be compared with voltage sag in order to get a difference voltage that will be injected by DVR system to maintain load voltage supply. PWM technique is using to control this variable voltage. In order to maintain load voltage supply, reactive power must be injected by DVR system. Practically, the capability of injection voltage by DVR system is 50 % of nominal voltage. It is sufficient for mitigation voltage sag because from statistic show that many voltage sag cases in power system involving less than 0.5 p.u. voltage drop [2].

3. ATP-EMTP for modeling in power system

EMTP is a abbreviation for Electromagnetic Transients Program. Licensing to use ATP (Alternative Transients Program) is free of all charge for all who have not engaged in EMTP commerce, so it's ideal for education purposes. ATP is a universal program for digital simulation of transient phenomena of electromagnetic as well as electromechanical nature. With this digital program, complex networks and control systems of arbitrary structure can be simulated. ATP has extensive modeling capabilities and additional important features besides the computation of transients.

Typical EMTP studies are: lightning and switching transients analysis, statistical and systematic overvoltage analysis, machine modeling, motor startup, shaft torsional oscillations, ferroresonance, power electronic applications, FACTS devices: STATCOM, SVC, UPFC, TCSC modeling, harmonic analysis, etc [3].

3.1. ATPDraw

ATPDraw is a graphical preprocessor to the ATP-EMTP on the MS Windows platform. The ATPDraw is written in Borland Delphi. In the program the user can build up an electric circuit, using the mouse, by selecting predefined components from an extensive palette. Based on the graphical drawing of the circuit, ATPDraw generates the ATP file in the appropriate format. All kinds of standard circuit editing facilities (copy/paste, grouping, rotate, export/import) are supported. Circuit node naming is administrated by ATPDraw [3].

4. Simulation of voltage sags by using ATPDraw

In this part I pesent my first model in ATPDraw (Fig. 3). We can see there one sector of Slovak power network. As power source the generator in nuclear power station in Jaslovské Bohunice is modeled (1). There is a load, represented with a big Slovak company, Duslo Šaľa, a.s (2). When the load is connected (at the time 0,1 second), we can see a voltage sag on the consumer side, (Fig.4, part a)). The customer side is represented by load in Križovany (3). The circuit-breaker is switched off at time 0,3 second. After this time voltage is again in nominal value. There is yet one more part of this simulation model. It's a DVR device (4), which is connected in series with line wire.

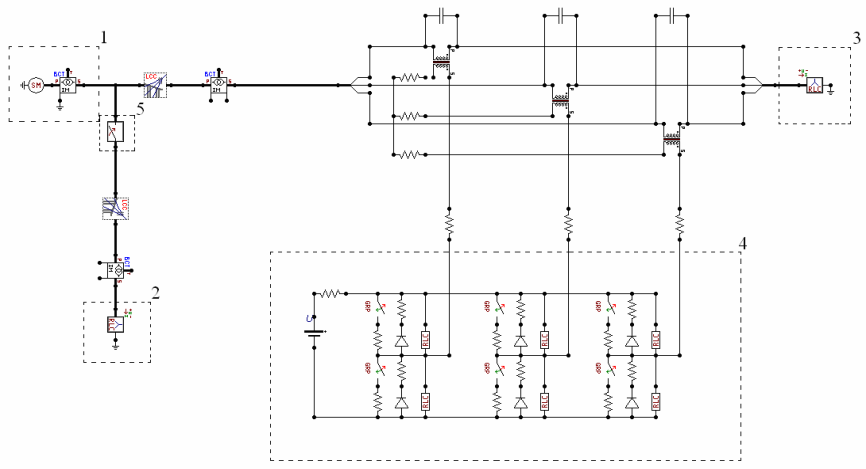

Fig. 3. The model of electricity supply system with DVR device

This device is out of service in this time, because the elements of power electronics are without control, without control signal on their input. This is object of my next work. I have to design the control algorithm of DVR device, which will be compensating the voltage sag from Fig.4, part a). Fig. 4 presents waveforms from specific part of the model. On the picture b) we can see a waveform of current on the customer side (on the load in Križovany). On the picture c) is displayed a voltage curve on the generator in Jaslovské Bohunice and on the picture d) we can see a current through a circuit breaker (5).

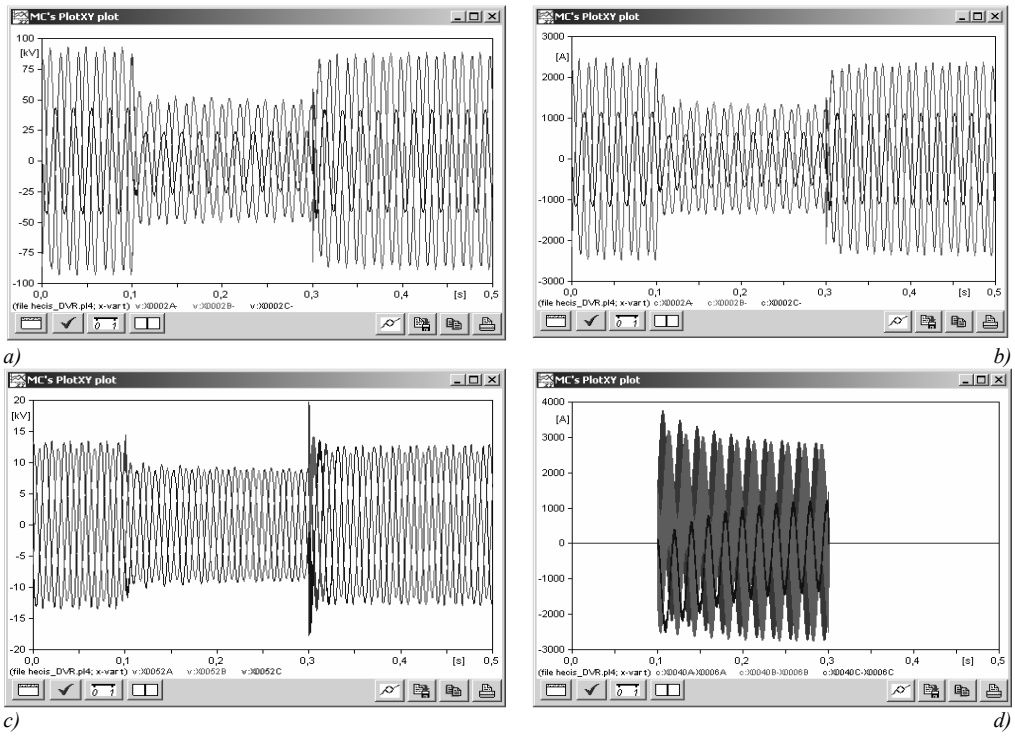

Fig. 4. Shape of the voltage curve during voltage sag

5. Conclusion

This paper described voltage sags and interruptions problem. It's a particularly topical problem, because the impact of these disturbances on sensitive equipment is severe. DVR is a series compensator which is able to protect a sensitive load from these disturbances and it is presented in this paper. The voltage sag is simulated in program ATPDraw and the results of this simulation are presented in this paper. In my next work I want to compensate this voltage sag with DVR device.

References

[1] PLATTS, research&consulting, *Voltage sags,* 2004, http://www.we-energies.com/powerquality/voltagesags.pdf.

[2] WAHAB, S.W., YUSOF, A. M., *Voltage Sag and Mitigation Using DVR System*, ELEKTRIKA, 8(2), 2006.

[3] http://emtp.org/

Transcom 2009, 22-24 June 2009
University of Žilina, Žilina, Slovak Republic

Overview of Voice Recognition Tools Based on HMM

[*]Ján Krajčovič
[*]University of Žilina, Faculty of Electrical Engineering,
Department of Control and Information Systems,
Univerzitná 2, 01026 Žilina, Slovakia, Janko.Krajcovic@gmail.com

Abstract. In this paper I will make a research of available tools dedicated to speech recognition based on Hidden Markov Models. Some of these tools were tested and their evaluation is introduced in the conclusion. A part of this paper is a table showing attributes of mentioned tools as well as their basic features as are types of parameterization, training types, licensing and so one.

Keywords: Hidden Markov Models, Hidden Markov Toolkit, Speech Recognition.

1. Introduction

Currently, Hidden Markov Models (HMM) with their attributes belong to the most used speech recognition technique. Following chapters bring a basic overview of tools based on Hidden Markov Models with their descriptions and basic features.

1.1. Hidden Markov Toolkit

HTK (Hidden Markov Toolkit) is a system which is well known in laboratories over the world. It is a set of tools dedicated to manipulation with Hidden Markov Models for purposes of speech recognition. Moreover, with small changes the toolkit is also applicable in other areas as are voice synthesis, recognition of DNA (Deoxyribonucleic Acid) sequences and so one. The HTK itself consists of libraries written in C programming language and is available like an open source ready to be modified and improved. HTK directly supports discrete, continues and semi continues HMM. The usage of HTK is very wide but mainly focused on speech recognition therefore HTK offers tools for voice recording, parameterization, initialization of HMM, recognition itself and in addition module for results interpretation [1].

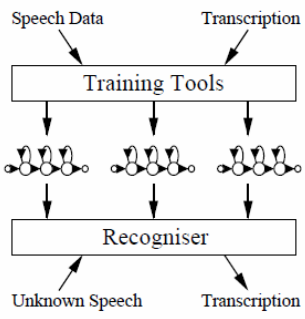

Fig. 1 Basic concept of HTK

1.2. An Application Toolkit for HTK

ATK (An Application Toolkit for HTK) is API (Application Programming Interface) for HTK. The ATK itself consists of a set of classes programmed in C++ which are an interface to HTK libraries. This improvement enables to use a HTK recognizer in an arbitrary application because it is easy to integrate this bug free speech recognizer [2].

Furthermore, ATK supports also speech synthesis in English by embedding the CMU (Carnegie Mellon Statistical Language Modeling) module. By using of all its available options it is pretty easy to build up a spoken dialog system. The fig. 2 shows a basic recognition system created of ATK components. The essential ATK components are:

- Dictionary – is a set of words which will be used in the process of speech recognition.
- Grammar – defines allowed word orders.
- HMM set – contains models of each word used in the dictionary.

Set of HMM model as well as grammar and dictionary can be either stored in external files or modified on the fly of the application.

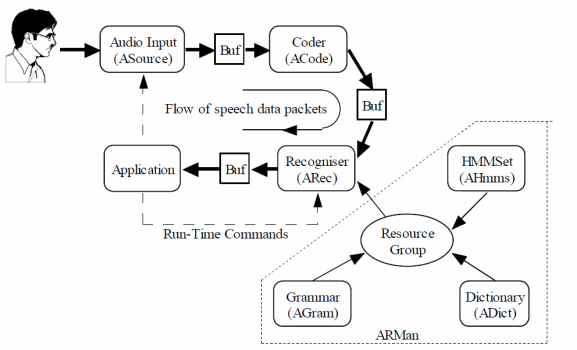

Fig. 2 Basic recognition system

For more complex solutions ATK comes with the AIO [Asynchronous Input/Output Control Component] component dedicated to controlling of fully spoken speech interfaces. Example of such a system is shown on fig. 3.

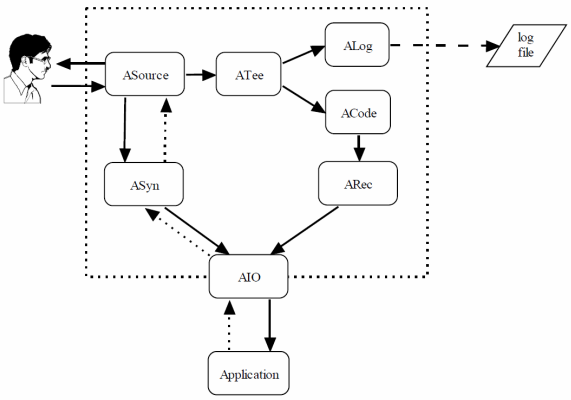

Fig. 3 More complex speech recognizer with AIO block

The AIO block takes care of all internal communication and also coordinates activities between speech recognizer and voice synthesizer. In order to issue a prompt AIO sends a message into voice synthesizer and at the same moment activates the speech recognizer which will be awaiting a speech to be recognized. By this manner we can build up a complex system which will put questions to an user and changes them according to recognized answers. This communication is constrained by defined dictionary and grammar.

1.3. SPHINX

The system SPHINX has been developed at Pittsburg University [3], [4] and was intended for speech recognition by using huge dictionaries. The heart of SPHINX is based on discrete hidden Markov models and parameters derived from LPC coefficients. For purposes of reduction of the coarctic effect SPHINX uses models at the level of words and general trifon model. The first version of SPHINX had compared recognized speech with stored samples of speech. Later, the system had been based on phonetic rules and DTW (Dynamic Time Wraping) [4] algorithm. The latest approach in development has had inclination to statistic models based on HMM. Because SPHINX works with huge dictionaries offers also a possibility to be phoneme oriented. Used phoneme model has seven states and is suitable for modeling of longer and long words. The same model was also used by IBM in their recognizers.

Innovations in modeling and redesigning of algorithms brought a version of recognizer which was user independent and was able to recognize a speech with high accuracy [3]. The process of training is performed in two iterations of forward – backward algorithm. In addition, in the first iteration the model of phoneme is reestimated by using of training data. In the second iteration, these models are used for generating of trifons. Nowadays, SPHINX is available in four major versions which differ in accuracy of speech recognition, usage, size of the dictionary and so one.

1.4. Edinburg Speech Tools

EST (Edinburg Speech Tools) is available in the form of libraries written in C++ and support reading, recording and parameterization of signals in different formats which are among each other convertable.

EST works almost with all operation systems and moreover is freeware and enables his unlimited distribution. Regarding of the signal processing EST can offer options like windowing, linear prediction, LPC, DFT, filter bank, Fourier analysis, detection of frequencies and creating of spectrogram.

Regarding of the grammar in EST supports different types of grammars e.g. stochastic context free grammar.

In the area of linguistic it is possible to use a system for saving and processing of linguistic units as well as tool for automatic creating of trees, deciding of regress trees CART.

2. Comparison table

This chapter contains a table which shows main features of exanimate tools which should be concerned in the phase of designing of a speech recognizer.

Table 1 Overview of HMM tools

System	*Licensing*	*Developed by*	*Model type*	*Parametrization*	*Training*
HTK - ATK	Freeware	Cambridge University UK	Words, phonemes, trifons	MFCC, LPC, LPC Cepstra, MelSpectrum	Flat start, Bootstrap
SPHINX	Freeware	Carnegie Mellon University USA	Phonemes, trifons	LPC	Bootstrap
EST	Freeware	Edinburgh University UK	Words, phonemes	F-bank, LPC, MelSpec	Flat start

3. Conclusion

At the present days hidden Markov models are very popular technology in the filed of the speech recognition hence we can come across plenty of available tools based on this technology. In this paper I did a basic overview of the most popular tools manipulating with HMM.

With each decision to build up a speech recognition system we should take into consideration factors like type of models (words, phonemes,..), parameterization type, licensing, possibility of real-time speech recognition, possibility to make own modifications and apply new ideas or algorithms and so one.

According to my trials and experiences, HTK offers the best environment for speech recognition from tools exanimate in this paper.

Advantage of HTK toolkit is that is available like freeware in form of C source codes and offers wide range of tools usable in the whole speech recognition process. Whether it is a tool for creation of dictionary, tools for creating and testing grammar definitions or tools making the speech recognition itself with possibility to compare and evaluate results for instance in format of confusion matrix.

Generally, HTK together with its extension ATK is regarded by experts as system which achieves excellent accuracy in speech recognition and is frequently the subject of issued papers, discussions and newly proposed methods of speech processing.

References

[1] S. Young, G. Everman, M. Gales, T. Hain: The HTK book, Cambridge University Engineering department, 2001 - 2006

[2] S. Young: ATK, Cambridge University Engineering department, 2007

[3] K.Lee, K. Hon: An overview of the SPHINX speech recognition system, IEEE Transactions on Acoustics, Speech and Signal Processing, ASSP-38(1), 35-44, 1990

[4] X. Huang, F. Alleva: The SPHINX-II speech recognition system: an overview, Computer Speech and Language, 7(2), 137-148, 1992

Transcom 2009, 22-24 June 2009
University of Žilina, Žilina, Slovak Republic

Parameterization and its Influence on Speech Recognition

[*]Ján Krajčovič, [*]Martin Hrnčár
[*]University of Žilina, Faculty of Electrical Engineering, Department of Control and Information Systems, Univerzitná 2, 01026 Žilina, Slovakia
Janko.Krajcovic@gmail.com, hrncar@fel.uniza.sk

Abstract. This paper deals with the MFCC parameterization and its modifications in the process of speech recognition. For the purposes of this paper, several attempts in order to prove an influence of the parameterization type on the correctness of speech recognition have been done. The influence was measured on recognizer based on HTK libraries. In the conclusion of this paper we compare chosen parameterizations regarding the correctness of the recognition and training time.

Keywords: Parameterization, HTK, MFCC, speech recognition.

1. Introduction

The choice of parameterization is very important because it can significantly influence the reliability, the stability and mainly the accuracy of a speech recognizer.

In order to suppress redundancy of voice signals and proceed with smaller volume of data was created parameterization. The main purpose is to extract only the most important features of the signal which can sufficiently describes original signal but with less dataflow.

HTK (Hidden Markov Model Toolkit) supports several kinds of parameterizations but the most frequently used is MFCC (Mel Frequency Cepstral Coefficients) parameterization with its variations.

For instance, to twelve MFCC coefficients is possible to add zero cepstral coefficient (extension _0), coefficient of total energy in the frame (extension _E), delta cepstral coefficient (extension _D) and acceleration coefficient (extension _A). This process is displayed in the Fig. 1 which also illustrates signal processing through MFCC with energy and difference coefficient.

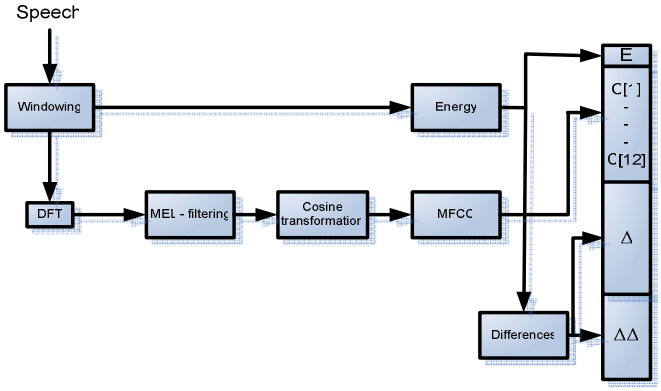

Fig. 1 Signal processing with MFCC

2. Mel Frequency Cepstral Coefficients

MFCC is regarded as the most frequently used type of parameterization in the process of speech recognition. MFCC is based on nonlinear scale of filter banks on which are applied rules of signal processing. Calculation of MFCC coefficients is performed by cosine transformation DCT (Discrete Cosine Transform) which has also DC component available as parameter C_0.

This transformation evaluates the shape of spectrum by using its frequency or sequential attributes. That is very important regarding of noise resistance. Individual coefficients among each other are little linear depend what is significant feature for speech recognition by using of HMM (Hidden Markov Model) [1][1].

Calculation of MFCC coefficients is done by using following formula:

$$C_k = \sum_{j=1}^{N} m_j \cos\left(k\left(j - \frac{1}{2} \right) \frac{\pi}{N} \right), \tag{2.1}$$

where m_j is logarithm from the filter banks, for $k = 0, 1,..$up to number of MFCC coefficients (usually 10 up to 15), N is number of filter banks (usually 20 up to 25) [4].

2.1. Energy measurement

In order to extend MFCC coefficients or MEL filter bank was established energy measurement [4]. The energy is calculated as logarithm of signal energy, which for speech is calculated from samples F_{SN}.

$$E = \log \sum_{n=1}^{N} S_N^2 \ . \tag{2.2}$$

2.2. Delta and acceleration coefficients

In the process of speech recognition is important to take into consideration also dynamic parameters of the speech [3], [4]. Therefore, it is suitable MFCC method, which does not consider dynamic information because works on small speech segments, extends with information about the environment. It can be achieved by introducing of delta and acceleration coefficients. In order to calculate a delta coefficient we can use following formula:

$$\Delta c(n) = m \sum_{k=-L}^{L} k.c(n+k), \tag{2.3}$$

where m is normalization constant and L is number of items of the feature vector. Acceleration coefficient, which is calculated as difference of delta coefficients are determined by following formula:

$$a(n) = \Delta\Delta c(n) = m \sum_{k=-L}^{L} k.c(n+k). \tag{2.4}$$

3. Experiment

For purposes of this experiment we have created the HTK speech recognizer with three hundred words in the testing database. In order to simulate an influence of parameterization type we had to consider different parameterization types in configuration files as well as the length of feature vectors, see table 1. As default MFCC parameterization was used unlike zero coefficient (DC component), dynamic coefficient and normalization of the MFCC which were used in six combinations according to the table 1.

Table 1 Used parameterization types

Type of MFCC parameterization	***Length of the feature vector***	***Description of used MFCC coefficients***
MFCC_0_Z	13	Normalized MFCC coefficients with zero coefficient
MFCC_0_D_Z	26	Normalized MFCC coefficients with zero and delta coefficient
MFCC_D_A	36	MFCC coefficients with delta and acceleration coefficients
MFCC_D_A_Z	36	Normalized MFCC coefficients with delta and acceleration coefficients
MFCC_0_D_A	39	MFCC coefficients with delta, zero and acceleration coefficients
MFCC_0_D_A_Z	39	Normalized MFCC coefficients with delta, zero and acceleration coefficients

In order to determinate correctness of the speech recognition we used HTK tool called HResults [1]. Also the log file of the recognizer was extended by the timestamps which were used in the final experiment, comparison of time costs. Results of the experiment are shown in figure 2.

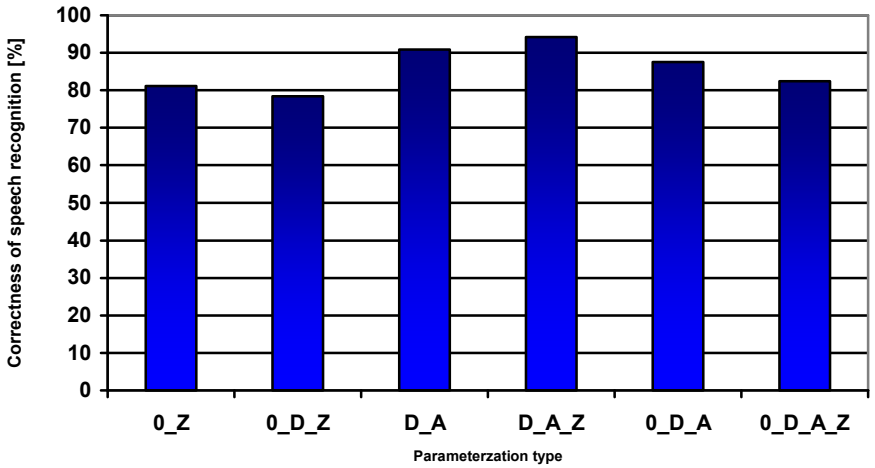

Fig. 2 Correctness of the speech recognition

The process of training itself is very time demanding process and requires a lot of resources. From the figure 3 is visible that the chosen parameterization type has a significant influence on the spent time and varies with chosen extensions of MFCC.

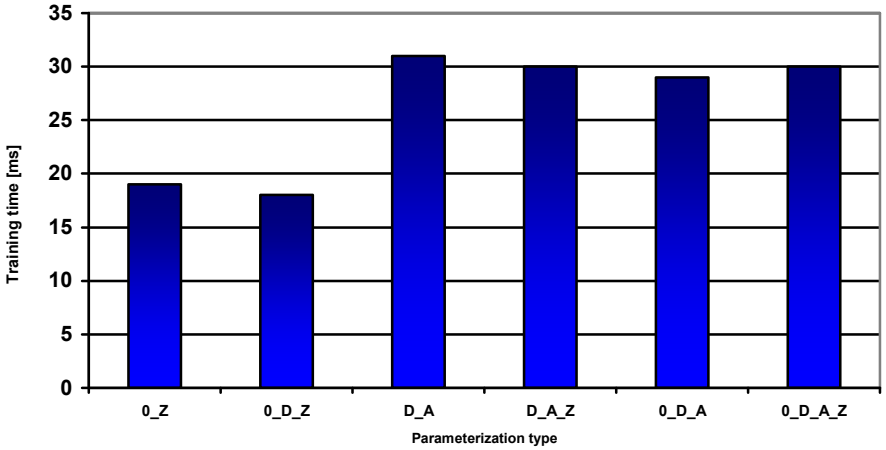

Fig. 3 Time spent in the process of training

4. Conclusion

The purpose of this paper was to compare the correctness of speech recognition regarding the used parameterization. Speech recognizer built in HTK was used as the testing environment as well as measuring tool.

On the basis of performed experiments we can come to the conclusion that the best type of the parameterization is the usage of normalized MFCC coefficients with delta and acceleration coefficients. Further, we can say that the omission of acceleration coefficient (extension _A) led to about 13% decrease of the correctness. On the other hand, this omission led to the 40% time saving, in comparison to the parameterization using acceleration coefficients.

It is suitable to use normalized MFCC coefficients (extension _Z) as they do not cause additional time consuming and, on the other hand, they contribute to the accuracy of the recognition.

If we need to build up a HMM recognizer with limited computing resources the best option seems to be the usage of MFCC parameterization together with zero coefficient carrying energy information.

References

[1] Young, S., Everman, G., Gales, M., Hain, T.: *The HTK book*, Cambridge University Engineering department, 2001 - 2006

[2] Zelenak, M.: *Rozpoznávanie reči pomocou HMM*, Bakalárska práca, FEI Bratislava, 2006

[3] Uhlíř, J., Sovka, P.: *Číslicové spracování signálú*, CVUT Praha, 2002, ISBN 80-01-02613-2

[4] Kotuliaková, J., Rozinaj, G.: *Číslicové spracovanie signálov 1*, FABER Bratislava, 1996, ISBN 80-967503-1

Transcom 2009, 22-24 June 2009
University of Žilina, Žilina, Slovak Republic

Train Performance Simulation

[*]Karel Kubátka
[*]University of Žilina, Faculty of Electrical Engineering, Department of Power Electrical Systems (DPES), Univerzitna 1, 01026 Žilina, Slovakia, karel.kubatka@kves.uniza.sk

Abstract. This paper gives a short introduction to a train performance simulation with supply energy consumption optimizing. The first part describes the mathematic model of a train dynamics. The second part introduces the MKSV simulation software. Third part of this paper describes the future improvements of simulation models, which will enable more exact power consumption calculations.

Keywords: Train ride simulation, track resistance, tachogram, chronogram, power consumption.

1. Train dynamic model

We understand under the term "train performance simulation" an algorithm, which computes speed or time diagrams by solving a system of differential equations. Results of the simulation are usually speed or time vs. distance graphs. The simulation is based on physical laws describing the movement of the train.

The advantage of the computer simulation is a relatively high accuracy of calculation and the short calculating time, therefore it is not necessary to make long and expensive test runs. Results are available as numeric data and as graphs.

1.1. Tracks resistance

Resistive forces applied during train ride can be separated into:

- Vehicle resistance
  - Rolling resistance F_0 (specific rolling resistance p_0)
  - Inertial mass resistance F_a (specific p_a)
  - Break resistance F_b (specific break resistance p_b)
- Track resistance
  - Slope resistance F_s (specific slope resistance p_s)
  - Curvature resistance F_r (specific curvature resistance p_r)
  - Tunnel resistance F_{tu} (specific tunnel resistance p_{tu})

All three components of the track resistance are usually given by the specific track resistance as a function of distance. On the other hand, regard to low values of specific additional resistance from the route curvature p_r, we can ignore this parameter.

1.2. Rolling resistance

Rolling resistance consists of friction, bearing and aerodynamics resistances component. For every vehicle the specific rolling resistance is intended by measurement and can be expressed by Davis type formula [4]:

$$p_0 = \frac{F_0}{G} = \frac{A}{G} + \frac{B}{G} \cdot V + \frac{C}{G} \cdot V^2 = a + b \cdot V + c \cdot V^2 \, [N/kN; km/h]. \qquad (1)$$

1.3. Train motion equation

For the train performance calculation, the locomotive traction characteristics as well as rolling and track resistances have to be known. Applied traction effort F_t of the train set will be used to generate the inertial mass resistance (acceleration effort) F_a for the train set and to overcome the operation resistance (F_{0V}, F_s). When breaking, traction effort is set to zero and breaking effort F_b is applied:

$$F_t = F_a + F_{0L} + F_{0V} + F_s + F_b [N;N,N,N,N,N]. \tag{2}$$

And:

$$F_a = F_t - F_{0L} - F_{0V} - F_s - F_b [N;N,N,N,N,N]. \tag{3}$$

The inertial mass resistance and its specific value can be expressed as:

$$F_a = m \cdot \xi \cdot a \Rightarrow p_a = \frac{m \cdot \xi \cdot a}{G} \Rightarrow p_a = 102 \cdot \xi \cdot a \, [N/kN;1,m/s^2] \tag{4}$$

Finally, the train movement equation to be computed is given by:

$$\frac{dV}{dt} = \frac{1}{28{,}32 \cdot \xi \cdot (G_L + G_V)} \cdot (F_t - G_L \cdot p_{oL} - G_V \cdot p_{oV} - (G_L + G_V) \cdot p_s - F_b) \tag{5}$$

G – Weight (kN),
ξ – Rotational inertia coefficient (-).

1.4. Calculation of the energy consumption time behavior

Power drain time behavior is a numeric integral of electric input of the locomotive.

$$W_{celk} = \sum_{n+1}^{n} W_i + W_p + W_0 [kWh] \tag{6}$$

W_i – power drain in a time interval
W_p– power drain for auxiliaries
W_0– power drain for electric heating

Calculation of power drain for auxiliary drives is difficult to establish, because the electric input of auxiliary drives depends on service regulation. We simplify the auxiliary power consumption using specific power drain constant:

$$W_p = \kappa \cdot W_i \tag{7}$$

κ - specific power drain for auxiliary drives (0,02 DC track – 0,03 AC track)

Power drain for electric heating includes heating, air-conditioning, or power supplying of cars.

$$W_0 = k_{kW} \cdot G_V \cdot \varphi \cdot t_0 \tag{8}$$

φ – specific power drain for power supply (0,1 ÷ 0,75)
G_D – pressure vehicles

Actual energy consumption calculation used in simulation:

$$W_{celk} = \sum_{i=1}^{n} \frac{1}{3{,}6} \cdot F_{ti} \cdot V_i \cdot \frac{1}{\eta_L} \cdot \Delta t_i + W_p + W_0 [kWh; kN, km/h, kWh, kWh] \qquad (9)$$

Specific energy consumption measured on pantograph:

$$w = \frac{W_{celk}}{M \cdot L} [Wh/tkm] \qquad (10)$$

2. Train performance simulator MKSV

This simulation program was built in C# programming language (Microsoft Visual Studio 2008) because of following advantages:

- User friendly graphic interface
- Multi-platform programming
- High level coding
- Free download for non-commercial use.

You can see the program's main window in Fig. 1.

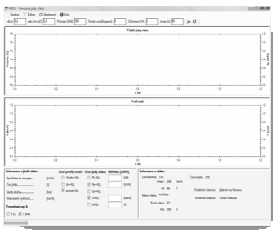

Fig. 1. MKSV main panel 1

2.1. Program structure

Simulation output graphs with following input parameters are shown on Fig. 2 and 3:

- Locomotive 151 ČD – max. speed 160 km/h, max. power 4 MW,
- Load – train EC, weight 350 t
- Track – max. speed 100km/h, length of track 36 km

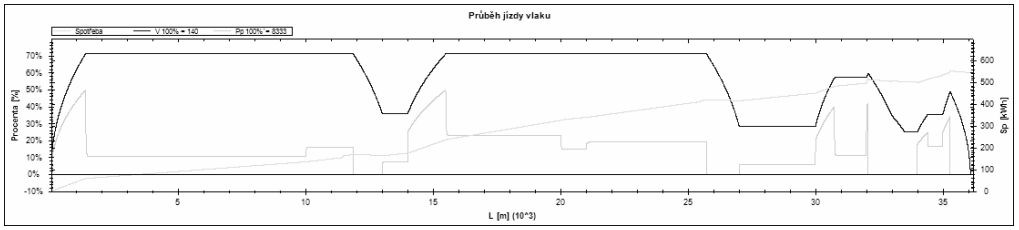

Fig. 2. Graph of train ride – $S_p = f(L)$, $V = f(L)$, $P_p = f(L)$

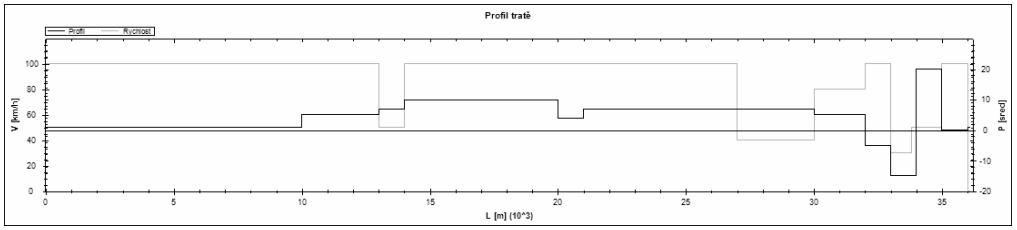

Fig. 3. Graph of track profile – $p_s = f(L)$, $V_{trat} = f(L)$

Input parameters:

1. Weight of locomotive
2. Rotating mass coefficient
3. Rolling resistance constants
4. Num. of traction motors
5. Line voltage
6. Rated current
7. Maximum vehicle speed
8. Brake deceleration

Output parameters – graphs:

1. $F_t = f(L)$
2. $F_t = f(t)$
3. $P_p = f(L)$
4. $S_p = f(L)$
5. $V = f(L)$
6. $V = f(t)$
7. $t = f(L)$
8. $I_m = f(L)$
9. $p_s = f(L)$
10. $V_{trat}=f(L)$

3. Optimization of simulation

This program is not intended only for train performance simulation, but also for power drain optimizing. Now, the program simulates the train as one mass point (Fig. 4a)). For simulation with optimized power drain, we must consider the train as set of mass points (Fig. 4 b, c)). Every car of the train will be simulated separately, having own parameters as weight, length and rolling resistance. The resistive effort F_{0Vi} of each car will be calculated. Resulting train force F_{0V} will be calculated as sum of partial vehicle forces (10).

$$F_{0V} = \sum_{0}^{i} F_{0Vi} \qquad (11)$$

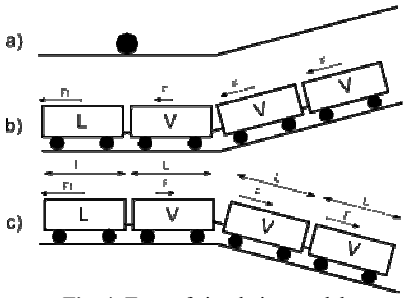

Fig. 4. Type of simulation model

4. Conclusion

Train performance simulation technique has been discussed considering only one mass point model. The simulation gives satisfactory results on speed and energy consumption performance. Application MKSV can be used to predictive computation on journey time or energy-based cost. This model will be improved with multi point simulation model with energy optimization of the service.

References

[1] Drábek, J. *Dynamika a energetika elektrické trakce*. Bratislava: ALFA, 1987.

[2] Jansa, F. *Dynamika a energetika elektrické trakce*, Praha: NADAS, 1980.

[3] Kubátka, K. *Simulace jízdy vlaku*, Žilina: Diplomová práce, 2008

[4] Bih-Yuan Ku, Jang, J.S.R., Shang-Lin Ho, *A modulized train performance simulator for rapid transit DC analysis*, Proceedings of the 2000 ASME/IEEE Joint Railroad Conference, 2000, ISBN: 0-7803-6328-0

Transcom 2009, 22-24 June 2009
University of Žilina, Žilina, Slovak Republic

Induction Motor Drive Fed by Matrix Converter with Takahashi Direct Torque Control

*Dragan Kuzmanović, *Jiří Lettl
*Czech Technical University in Prague, Faculty of Electrical Engineering,
Department of Electric Drives and Traction,
Technická 2, 166 27 Prague 6, Czech Republic, lettl@fel.cvut.cz

Abstract. Matrix converter belongs to the group of direct AC-AC converters, i.e. converters that transform energy from one AC power system into another one without an intermediate DC link with an energy storage. The absence of the DC link makes the control of the converter much more complex comparing to indirect converters. Instead of constant DC link voltage the matrix converter generates output voltages by combining three input phase voltages that are not of constant values. Direct Torque Control (DTC) is a modern control technology which uses a simple control algorithm. It directly controls motor torque and flux values without using a modulator and without the need for generating precise output voltage vectors like in the case of Field Oriented Control. That makes it a good candidate for use in drives fed by the matrix converter.

Keywords: Matrix Converter, Takahashi Direct Torque Control.

1. Introduction

The concept of the matrix converter lies in direct switching of the input phases to the output phases. That is achieved by using a 3x3 matrix of bidirectional switches (Fig. 1a). Bidirectional switches enable energy flow in both directions. Anti parallel diodes increase the reverse blocking capability of the switches.

There are two main tasks that the matrix converter performs in normal operation:

- generating the required output voltages by combining the input phase voltages,
- directing the converter output phase currents into the input phases in such a way to provide the sinusoidal input current with a required power factor (usually 1).

Since it is easier to analyze these tasks separately the matrix converter is often observed as a combination of a virtual current source rectifier and a virtual voltage source inverter connected by a virtual DC link (Fig 1b). Every switching combination of the virtual rectifier / virtual inverter configuration has a corresponding switching combination of the real matrix converter.

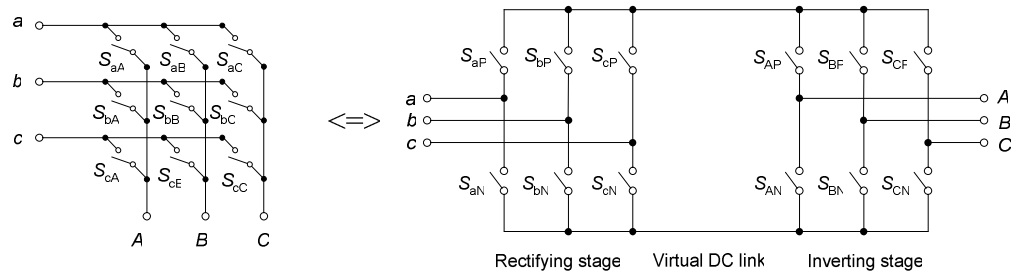

Fig. 1. Matrix converter (a) and indirect representation of the matrix converter (b).

Owing to the "independent" operation of the virtual rectifier and the virtual inverter stages, Indirect Space Vector Modulation can be applied to the matrix converter. This modulation method enables generation of desired voltage vectors at the output and at the same time generation of the input current vector which rotates at the same speed like the converter input voltage vector and with the constant angle displacement towards it. The generation of these vectors is illustrated in Fig. 2.

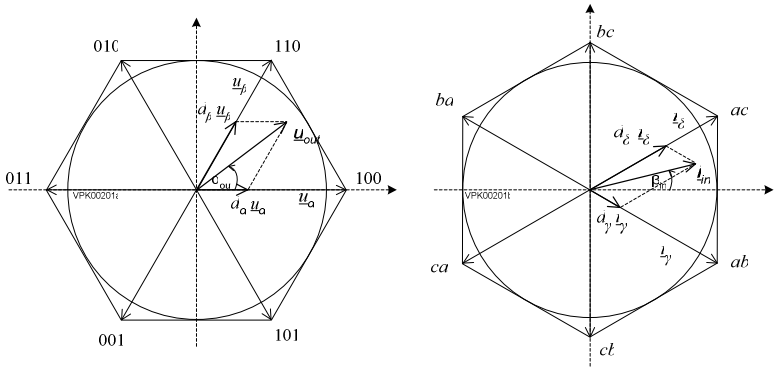

Fig. 2. Inverter stage SVM (a) and rectifier stage SVM (b).

2. Takahashi Direct Torque Control

A principle of DTC is very simple. The estimated torque and flux values are constantly compared to their set points and if they are out of the tolerance bands (Fig. 3a) an adequate switching combination is applied at the converter output which will drive the torque and flux to their set values. There are several types of the DTC: Depenbrock DTC, Takahashi DTC, DTC Using the Space Vector Modulation, DTC Using the Discrete Space Vector Modulation, Neuro-Fuzzy DTC, etc.

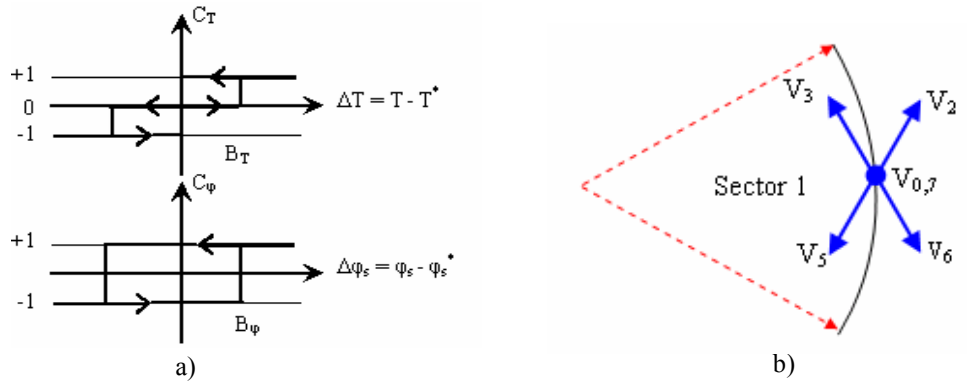

Fig. 3. Torque and Flux hysteresis (a) and voltage vectors used in the first sector (b).

Takahashi DTC operates on a six sectors flux vector circle. In each sector four active and one zero vectors are employed in order to keep the torque and flux values within their limits (Tab. 1). For example in the first sector (Fig. 3b) vector V_2 will increase torque and flux, V_3 will increase torque but decrease flux, V_5 will decrease torque and flux, and V_6 will decrease torque and increase flux. By applying a zero vector, flux will remain constant ant torque will slowly decrease.

Sector		1	2	3	4	5	6
$C_o = -1$	$C_T = -1$	V_2	V_3	V_4	V_5	V_6	V_1
	$C_T = 0$	V_7	V_0	V_7	V_0	V_7	V_0
	$C_T = +1$	V_6	V_1	V_2	V_3	V_4	V_5
$C_o = +1$	$C_T = -1$	V_3	V_4	V_5	V_6	V_1	V_2
	$C_T = 0$	V_0	V_7	V_0	V_7	V_0	V_7
	$C_T = +1$	V_5	V_6	V_1	V_2	V_3	V_4

Tab. 1. Voltage vectors lookup table.

Flux vector is determined from the stator voltage using the following equation (voltage drop across the stator resistance is neglected):

$$. \overline{V}_S \approx \frac{d\overline{\psi}_S}{dt} \Rightarrow \Delta\overline{\Psi} = \overline{V}_S \cdot \Delta t \tag{1}$$

3. Model in MatLab

As the first step in the realization of the Takahashi DTC on an AM drive fed by the matrix converter, a model in MatLab Simulink was designed (Fig. 4).

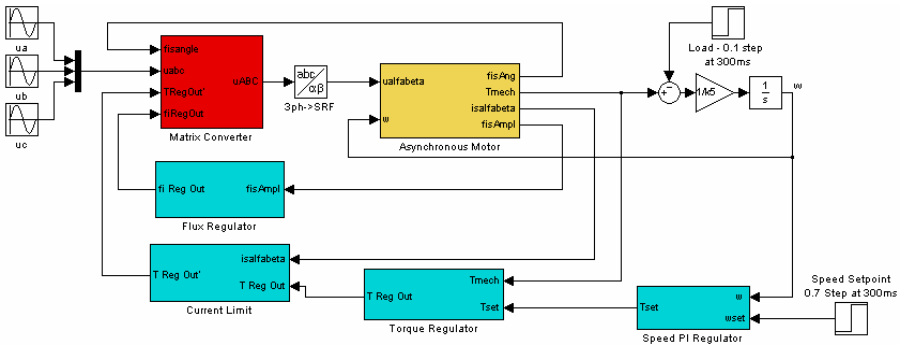

Fig. 4. Simulink model.

In the simulation 0.7 ω_n speed set point and 0.1 T_n load are applied to the system. The torque set value is limited to T_n and the torque tolerance band is ±0.1 T_n. The selected switching frequency is 20 kHz. Simulation results for the torque are presented in Fig 5. Red lines are set and blue actual values. It can be seen that the torque is successfully kept within the tolerance band.

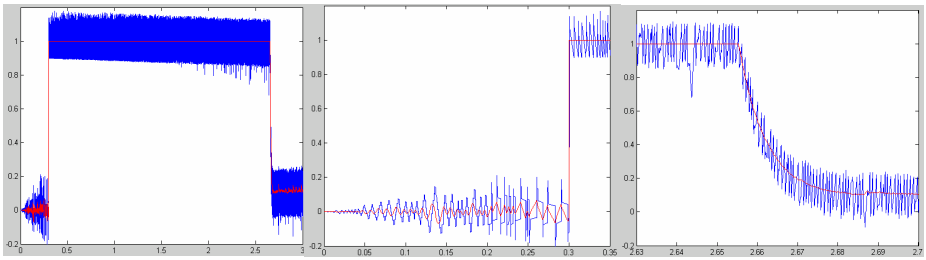

a) b) c)

Fig. 5. Simulation results: a) motor torque, b) enlarged detail (T_{set} changed from 0 to T_n), c) enlarged detail (T_{set} gradually changed from T_n to 0).

4. Practical Results

Finally, Takahashi DTC was applied to a real system consisting of a matrix converter (Fig. 6) supplying a 4 poles 6 kW induction machine with 22 Nm rated torque.

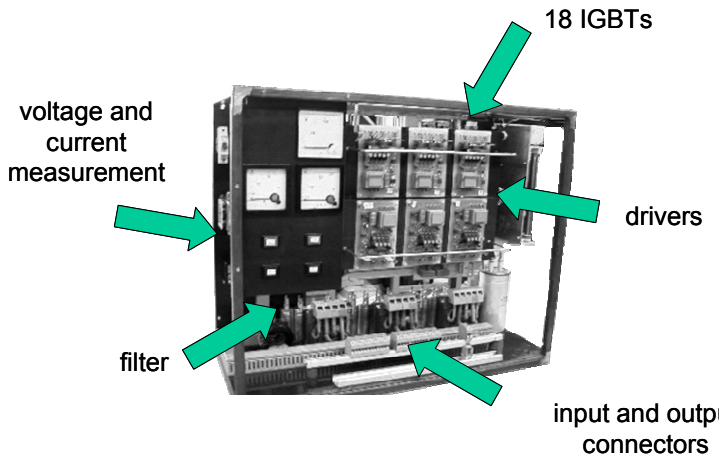

Fig. 6. Matrix converter used in the experiment.

The applied switching frequency was 6.67 kHz and torque tolerance was set to ±2 Nm. Some experimental results are shown in Fig. 7.

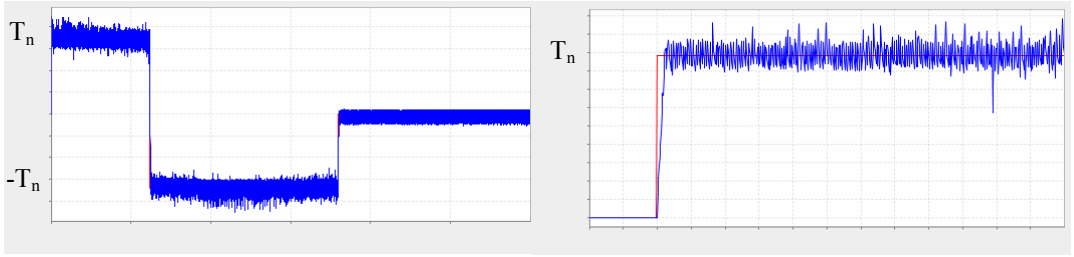

Fig. 7. Experiment results: a) motor torque, b) enlarged detail (T_{set} changed from 0 to T_n).

5. Conclusion

Experiment and simulation results presented in this paper prove that Takahashi DTC can be successfully applied to the induction machine drive fed by the matrix converter. The torque control achieved with matrix converter using this type of DTC is comparable to classical indirect AC/AC converters.

References

[1] KUZMANOVIC, D. *Model of matrix converter-fed asynchronous motor drive controlled by Takahashi direct torque control and matrix converter switching losses analysis,* Technical Study, ČVUT, Prague, 2007.

[2] BOLL, J., FUCH, F. W. *Direct control methods for matrix converter and induction machine,* Proceedings of the IEEE International Symposium on Industrial Electronics, ISIE, vol. 2, pp. 781-787, 2005.

[3] TAKAHASHI, I., NOGUCHI, T. *A new quick-response and high-efficiency control strategy of an induction motor,* IEEE Transaction on Industry Applications, vol. IA-22, no.5, pp. 1820-1827, 1986.

[4] LETTL, J., FLÍGL, S. *PWM strategy applied to realized matrix converter system,* Progress In Electromagnetics Research Symposium PIERS 2007 Proceedings, pp. 98-101, Prague, 2007.

Transcom 2009, 22-24 June 2009
University of Žilina, Žilina, Slovak Republic

Cosimulation of Two-Step Commutation Method of the Matrix Converter in Simulink/Modelsim

*Libor Linhart, *Jiří Lettl, *Miroslav Bednář, *Jan Bauer
*Czech Technical University in Prague, Faculty of Electrical Engineering,
Department of Electric Drives and Traction,
Technická 2, 166 27 Prague 6, Czech Republic, lettl@fel.cvut.cz

Abstract. This paper describes basic knowledge about two – step commutation method that was realized in our department. This commutation strategy was realized in VHDL for FPGA and was simulated in Simulink. But it was necessary to link Simulink with Modelsim that can simulate VHDL code. So these two sophisticated programs had to cosimulate. By virtue of this cosimulation can be uncovered, that theoretic calculations did not reflect some limitations of this two - step algorithm.

Keywords: Matrix Converter, Two – Step Commutation, .VHDL, Modelsim, Simulink

1. Introduction

In general, matrix converter is device, which allows connecting any of n input phases with any of m output phases. Therefore matrix converter consists of $m \times n$ bi – directional switches which are able to conduct currents and blocking voltage of both polarities depending on actual state of a modulation strategy. The bi – directional switch is realized in most cases by antiserial connected IGBT´s and each has antiparallel connected diode [4].

2. Modulation

Compact matrix converter, which is being developed on our department, uses indirect space vector modulation. The term “indirect” means that we can split matrix converter into virtual rectifier, inverter, and DC link. Thus the matrix converter can be controlled like an indirect frequency converter. Throw an efficient choice of switching pattern we can generate required curves on the output of the matrix converter. Modulator which realizes this switching sequence has to define the next switching state (switching combination of virtual rectifier and inverter) and the relative time of this state. But commutation strategy resolves the process of transition between two another states [2]. So it is possible to say that commutation strategy (or algorithm) is the functional part of modulator.

3. Two – step commutation method

Commutation process is conventionally switch – over of one output phase from one input phase to another one. Two – step method was realized to reduce commutation time and is established on idea that the maximum number of IGBT´s has to be switched on. Therefore some IGBT´s of unplugged input phases have to be switched on and they create a prearranged state for next commutation. This prearranged state must not cause an interphase short – circuit

and output current must not be interrupted. These are two important conditions for successful commutation.

The polarity of input phase – to – phase voltage is chosen as control variable for commutation. It means that the prearranged state is set based on polarity of phase – to – phase voltage between connected phase and other two phases. For example, if phase R was connected to output we would monitor polarity of voltage U_{RS} and U_{TR}.

If phase R is connected to output and the modulator will want to switch to phase S the following sequence of steps will be performed:

First step: All IGBT´s which are placed on the same side (load side or source side) like switched – on – IGBT on the phase S will be switched off. This IGBT on phase S will be let switched on.

Second step: Second IGBT of phase S will be switched on. The new prearranged state will be set. Now we have to realize that the new prearranged state will be set based on polarity of voltage of another phase than in previous case. Now polarity of voltages U_{ST} and U_{RS} is relevant.

Stand diagram of two – step commutation shows a graphical representation of entire algorithm and was introduced in [2]. There are four prearranged states for each input phase depending on voltage polarity and each of them has two possible states after commutation.

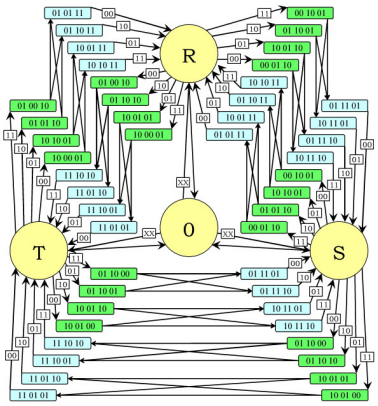

Fig. 1. Stand diagram of two-step commutation.

4. Practical realization

Control structure of compact matrix converter consists of FPGA and one – desk PC. Modulator with commutation blocks was implemented in FPGA and one – desk PC represents superior regulator preparing information about sectors of input current and output voltage. This information and relative time is sent to modulator in FPGA via PC 104 bus. On the basis of this inputs modulator finds the switching combinations and through the commutation blocks realizes it [1].

Whole commutation algorithm was developed in VHDL language for FPGA. Each output phase has one commutation block which realize connecting of input phase R, S or T. Input to commutation block is signal MTSR (modulation switching word) which acquaint with required connection. Output from commutation block is signal which is sent direct on IGBT drivers.

For simulation and debugging of two – step algorithm was created model of one output phase of matrix converter in MatLab – Simulink. It is also suitable for comparison with existing four – step algorithm. This model includes cosimulation block "Link for Modelsim" because MatLab can work with VHDL code only under participation with Modelsim from Mentor Graphics [3].

5. Simulation

In Fig. 2 you can see the model of one output phase of matrix converter. It includes 6 IGBT´s and 3 voltage sources that represent power parts of model. Control of IGBT´s is

realized throw the cosimulation block. Input signals to this block are *pol* (polarity of input phase-to-phase voltage), *mtsr* (modulation switching word – switching request which tells to commutation block which phase is required), and some additional signals like blocking of commutation, start delay for initializing, etc. These signals are transported to Modelsim with sampling period 21 ns. In Modelsim VHDL algorithm is running. Output signals from Modelsim are transported back to Simulink where we can display it or put it on IGBT´s. Therefore we have feedback to the "real" device and we can verify behaviour of whole circuitry. Some simulation result in Modelsim is shown in Fig. 3 and we can see, that we have there no information about magnitude of voltage and what currents flow throw IGBT´s. Only on basis of Fig. 4 (which represents the same situation in Simulink) we can analyse whole two – step algorithm.

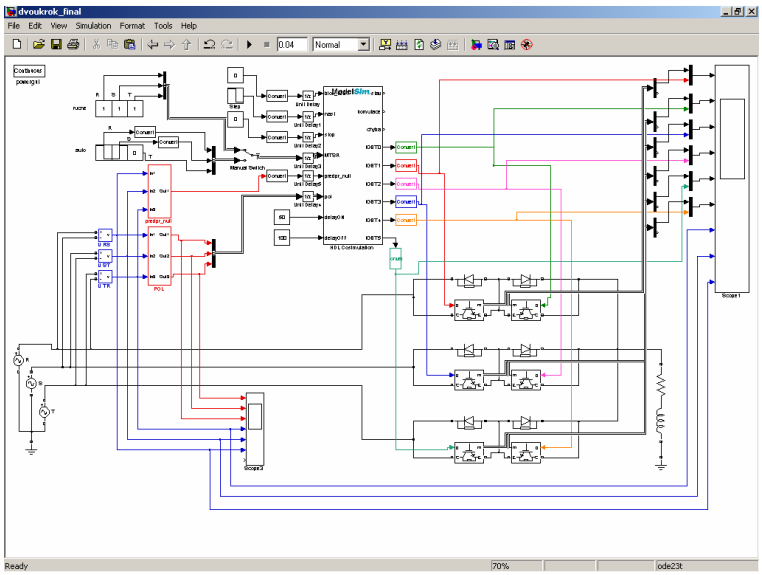

Fig. 2. Simulink model of one output phase of the matrix converter

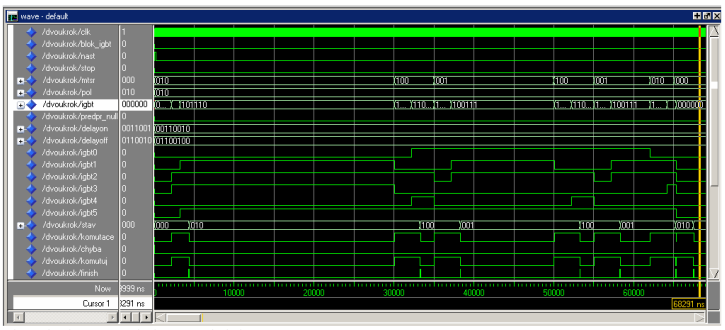

Fig. 3. Some simulation result in Modelsim

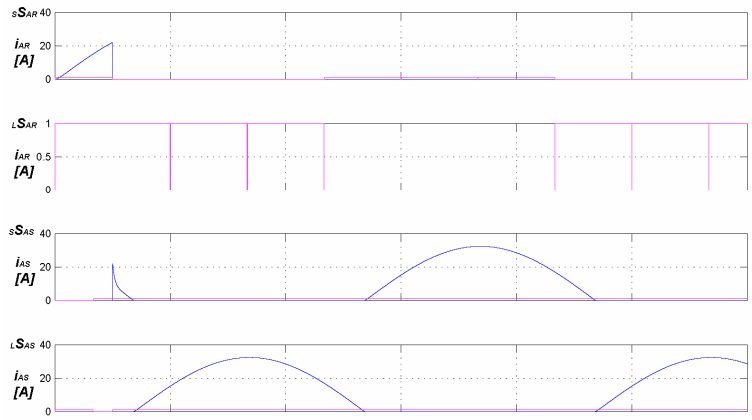

Fig. 4. Currents of phase R and S in Simulink

6. Conclusion

The developed two – step method is two – time faster than existing four – step method. But the cosimulations in MatLab and Modelsim have demonstrated that two – step method has some limitations that are not respected in theoretical analysis. Some preliminary diode of disconnected input phase can be positive polarized closely before (or after) changing polarity of input phase – to – phase voltage. It causes that one output phase of matrix converter is connected with two input phases for a short time. Two – step method is inapplicable in this short time area. Thus we cannot tell that two – step method is a single and correct solution. By that time the solution consists in combining of both methods.

References

[1] POŠTA, P. *State Automatic Modulator for Compact Matrix Converter.* ČVUT, Prague, 2007 (in Czech).

[2] LINHART, L. *Modulation Strategy of Matrix Converter.* ČVUT, Prague, 2008 (in Czech).

[3] LINHART, L. *Simulink and Modelsim Interconnection.* ČVUT, Prague, 2007 (in Czech).

[4] FLÍGL, S. *Matrix Converter in Hybrid Drives.* ČVUT, Prague, 2007.

[5] LETTL, J., FLÍGL, S. *PWM strategy applied to realized matrix converter system,* Progress In Electromagnetics Research Symposium PIERS 2007 Proceedings, pp. 98-101, Prague, 2007.

[6] LETTL, J. *Matrix converter induction motor drive*, 12th International Power Electronics and Motion Control Conference EPE-PEMC 2006 Proceedings, pp. 787-792, Portoroz, 2006.

[7] LETTL, J. *Control design of matrix converter system,* International Aegean Conference on Electrical Machines and Power Electronics ACEMP´07 Proceedings, pp. 480-484, Bodrum (Turkey), 2007.

[8] ŠIMÁNEK, J., NOVÁK, J., DOLEČEK, R., ČERNÝ, O. *Control algorithms for permanent magnet synchronous traction motor*, EUROCON 2007 Conference Proceedings, Warsaw, 2007.

[9] ZDĚNEK, J. *Efficient system software architecture of traction vehicle distributed control computer using DMA communication channels,* EDPE 20078 Conference Proceedings, pp. 1-6, High Tatras (Slovakia), 2007.

[10] ZDĚNEK, J. *Traction vehicle distributed control computer system architecture with auto reconfiguration features and extended DMA support*, EPE-PEMC 2008 Conference Proceedings, pp. 139-145, Poznan, 2008.

Transcom 2009, 22-24 June 2009
University of Žilina, Žilina, Slovak Republic

Pulsed Eddy Currents as a New Approach in Nondestructive Evaluation of Conductive Materials

Milan Smetana, Tatiana Strapacova
University of Zilina, Faculty of Electrical Engineering, Department of Electromagnetic and Biomedical Engineering, Univerzitna 1, 01026 Zilina, Slovakia, smetana@fel.uniza.sk

Abstract. Pulsed eddy current (PEC) is a new method of nondestructive evaluation (NDE). This method uses a broadband pulse excitation with rich frequency information. Also feature points extraction and response signal for defect detection and characterization. This paper introduces some basic aspects of PEC method. Selected results of the numerical simulations performed on the material specimen (stainless steel SUS316L) and based on the Finite element method (FEM) are presented and discussed.

Keywords: pulsed eddy current excitation, transient analysis, material defect, finite element method.

1. Introduction

Pulsed eddy current (PEC) sensing is a new technique that has been particularly developed for sub-surface crack measurements, crack reconstruction and depth estimation in conductive materials. Stratified conductive materials play an important role in pipeline, aeroplane, water jet-peened components, etc. In contrast to the conventional eddy current testing with sinusoidal excitations, pulsed eddy current testing taking pulses as excitation can minimize power consumption. This fact is more promising in the development of portable instruments.

The basic advantage of a transient system is that the circuitry is relatively simple compared with that needed for broad band alternating current testing. A single transient response contains as much informations as an entire spectrum of frequency domain excitations. In order to extract the information, the signals must be first analyzed [1].

The theoretical study for PEC has been conducted for several years and began with the analytical modelling for time-harmonic ECT inspection on layered structures, followed by numerical simulations using the FEM method. After the time-stepping solver was introduced in FEM, 2D and 3D FEM simulations are commonly used to PEC problems. For analytical modelling of PEC, the approach is based on time-harmonic formulation and analysis of the magnetic field in conjunction with either Fourier transform (FT) or Laplace transform (LT) [2] .

Numerical simulations of electromagnetic NDT problems can be time-consuming in comparison to analytical methods which provide fast closed-form solutions to these problems.

2. PEC sensing

PEC data analysis is mainly carried out in the time domain. PEC testing applies a broadband pulse as excitation and analyzes the transient voltage response. Because the penetration depth of eddy current testing depends on excitation frequency, PEC testing can detect deeper and fetch more informations. Pulses can be easily generated and controlled by

the intensity of excitation. Responses of pulse often come when excitation step is over and no overlap between excitation and response will occur. PEC testing is thus more robust to interference. The response signal with the system probe located on defect-free area is taken as a reference response. A differential response is obtained by substracting the reference response from the testing sample response. Differential response is usually used for feature extraction as well for defect clasification and quantification. Features commonly used are the peak value (PV) and the arrival time (PT) of the positive peak of differential response and the arrival time of the rising point (TR) [3].

3. Numerical simulations results

All the numerical simulations calculations were performed using the Finite element method (FEM) as follows: The artificial notch was situated into the middle of the material, (Fig.1). Material properties were set according to the real material parameters for SUS316L stainless steel, σ=1.6 MS, μ_r=1. Material defect has no conductivity, σ=0 S, μ_r=1. Such types of defects can be presented as fatique cracks or electric discharge machined notchs.

Modelled ECT coil (absolute coil type, Fig. 1) was situated above the material with lift-off distance d=1 mm and has 40 turns (N=40). The voltage source was used for driving of the coil. Amplitude of the driving coil signal was set to U=10V. Simulated problem was solved for three time durations of the driving signal: t_{w1}=0,01s, t_{w2}=1ms, t_{w3}=0,1ms, respectively. Current signal was the response for next data processing.

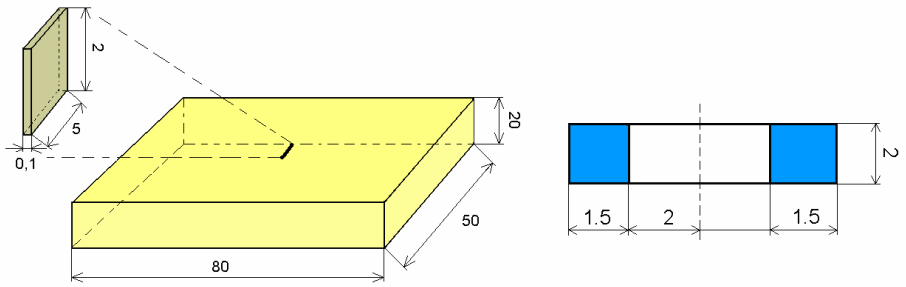

Fig.1 - Dimensions of the simulated material with artificial notch and coil

Simulation results for t_{w1}=0,01s

Time duration of the driving pulse was t_w=0,01s. As can be seen from Fig.2, the persistence of the system relatively large. Transient response is over for about 15 times of time duration of the driving pulse. This fact is according to the time constant of the circuitry. Current peak value reaches almost 15A . Using such time duration of the driving signal, the repetition frequency of the signal can be set up up to 5 cycles over period . Using higher repetition frequency causes overlapping the response signal with next response signal. Thus material defect can not be correctly evaluated. Repetition frequency of the driving pulse have to be set according to the time constant of such circuitry.

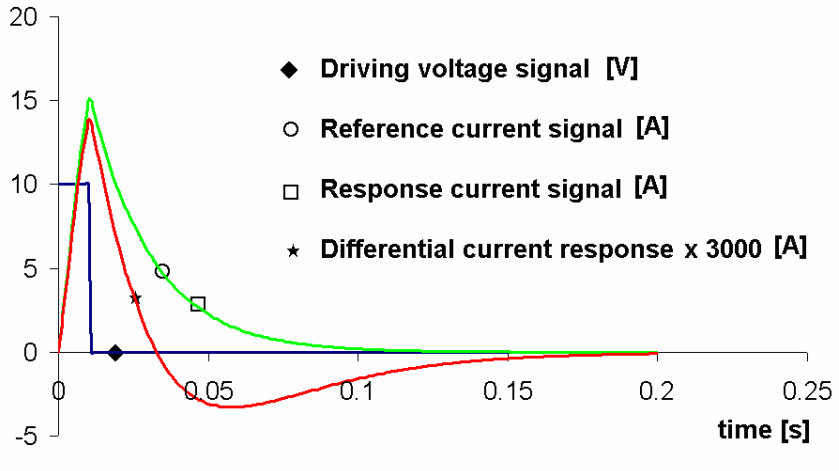

Fig.2. Time dependences of the signals for t_{w1}=0,01s

Simulation results for t_{w2}=1ms

As can be seen from Fig.3, time duration of the driving pulse was t_w=1ms.Current peak in this case reaches almost 1,8A. Transient response is over about t=200 ms, it means for about two hundred times of time duration of the driving pulse. Persistence of the system is relatively large.

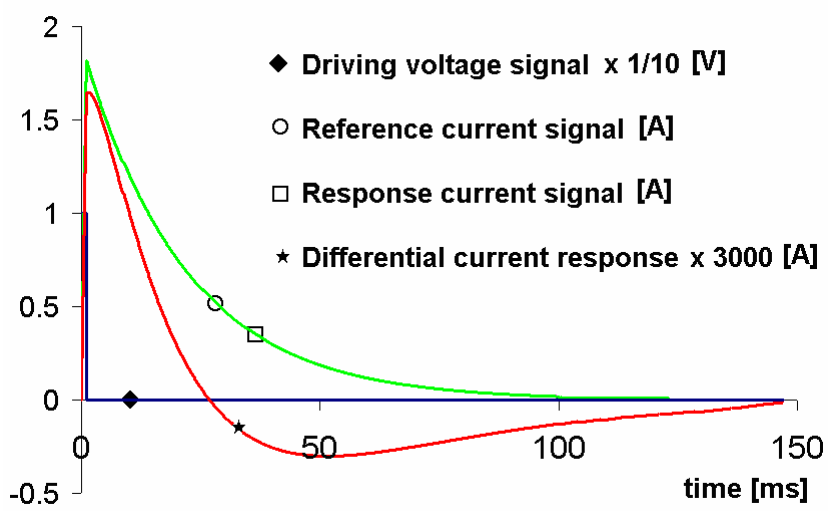

Fig.3. Time dependences of the signals for t_{w2}=1ms

Simulation results for t_{w3}=0,1ms

Fig.4 presents that persistence of the system using such time duration of the driving pulse is large. Transient response is over about $0,1x10^6$ times of the pulse duration. Amplitude of the current peak reaches almost 0,25A.

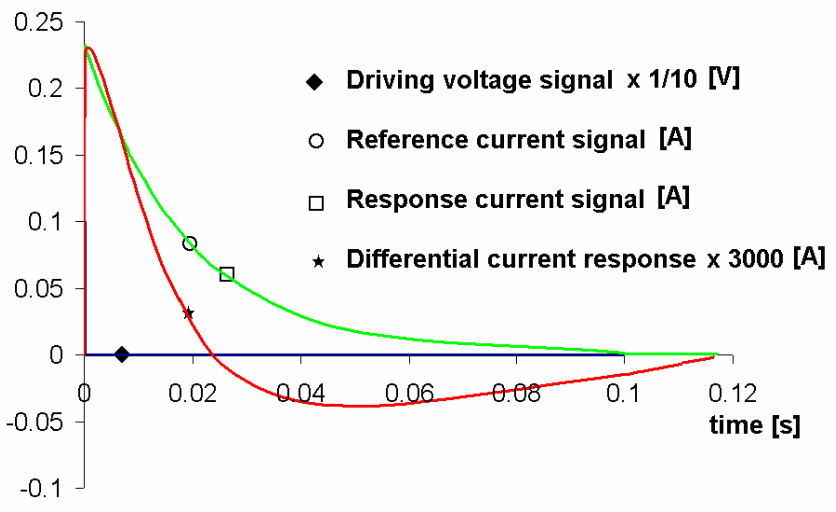

Fig.4. Time dependences of the signals for t_{w3}=0,1ms

4. Conclusion

PEC method is a new powerful tool to inspect conductive materials. Because of many advantages of this method ,material crack information can be widely used and analysed as well as in time domain also in frequency domain.

When comparing simulations results for all the time durations (frequencies) of the driving signal, it can be seen two main aspects: The shorter is the time duration of the driving pulse, the smaller is the current peak value. Persistence of the circuitry is defined by the time constant of such circuitry, where a 1.order transient response is present. Amplitudes of the reference and response signals and their differential responses are in same ratio for all the simulations because of linearity of the problem. Transient responses times for every simulation are superimposed . It means that the shorter is time duration of the driving pulse, the longer is the transient response time for such system. Because of low values of the differential responses (10^{-4} A and lower), all of the PEC apparatus devices have to be low-noise components. By analyzing obtained differential responses in frequency domain (using Fourier transform or another transforms), material crack can be explain in more detail. This is the aim for our further work.

Acknowledgement

This work was supported by the Slovak Research and Development Agency under the contract No. APVV-0194-07.

This work was supported by the VEGA project No. 1/0308/08

References

[1] BOWLER, R. Pulsed eddy-current response to a conducting half-Space.IEEE Transactions on magnetics, Vol.33, May 1997.

[2] LI, Y., TIAN, G.Y., SIMM, A. Fast analytical modelling for pulsed eddy current evaluation. NDT&E International 41 (2008), pages 477-483

[3] CHEN,T.,TIAN, G.Y., SOPHIAN, A., QUE, P.W. Feature extraction and selection for defect classification of pulsed eddy current NDT. NDT&E International 41 (2008), pages 467-476

Transcom 2009, 22-24 June 2009
University of Žilina, Žilina, Slovak Republic

Determination of Limit Values of Maintenance Priority of 110 KV VMM Low-Oil-Content Breakers

*Břetislav Stacho, *Stanislav Rusek
*Department of Electrical Power Engineering VŠB - Technical University of Ostrava,
17. listopadu 15, 708 33 Ostrava – Poruba, {bretislav.stacho.fei,stanislav.rusek}@vsb.cz

Abstract. Paper deals with application of reliability centred maintenance (RCM) to 110 KV VMM low-oil-content breakers. Brief procedure to determine the technical condition and operational importance is described in this paper. Maintenance priority of appropriate power breaker is determined by these two values. Main part of this paper is the determination of limit values of maintenance priority. It means assign the specific maintenance activity to particular power breakers according to resulting values of maintenance priority.

Keywords: Maintenance priority, type power breaker, diagnostic, technical condition.

1. Introduction

From the principle view we chose two different approaches to apply RCM onto distribution network elements: *optimisation of maintenance cycle* and *determination of maintenance priority*.

First approach is performed by the principle of finding the minimum of cost function. Maintenance, outage and failure repair cost are expressed as a function of maintenance rate. Optimisation of maintenance cycle is suitable for type of elements, which are high number in distribution network and which have not high importance (e.g. MV/LV DTS and MV lines [1]).

Second approach leads to determination of appropriate equipments maintenance priority, which further leads to determine either the optimal order of elements to maintenance or the adequate maintenance activity for particular element. Maintenance priority determination is suitable for type of elements, which number is not such high in distribution network and its importance is quite high, so it is suitable for 110 kV voltage level elements.

It results from two last paragraphs that we decided to use the *determination of maintenance priority* approach for application of RCM to 110 KV VMM low-oil-content breakers.

2. Determination of maintenance priority

Maintenance priority is determined according to evaluation of technical condition and operational importance of power breakers [2]. The resulting value of maintenance priority is determined according to formula 1, where KTS is the coefficient, which prefers the technical condition compared to operational importance. If this coefficient equals 0,5, the technical condition has the same weight as the operational importance. If KTS equals 0,3, the technical condition will share in the resulting maintenance priority by 70%, the operational importance will share by 30%.

The value of maintenance priority of the power breakers estimates maintenance activity. The higher priority, the earlier maintenance.

$$Priority = \left[100 - Technical\ condition\ (\%)\right] \cdot \left(1 - K_{TS}\right) + \\ + Operationa\,l\ Importance\ (\%) \cdot K_{TS} \quad (1)$$

2.1. Evaluation of technical condition and operational importance

Technical condition of power breakers are determined by results of diagnostic measuring and inspection. The most important criteria of technical condition are the *diagnostic measuring, tightness of quenching chamber, tightness of pressure system of a drive, insulator condition* and *time since last RM (routine maintenance)*.

Power breakers operational importance depends mainly on number and importance of connected customers and on power breaker backup possibility.

Description of all criteria technical condition and operational importance, its weights and evaluation range and description of resulting evaluation of technical condition or operational importance are not performed in this paper. All you can see in reference [3].

3. Determination of limit values of maintenance priority

We created the **type power breakers** to determine the limit values of maintenance priority, which define the specific maintenance activity. We created them by all possible combinations of values, which the power break can take in terms of technical condition and operational importance.

3.1. Type breakers creation

We focused on most important criteria, which mostly influence the technical condition (tightness of quenching chamber, tightness of pressure system of a drive, insulator condition, time since last RM and diagnostic tests evaluation) and we determined its combinations according to evaluation range, which the criteria can take (see Tab. 1).

Breaker name	Diagnostic	Tightness of quenching chamber	Tightness of pressure system of a drive	Insulator condition	Time since last RM
B 1	1	100	100	90	1.1.2008
B 2	1	100	100	90	1.1.2006
B 3	1	100	100	50	1.1.2008
B 4	1	100	100	50	1.1.2006
B 5	1	100	80	90	1.1.2008
B 6	1	100	80	90	1.1.2006
B 103	3	25	80	50	1.1.2008
B 104	3	25	80	50	1.1.2006
B 105	3	25	50	90	1.1.2008
B 106	3	25	50	90	1.1.2006
B 107	3	25	50	50	1.1.2008
B 108	3	25	50	50	1.1.2006

Tab. 1. Type breakers for determination of limit values of maintenance priority

Evaluation ranges of criteria in Tab. 1 :

Diagnostic: 1 – able for operation, 2 – deterioration of condition, 3 – eventual temporary operation with tighter conditions

Tightness of quenching chamber: 100% – tight chamber, 50% – small escape, 25% – major escape.

Tightness of pressure system of a drive: 100% - without escape, 80% - small leakage, 50% - major leakage.

Insulator condition: 90% – small glaze damage, pollution (oil, dust etc.), 50% – more extensive damage.

Time since last RM: 1.1. 2008 – means 1 year from last RM, 1.1.2006 – 3 year from last RM

In Tab. 1 there is shown the firs six and the last six type power breakers determined by method mentioned above. It was created 108 power breakers in all (3 criteria have three possible evaluations and 2 criteria have two possible evaluations $\Rightarrow 3^3 . 2^2 = 108$).

We calculated the maintenance priority of these type power breakers (chapter 2) in program *RCM*, which was developed at Department of Electrical Power Engineering VŠB-TU of Ostrava. Calculation was performed for three values of operational importance: minimal (25%), middle (60%) and maximal (88%). Resulting values of maintenance priority together with input data sorted in increase order of priority are shown in Tab. 2.

breaker name	tightness of quenching chamber	tightness of pressure system of a drive	insulator condition	construction age	time since last RM	diagnostic (%)	technical condition (%)	importance (%)	Priority Kt - 0,3 (%)
B 6	**100**	**80**	**90**	1990	**1.1.2006**	**100**	53,3	88	**59,1**
B 7	**100**	**80**	**50**	1990	**1.1.2008**	**100**	53,1	88	**59,2**
B 37	**100**	**100**	**90**	1990	**1.1.2008**	**66**	50,5	88	**61,1**
B 4	**100**	**100**	**50**	1990	**1.1.2006**	**100**	47,8	88	**62,9**
B 13	**50**	**100**	**90**	1990	**1.1.2008**	**100**	45,9	88	**64,3**
B 8	**100**	**80**	**50**	1990	**1.1.2006**	**100**	42,1	88	**67,0**
B 17	**50**	**80**	**90**	1990	**1.1.2008**	**100**	40,4	88	**68,1**
B 38	**100**	**100**	**90**	1990	**1.1.2006**	**66**	40,0	88	**68,4**
B 39	**100**	**100**	**50**	1990	**1.1.2008**	**66**	39,9	88	**68,5**
B 14	**50**	**100**	**90**	1990	**1.1.2006**	**100**	36,3	88	**71,0**
B 23	**50**	**50**	**50**	1990	**1.1.2008**	**100**	25,4	88	**78,6**
B 20	**50**	**80**	**50**	1990	**1.1.2006**	**100**	25,2	88	**78,7**
B 73	**100**	**100**	**90**	1990	**1.1.2008**	**31,9**	24,4	88	**79,3**
B 26	**25**	**100**	**90**	1990	**1.1.2006**	**100**	24,2	88	**79,5**
B 27	**25**	**100**	**50**	1990	**1.1.2008**	**100**	24,2	88	**79,5**
B 50	**50**	**100**	**90**	1990	**1.1.2006**	**66**	24,0	88	**79,6**

Tab. 2. Maintenance priority of type power breakers (with max. importance) with highlighted limit values

In Tab. 2 the type power breakers (with maximal importance) placid around determined limit values (see chapter 3.3) are shown.

3.2. Determination of approximate limit values of maintenance priority

To find out the limit values of maintenance priority we use values from Tab. 2. These approximate limit values are determined by breakers position, when the breaker was for the first time evaluated by 3rd diagnostic level (33%) (B 73) and the position when breaker was for the last time evaluated by 1st diagnostic level (100%) (B 36). In this way determined approximate limit values of maintenance priority are shown in Tab. 3.

	importance		
	min	middle	max
1st time evaluation by 3rd diag. level	[1]60,7	[2]71,1	[3]79,3
last time evaluation by 1st diag. level	[2]68,4	[3]78,8	87

Tab. 3. Approximate limit values of maintenance priority

We decided from Tab. 3 that we use three limit values of maintenance priority, so the four different maintenance activity:

1) less than [1]60% - only perform the diagnostic measuring and inspection in fixed intervals
2) [1]60% ÷ [2](68,4÷71,1)% - power breaker is put into maintenance plan to next year
3) [2](68,4÷71,1) ÷ [3](78,8÷79,3) - plan the maintenance as soon as possible, it is not necessary to shut down the power breaker
4) up to [3](78,8 ÷ 79,3) - power breaker has to be shut down immediately

3.3. Resulting determination of limit values of maintenance priority

In the course of closer observation of maintenance priority values of 108 type breakers (with three values of operational importance) were the limit values of maintenance priority specified and are together with substantiation expressed subsequently:

First limit level [1](60%)

a) **min. importance:** Power breaker has minimal importance, so it will be put into maintenance only in case of 3rd level of diagnostic evaluation.

b) **middle import.:** It will be put into maintenance in case of 2nd diag. level evaluation and the maintenance was not perform in last 3 years. It will not be put into maintenance even if it has small escapes in quenching chamber and in a pressure system of a drive, if the last RM was performed last year (improbable and in addition next year it will be put into maintenance by influence of increasing time of last RM

c) ***max*. importance:** It will be put into maintenance in case of 2nd diag. level evaluation. It will not be in case of small escapes in pressure system of a drive and in case of insulator deterioration (It was put into maintenance last year ⇒ see middle importance)

Second limit level [2](68,2%)

a) **min. importance:** We have to carry out the maintenance as soon as possible in case of 3rd diag. level evaluation, last RM was carried out 3 years ago and it has small escapes

in pressure system of a drive. We have not to carry out in case of 2nd diag. level evaluation, it have major escapes and last RM was carried out one year ago (improbable).

b) **middle import.:** We have to carry out the maintenance as soon as possible in case of 2nd diag. level evaluation, 3 years without maintenance and it has escapes in pressure system of a drive. We have not to carry out in case of 1st diag. level evaluation, 3 years without maintenance and small escapes.

c) **max. importance:** We have to carry out the maintenance as soon as possible in if it has for the first time 2nd diag. level evaluation and at the same time the maintenance was not carried out last three years. We have not to carry out in case of 100% diag. evaluation when it has maintenance last year and it has small escapes.

Third limit level [3](79%)

a) **min. importance:** Power breaker will never be immediately shut down, because it has not sufficient importance.

b) **middle import.:** Breaker will be immediately shut down in case of 3rd diag. level evaluation and it has major escapes, or in case 2nd diag. level evaluation and it has a huge escapes. It will not be shut down immediately in case of 2nd diag. level evaluation and it has major escapes, or in case of 3rd diag. level evaluation and it has minimal escapes.

c) **max. importance:** Power breaker will be immediately shut down in any case of 3rd diag. level evaluation.

4. Conclusion

In this paper was performed the brief design to determine the maintenance priority of 110 KV VMM low-oil-content breakers, which is important value if we want apply the RCM to these power breakers. Main part of paper was determined the limit values of maintenance priority.

By the help of created type breakers these values was determined subsequently. If the power breaker has less value of maintenance priority than 60% then only the diagnostic measuring and inspection in fixed intervals will be performed. If the value is in range 60%÷68,2% then Breaker is put into maintenance plan for the next year. If the value is in range 68,2%÷79% then the maintenance has to be performed as soon as possible, but Breaker has not to be shut down immediately. In case of bigger value then 79% the power breaker is immediately shut down.

Acknowledgement

The support for this research work has been provided by the GAČR project 02/09/1842.

References

[1] RUSEK S., STACHO B.: Application of reliability centred maintenance of distribution network elements into practise. Impact journal Przeglad Elektrotechniczny 9/2008, Ročník LXXXIV (84), PL ISSN 0033-2097, str 68-69, Warszawa, Polska.

[2] STACHO B.: Design of Reliability Centred Maintenance algorithm to distributive network elements. Work to doctoral examination, 2008, Ostrava.

[3] STACHO B., RUSEK S.: Design of RCM algorithm to 110 kV VMM low-oil-content breakers. In proceedings of the international Conference EPE 2009, Dlouhé Stráně

Transcom 2009, 22-24 June 2009
University of Žilina, Žilina, Slovak Republic

Costs of Improper Quality of Energy Services in the Context of Value Services Analysis

[*]Renata Stasiak - Betlejewska,
[*]The Czestochowa University of Technology, Faculty of Management, Division of Production Engineering, Armii Krajowej 19 B, 42 – 200 Częstochowa, Poland, renatastasiak@wp.pl

Abstract: The electrical power engineering is a technical system, which is obligated to the assurance of the incessant electricity supply. It determines a quality of that kind of service in a considerable degree. An analysis of nonconformities, which influence on the costs structure of improper quality of energy services, was made in this article.

Keywords: the market of energy services, costs of quality, Pareto – Lorenz diagram.

1. The market of electric energy in Poland

The electrical power engineering is an infrastructure industry about character of natural monopoly. The electric energy constitutes about the 13% in the structure of demand for carriers of the final energy in Poland, in addition it is a constituting participation about 15% in industry.

The electroenergetics is technical system, which is obligated to the assurance of incessant electricity supply. Three subsystems consist the composition of this system: the subsystem of the electric energy generating, the subsystem of the electric power transmission and the subsystem of electric energy distribution. The subsystem of the production includes power stations and intercepting, combined heat and power stations and hydroelectric power stations, which the total installed power is taking out 33000 MW. The subsystem of electric energy distribution is being created by networks of high voltages: 750 kV, 400 kV, 220 kV, of which the total length at the end of 1996 amounted to almost 13000 kilometers. They are coupled with themselves as well as they are powering the distribution network with the help of over 80 large transformer stations. Polish Electric Networks represents the subsystem of the electrical power transfer electrical power. This company is an owner of transmission grids wealth and a majority share packet in the pumped - storage power station. Lines and energy stations form the subsystem of distribution about stretching 110 kV, for averages (from 6 - 30kV) and low (below 1kV). General length of power lines about stretching 110 kV and lower took out at the end of 1996 681000 kilometers. In Poland, 33 power plants constitute the subsystem of distribution [2].

The electric energy purchase by only one company (PSE S.A.), related to prices established by the minister of the economy, has been practically a nature of the electric energy market's model till 1998. PSE S.A. sold the purchased energy to distribution companies at wholesale prices, and these ones sold it to final recipients according to official prices established by the minister of finance. These prices were established without taking into consideration incurred costs by individual distribution units and not always they have had character of economic prices. However it determined incomes of the entire sector.

The electrical power sector is in the process of transformations, which surrendered for considerable acceleration on the turn of eightieth and ninetieth years. The energetics was strongly monopolized till the end of year 1988. Energy circles were closed down in 1988 and workshops fitting into their composition were converted into independent state enterprises.

2. The costs structure of improper energy services quality

Costs lowering based on the processes improvement and the optimization is determined with name of the value engineering. The value engineering is often determined also as the value analysis and it also means the production method consisting on increasing the frugality of expended stores at holding required product quality and possible of product quality improvement. Getting the same achievements in the field of production and services at lower costs, owing to objects, products, the technology and the organization streamlining, is an aim of this analysis [2].

According to the main principle of value analysis, both a registration of the existing state in the sphere of its structure and functioning and identification of functions fulfilled by this system should be the main point of departure for changes in the given system (for company). This approach is aiming at the criticism of functions fulfilled currently by systems and function correcting, which are lowering product value.

The structure of costs resulting from improper energy services quality was the object of examinations, carried out on the area of one of the power plants in Poland, in December of 2000.

2.1. The costs structure in the monthly period

Causes of nonconformities, which influenced on creating of the definite costs structure of energy services in the monthly period are presented in the table 1.

Symbol of nonconformities	The name of nonconformities	Percentage share [%]	Accumulated share of nonconformities [%]
N 3	Thefts of the electric energy	37,5	37,5
N 1	Debt of enterprises	34,0	71,5
N 2	Decreasing electricity consumption	20,8	92,3
N4	Holiday breaks	7,7	100,0

Tab. 1. Nonconformities having influence on the costs level of energy services in the monthly period. Source: own study.

The Pareto – Lorenz diagram was made on the base of identified nonconformities [1], which is presented at the figure 2. Basing on the analysis of the Fig. 2 it can be stated that, two nonconformities, like thefts of electric energy and the debt of enterprises are responsible for the 71.5 % nonconformities having the influence on the costs structure of energy services. Other nonconformities cause the 28.5 % of appearing costs of improper energy service quality.

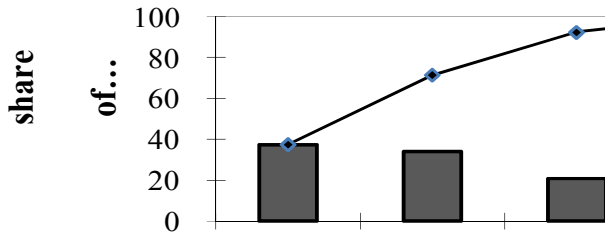

Fig. 2. The Pareto – Lorenz diagram for nonconformities influenced on the costs structure of energy services in the monthly period.

Source: own study.

2.2. The costs structure in the quarterly period

Causes of nonconformities, which influenced on creating of the definite costs structure of energy services in the quarterly period, are presented in the table 2.

Symbol of nonconformities	The name of nonconformities	Percentage share [%]	Accumulated share of nonconformities [%]
N 1	Debt of enterprises	39,6	39,6
N 3	Thefts of the electric energy	32,1	71,7
N 4	Holiday breaks	15,1	86,8
N 2	Decreasing electricity consumption	13,2	100,0

Tab. 2. Nonconformities having influence on the costs level of energy services in the quarterly period

Source: own study.

The Pareto – Lorenz diagram was made on the base of identified nonconformities (Tab. 2), which is presented at the figure 3.

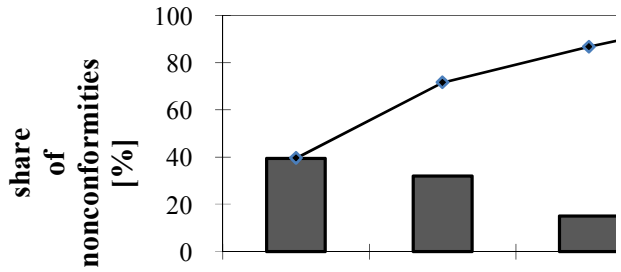

Fig. 3. The Pareto – Lorenz diagram for nonconformities influenced on the costs structure of energy services in the quarterly period. (Source: own study)

It results from analysis of the Fig. 3, two nonconformities, like the debt of enterprises and thefts of the electric energy, are responsible for the 71.7 % of nonconformities. Other nonconformities cause the 28.3 % of appearing costs of improper energy service quality.

2.3. The costs structure in the period of the half year

Nonconformities, which influence on the costs structure of energy services in the period of the half year, are presented in the table 3 and figure 4.

Symbol of nonconformities	The name of nonconformities	Percentage share [%]	Accumulated share of nonconformities [%]
N 1	Debt of enterprises	39,5	39,5
N 3	Thefts of the electric energy	30,2	69,7
N 2	Decreasing electricity consumption	19,3	89,0
N 4	Holiday breaks	11,0	100,0

Tab. 3. Nonconformities having influence on the costs level of energy services in the period of the half year. Source: owny study.

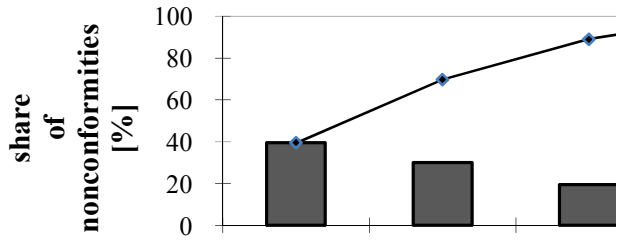

Fig. 4. The Pareto – Lorenz diagram for nonconformities influenced on the costs structure of energy services in the period of the half year. (Source: own study)

It results from analysis of the Fig. 4 that, the 69.7% of nonconformities are effect of two nonconformities like debts of enterprises and thefts of the electric energy. Other nonconformities cause the 30.3% of appearing costs of improper energy services quality.

3. Conclusion

The following nonconformities, which have the influence on the costs structure of improper quality of energy services were identified in the effect of research. The main causes of the nonconformities having the influence on the level of energy services costs are: the debt of enterprises (caused mainly by rising prices of the electric energy and the low collection rate of companies debts), thefts of the electric energy (connected with both thefts of a power line and the illegal drawing of the electric current), rock bottom of the energy selling (connected with the rock bottom of consuming energy and power failures caused by disruptions in the web).

These identified nonconformities result from wrong finance situation of enterprises in Poland and high prices of energy. The high price level is the effect of the specific of Polish energy market, which is complicated by monopoly market, which had been till 2008 year.

References

[1] BORKOWSKI S., ČOREJOVA T. *Instrumenty rozwiązywania problemów w zarządzaniu*. Wydawnictwo WSZiM w Sosnowcu, Sosnowiec 2004.

[2] STEWART R.B.. *Fundamentals of Value Methodology*. Xlibris Corporation. United States of America. 2005.

[3] DURLIK I. *Demonopolizacja i prywatyzacja elektroenergetyki*, EiOP 2/97.

[4] HAMROL A., MANTURA W. *Zarządzanie Jakością – Teoria i Praktyka* , PWN, Warszawa - Poznań 1999.

[5] KŁYSZ M. *Rynek energii elektrycznej w Polsce*, „Przegląd Organizacji", Nr 6, 1999.

[6] *Biuletyn Informacyjny GZE S.A.* „Łącznik".

Transcom 2009, 22-24 June 2009
University of Žilina, Žilina, Slovak Republic

Prosthetic Heart Valve Crack Signal Simulation in Eddy Current Testing

*Tatiana Strapáčová, **Milan Smetana
*University in Žilina, Faculty of Electrical Engineering, Department of Electromagnetic and Biomedical Engineering, Univerzitna 1, 01026 Žilina, Slovakia, strapacova@fel.uniza.sk, **smetana@fel.uniza.sk,

Abstract. Dysfunction of prosthetic heart valves is a common complication after heart valve replacement, affecting both biological and mechanical prostheses. The periodic evaluation of the state of the prostheses, non-destructive test of each individual valve may help to detect the fractures presents in heart valve replacements and so prevent the damages of a valve. Prosthetic heart valves of the Bjork-Shiley Convexo-Concave (BSCC) type have long been used extensively in implants; however, there have been reports of cases where one component of the valves failed, leading to the demise of the patient. To this end this paper presents a method for noninvasive electromagnetic evaluation of conductive heart valve replacements, using an eddy current testing. The first part of the article describes a principle of conventional eddy current method. Description of simulated problem, obtain results and their interpretation in the medicine are presented in the second part of the article.

Keywords: Electromagnetic method, eddy current, heart valve replacement, fracture of outlet strut

1. Introduction

The human heart has four valves which control the one-way flow of blood through its four chambers. Heart valves could be affecting by different type of diseases such a stenosis, incompetence or regurgitation. If the application of corrective actions (medication therapy or percutaneous mechanical procedure) is not possible, one alternative is to replace the malfunctioning valves with prosthetic devices. Artificial heart valves must be designed to survive more than 109 cycles over 40 years of operation. Thus, the fatigue represents one of the primary driving forces for safe operation of these devices. The inability to maintain the long term performance of critical devices in the future may lead to catastrophic failure and patient loss of life. One of the most common mechanical prosthetic heart valves that were implanted extensively was the Bjork-Shiley Convexo-Concave (BSCC) valve Fig.1. Approximately 86.000 BSCC valves are supposed to have been implanted worldwide, and 619 valves fractures have been reported to Shiley. In approximately two-thirds of the cases, it was reported the patient had died due to the valve fracture [2].

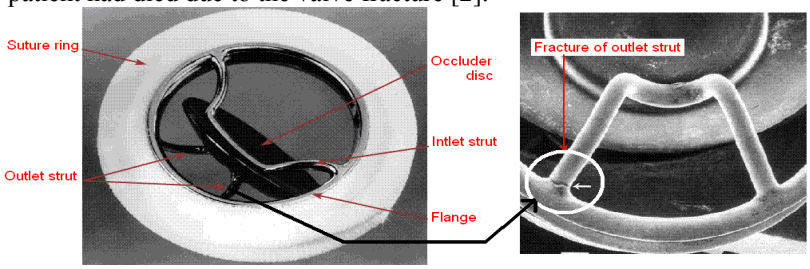

Fig.1 Bjork- Shiley Convexo Concave (BSCC)

BSCC heart valve contains a suture ring and two metallic struts, an inlet and outlet strut, which support a carbon occluder disk. While the inlet strut is integral to the suture ring, the outlet strut is welded to it. Occasionally the weld at one of the ends of the outlet strut develops a fracture and fails due to various reasons including mechanical fatigue and stress corrosion cracking. Although the valve in this condition performs normally, this may be a precursor to a fracture and eventual failure of the other leg of the outer strut, which leads to fatality. Hence, there is a considerable interest in detecting fractures of outlet strut in BSCC heart valves. In the present paper is propose an electromagnetic method eddy current testing- ECT for nondestructive examination of the outlet strut of BSCC valves.

2. Eddy Current testing - ECT

The eddy current inspection technique is widely used for quality assurance of metallic materials. In EC testing, the probe coil excited with alternating current is placed on an electrically conductive material (metallic biomaterials), eddy currents are induced in the material. Presents of inhomogeneities, defects, variations in electrical conductivity, magnetic permeability, and geometry of the material, and lift-off, etc. disturb the eddy current flow and, in turn, alter the coil impedance. The change in impedance is usually measured and correlated with defect dimension or the causes producing it. This method is applicable only to surface or near surface flaw detection because of the decrease in magnetic flux and eddy current density with depth. The depth of penetration of eddy current testing is limited by skin–effect, which depends on the operating frequency, the material conductivity, and the permeability.

2.1. Numerical Evaluation – Analysis model

The problem deals with pancake coil type, placed above an outlet strut of the BSCC heart valve replacement. The probe coil with dimensions Fig.2 moves parallel to the z axis in the section <-10; 10> mm, because the defect was positioned in the middle of material, where z=0. The probe coil had axis- symmetric shape and had 100 turns. It is supplied with current density **J** = 1A/mm^2 and frequency of the signal was f = 500 kHz.

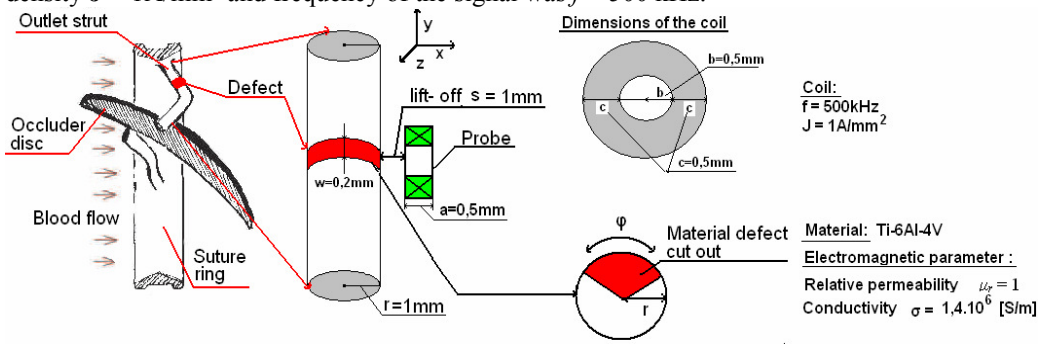

Fig. 2 Description of the simulated problem - dimensions of the material, coil and defect

Properties of the investigated material, dimensions and electromagnetic parameters of the material were set according to real dimensions and electromagnetic parameters of the outlet strut. The outlet strut was made of titan alloy type Ti – 6Al- 4V and has a conductivity σ=1.4×10^6 [S/m] and relative permeability μ_r = 1. The solution of the forward problem requires the determination of the impedance change of the probe. This parameter is evaluated by subtracting the values obtained for the material without defect from the values obtained for the material with defect. The defect was localized in the middle of the material, the defect

width was w=0.2mm and the defect depth r were changed during inspection. The defect opening angle φ was changed simultaneously with the defect depth. It makes 25 simulations done. The impedance change was calculated at the frequency 500 kHz and for lift-off of 1mm at different coil locations, starting from x = -10mm till x =10mm at every 1 mm along the crack direction.

2.2. Numerical evaluation – Analysis method

For the ECT based approach, the perturbed magnetic flux density due to the defect is studied. Parameters of the interest include the dimension and geometry of the coils, gauge of the coil wires, the current required to generate the desired magnetic field and sensitivity of the ECT coil probe. The ECT analysis is conducted by the magnetic vector potential **A** and electric scalar potential V. Fig.3 shows a configuration for typical eddy current problems. The solution domain is subdivided into conducting area Ω_1 and non-conducting area Ω_2. The eddy current in conductor is governed by following equations

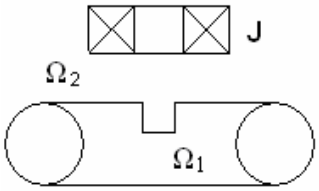

$$\frac{1}{\mu_0}\nabla^2\mathbf{A} = j\omega\sigma\left(\mathbf{A}+\nabla V\right). \tag{1}$$

$$\nabla\sigma\left(\mathbf{A}+\nabla V\right)=0\,. \tag{2}$$

Fig.3. A typical configuration for ECT

where μ_0 are permeability, ω angular frequency of AC current, and σ and the electric conductivity. The governing equation in air Ω_2 region is expressed by

$$\frac{1}{\mu_0}\nabla^2\mathbf{A} = -\mathbf{J}_0\,. \tag{3}$$

where $\mathbf{J_0}$ the applied current of the exciting coil. By solving this set of equations we get **A** and V. Then the induced voltage in the pick up coils and the impedance change in the pancake coil were obtained, [1], [3]

3. Numerical simulation results

The simulations results in graphic form Fig.4, shows a relation of coil impedance change from its movement above the given material it is possible to localize the defect in material relatively precisely. Five different curves represent five different depths of the defect for one opening angle φ=100˚. The amplitude of the impedance changed with changing defect depth. Coil impedance amplitude – reaction to corresponding changes. Waveforms at Fig.5 represent 5 simulations for various depths of the defect for one defect opening angle value φ = ‹ 80˚; 100˚›. It can be seen that representation does not correspond with real material defect description, where the defect has approximately a triangle shape. The curve with two maximal values -- peaks (for one depth of the defect value) can be seen on Fig.5. This is caused by small material defect opening angle. Path of eddy currents (which have to be enclosed and because they find a path with smaller resistance value) is shorter when they underflow the material defect in this case. This is shorter path unlike flow around the material defect.

From the obtained graphic relations it is possible to say that the ETC method is sensitive also for material defects with relatively small dimensions (tenths of millimeter) occurring in conductive heart valve prosthetic replacements.

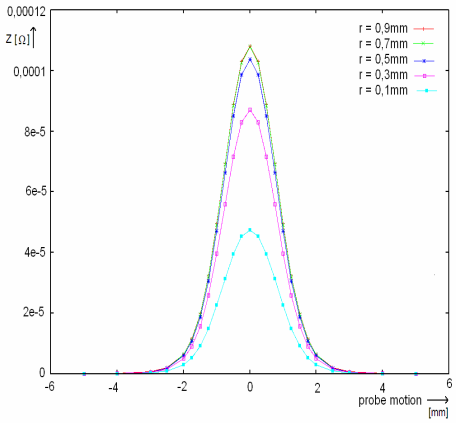

Fig. 4 The simulation result graphic presentation shows a relation of coil impedance change from its movement above the material φ = <40°; 140°> and the defect depth r was changed

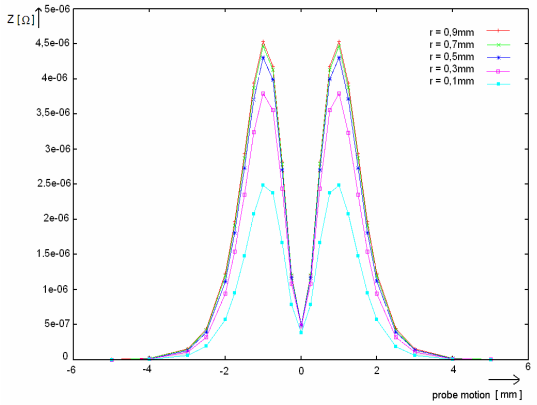

Fig.5 Graphical dependence of coil impedance change on the probe motion opening angle φ = <80˚; 100˚>

4. Conclusion

Prosthetic heart valves made from conductive materials are daily used in medical praxis. Their investigation is very important because a timely inspection of the heart valve replacements output strut „in vivo" will allow to avoid damages of these prosthetic replacement that could be incompatible with human being. The numerical simulations results affirm the feasibility of the detecting of defect which affects the outlet strut of the BSCC heart valve using ECT approach. The simulation tools are useful for gaining a better understanding of the underlying field distribution as well as improving the system designs. The advantage of this technique is that it provides a non-contact, non-destructive, highly sensitive three dimensional analysis of the heart valve replacement. The development of these methods, their application and optimizing of device components are studied in the meantime. Using of ECT in medical praxis prepare the way for non-invasive inspection of the prosthetic replacement and so make these evaluation fastener and accurately.

Acknowledgement

This work was supported by the Slovak Research and Development Agency under the contract No. APVV-0194-07.

This work was supported by the VEGA project No. 1/0308/08

References

[1] CHAN SHIU C., YUE LI, UDPA LALITA, UDPA SATISH S.*: Electromagnetic techniques for detecting strut failures in artificial heart valve,* Electromagnetic Nondestructive Evaluation, Vol 26 Studies in Applied Electromagnetics and Mechanics, G. Dobmann, ISBN 1- 58603-594-0

[2] RAIMOND GRIMBERG, SHIU C.CHAN, ADRIANA SAVIN, ROZINA STEIGMANN, ALINA BRUMA 1, LALITA UDPA 2, SATISH S.UDPA: *Electromagnetic health monitoring of BSCC prosthetic heart valves,* 17th World Conference on Nondestructive Testing, 25-28 Oct 2008, Shanghai, China.

[3] Weying Cheng, Zhenmao Chen, Kenzo Miya, Yoshikatu Yoshida: Numerical evaluation of the ECT signal from Multiple crack, Electromagnetic Nondestructive Evaluation (II), IOS Press, pages 92-98

Transcom 2009, 22-24 June 2009
University of Žilina, Žilina, Slovak Republic

Signals of Optoelectronic Transducer Processed in Flip-Flop Circuits

*MSc. Eng. Adam Szcześniak, **PhD. DSc. associate professor Zbigniew Szcześniak
*PhD student at the Mechatronics department of University of Technology in Kielce, Aleja Tysiąclecia Państwa Polskiego 7, Kielce PL - 25-314, e-mail: adam_szczesniak@o2.pl
** Department of Electrical and Computer Engineering, University of Technology in Kielce, Aleja Tysiąclecia Państwa Polskiego 7, Kielce PL - 25-314, e-mail: z.szczesniak@tu.kielce.pl

Abstract. This article is a presentation of a designed method using logic and flip-flop circuits which process signals from optoelectronic transducers. This enables a way to distinguish the direction and motion of optoelectronic transducers. More over method allows an increase of the accuracy of the optoelectronic transducer glass scale. Simulation of the method was carried out in Matlab-Simulink software. Verification of this method has been proven by a real device. Results from simulation research and a real system are enclosed.

Keywords: construction and rule of operation of photoelectric transducers, motion direction discrimination, increasing accuracy of the optoelectronic transducer, distinguishing motion direction.

1. Introduction

Presently the most popular are optoelectronic position transducers which consist of disc (or strip used for linear shift measurements) which has on its circumference a sequence of transparent and non-transparent fields. They respectively let in or absorb the light.
Optoelectronic transducers dedicated for length measurement are equipped with a glass scale. Its length is equal to the length of the measured position. In the case of the measuring angle optoelectronic transducers are equipped with rotating discs [1], [2].
Glass scale models of a beam of light which drops on the photoelement in such a way that on its end appear appropriate number of impulses. These are proportional to the linear or angular movement. In the measurement of the position there is great importance in the assurance of accurate and precise measurements. Decreasing the interval of shift quantization of an object can be achieved by using more precise methods of building optoelectronic transducers (its glass scale) or by applying appropriate methods of signal processing which is technologically much easier [4], [6], [7], [8], [9].

This article is a presentation of a designed method and a flip-flop circuit of interpolation of transducer signals which enables the distinguishing of its direction and increases the accuracy of the optoelectronic transducer.

2. Method of distinguishing optoelectronic transducer direction based on logical functions and flip-flop circuits.

In fig. 1. there is an introduced system of distinguishing the direction of motion and an idea of generating impulses for twice and four times increase of the glass scale accuracy. During the movement in a forward direction using the method of twice and four times increase

of accuracy on output of NAND3 (out_1_F Fig. 2.) and on output of NAND6 (out_2_F Fig. 2.) we obtain a sequence of impulses which repeat themselves with the period of signals from the transducer. The main function of distinguishing the direction performs a circuit which consists of flip-flops and TTL gates. JK flip-flops are synchronized with the pulse generator – CLK.

Two sinusoidal signals from the optoelectronic transducer (sine cosine) become digitalized and we obtain "A" and "G" signals respectively. Signal "A" is put on input of JK flip-flop and its negation on input K. If signal "A" is changing from 0 logic level to 1 logic level then during the first falling clock edge an output of this flip-flop becomes set to 1 logic level. (signal "B" Fig. 2). Output of this flip-flop is put on input J and its negation on input K of another JK flip-flop.

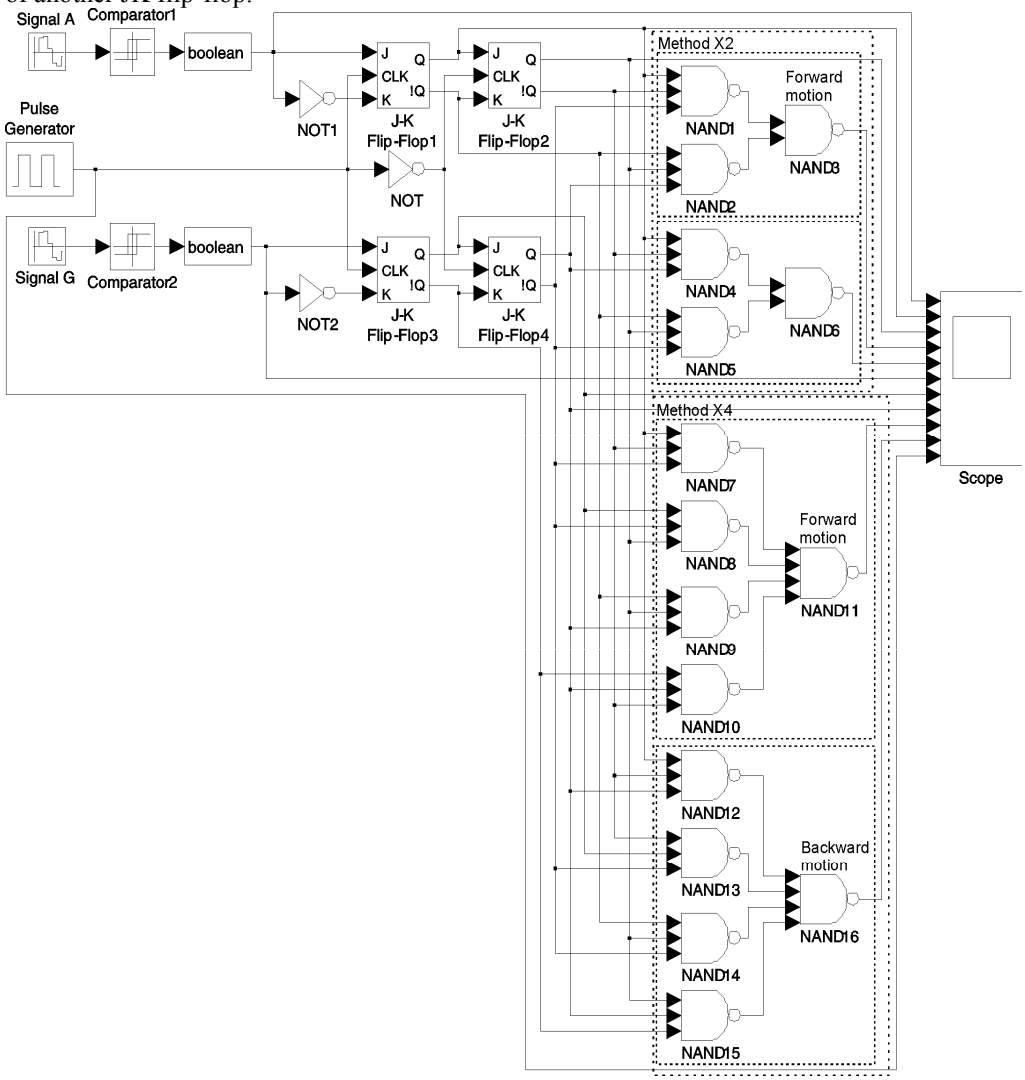

Fig. 1. Matlab-Simulink simulation diagram of the method of distinguishing movement direction of optoelectronic transducer based on logical functions and flip-flop circuits.

On its output appears logic state 1 which is delayed to an output of the previous flip-flop by clock impulse width. This delay is used to produce shift impulses according to a realization of

below function. In the same way signal G is processed. Its subsequent phases are shown in Fig. 2. as signals “E” and “F”.

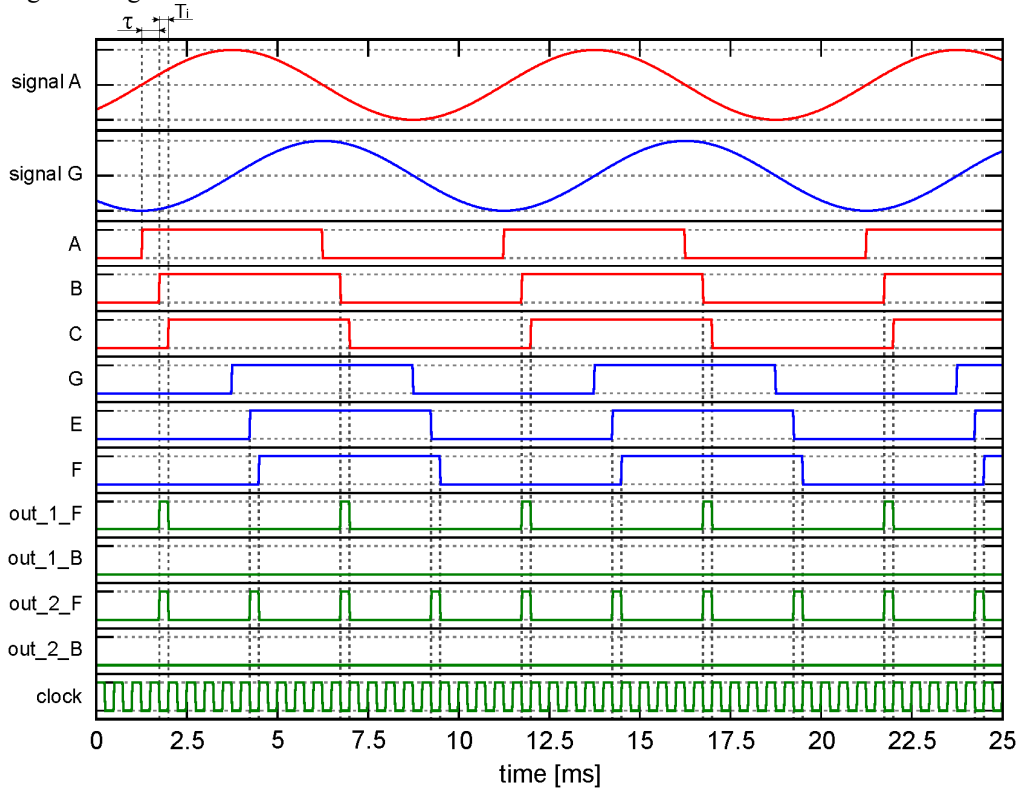

Fig. 2. Functions from simulation method of distinguishing optoelectronic transducer direction using logic functions and flip-flop circuits.

When we make a realization of logic functions for two times increase method:

for forward motion: $$out\_1\_F = B\overline{C}\,\overline{F} + \overline{B}CF \quad (1)$$

for backward motion: $$out\_1\_B = B\overline{C}F + \overline{B}C\overline{F} \quad (2)$$

and for four times increase method:

for forward motion: $$out\_2\_F = B\overline{C}\,\overline{F} + E\overline{F}C + \overline{B}CF + \overline{E}F\overline{C} \quad (3)$$

for backward motion: $$out\_2\_B = B\overline{C}F + E\overline{F}\,\overline{C} + \overline{B}C\overline{F} + \overline{E}FC \quad (4)$$

we will obtain impulses of transducer movement (counted in reverse counters), which sum indicates the position of the optoelectronic transducer.
Generally we can state, that motion impulses for forward direction can be obtained when:

- “G” = “0” and impulse generated from rising edge of signal “A” exist
- “A” = “1” and impulse generated from rising edge of signal “G” exist
- “G” = “1” and impulse generated from falling edge of signal “A” exist
- “A” = “0” and impulse generated from falling edge of signal “G” exist

Impulses for backward direction can be obtained when:

- "G" = "1" and impulse generated from rising edge of signal "A" exist
- "A" = "0" and impulse generated from rising edge of signal "G" exist
- "G" = "0" and impulse generated from falling edge of signal "A" exist
- "A" = "1" and impulse generated from falling edge of signal "G" exist

Taking into consideration the above and the glass scale symmetry division, using the described method, it can be obtained a multiplication factor 2 or 4 of the glass scale division. Direction of motion can change at any time so the greatest error of the direction of motion is equal to ¼ T for four times method of increase. (T – period of one channel of optoelectronic transducer). In the case of the first method this error is equal to ½ T. The above methods of distinguishing motion direction were presented in Fig. 2. which were registered during simulation research. For clarity, the method description assumed that the frequency (period) of the input signals is constant. This represents a situation of motor motion with constant velocity [3], [9].
Presented results Fig. 2. were obtained by simulating the diagram from Fig. 1. using Matlab-Simulink software. Practical circuit realization basing on above method for two times increase shows Fig. 3 [5].

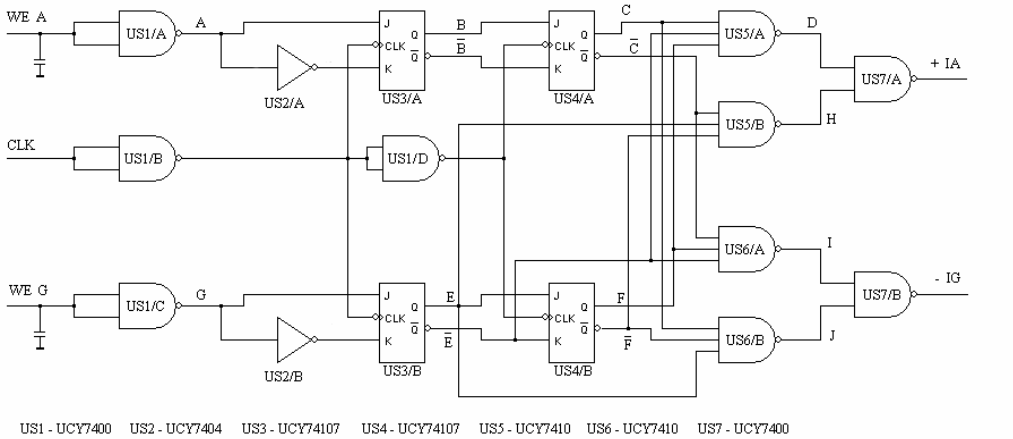

Fig. 3. Practical circuit realization of distinguishing optoelectronic transducer direction based on logical functions and flip-flop circuits.

3. Conclusion

1. Presented method and circuit were made using logic functions and flip-flop devices. System enables two times or four times increase of accuracy.
2. In this method the width of the increased impulses equals one half of the clock generator period. The frequency of the clock generator should be at least twice as high as the frequency of the increased signal.
3. This method causes delay τ (lower than the clock generator period) resulting of lack of synchronization between the signal from the transducer and the clock signal.

4. References

[1] **Ching-Fen Kao, Mao-Hong Lu** „Optical encoder based on the fractional Talbot effect" Optics Communications 250 (2005) 16–23 Elsevier

[2] **Feel-Soon Kang, Sung-Jun** Park A linear encoder using a chiaroscuro and its extension to switched reluctance motor drive Energy Conversion and Management 46 (2005) 1119–1128 Elsevier

[3] **Szcześniak Zb.** „Analysis of the position and velocity measurement line for the hydraulic press crossbar with the use of photoelectric transducer". Advances of Manufacturing Science and Technology, Polish Academy of Sciences, vol. 29 No 3/2005 pp. 75-84

[4] **Szcześniak Zb.** „Elektroniczny moduł dziesięciokrotnego zwiększania dokładności przetwarzania sygnałów optoelektronicznego przetwornika położenia". Elektronika i Telekomunikacja, Polska Akademia Nauk, Tom 51 nr 3/2005 ss. 439 - 447

[5] **Szcześniak Zb.** „Method of processing accuracy enhancement of the photoelectric position transducer signals". Metrology and Measurement Systems, Polish Academy of Sciences, vol. XII No 3/2005 pp. 315-322

[6] **Szcześniak Zb**. „Metoda interpolacji sygnałów elektrycznych optoelektronicznych przetworników w pomiarach położenia". Elektronika 2005. nr 1. str. 74-76.

[7] **Szcześniak Zb.:** „Methods of converting of electric signals from photoelectric position transducer for discrimination of its motion direction and for increasing its measurement accuracy". Electronics and Telecommunications. Polisch Academy of Sciences, Vol. 52 No 1 / 2006 pp. 23-30

[8] **Щесьняк Зб.,** Дорожовець М. „Метод помноження частоти вимірювального сигналу фотоелектричного перетворювача положення". Вісник НУ "Львівська Політехніка", "Комп'ютерні мережі та системи". N523. С.154-157. 2005р.

[9] **Szcześniak A. Szcześniak Zb. „**Mikroprocesorowe przetwarzanie sygnałów optoelektronicznego przetwornika położenia"
PRZEGLĄD ELEKTROTECHNICZNY (Electrical Review), ISSN 0033-2097, R. 85 NR 4/2009 str. 153 – 158

Transcom 2009, 22-24 June 2009
University of Žilina, Žilina, Slovak Republic

Equivalent Circuit Parameters Investigation of Switched Reluctance Motor

[*]Martin Šušota, [*]Pavol Rafajdus
[*]University of Žilina, Faculty of Electrical Engineering, Department of Power Electrical Systems,
Univerzitna 2, 01026 Žilina, Slovakia, Martin.Susota@kves.uniza.sk

Abstract. This paper deals with equivalent circuit parameters investigation of Switched Reluctance Motor (SRM). The parameters are: phase resistance and phase inductance versus current for various rotor positions. Different methods are described and used for phase resistance and inductance determination. The results of phase inductance are compared also with FEM analysis.

Keywords: switched reluctance motor, inductance, measurement, FEM.

1. Introduction

The equivalent circuit parameters investigation is very important task in the SRM from the point of view of the SRM torque ripple minimization. There exist many various methods how to investigate SRM parameters. If the SRM is under design process, the Finite Element Method (FEM) and also analytical approach are suitable. In the case of real SRM, some measurements are applicable. In this paper a real small SRM is analyzed. Its nameplate is shown in the Table 1a. and its photo is in Fig.1a. In this paper the equivalent circuit parameters (phase resistance, phase inductance) are measured and evaluated in dependence of rotor position and phase current, as it is described in the next chapters. An equivalent circuit of the SRM is in, the Fig. 1b [1, 2, 3, 4].

Table 1.
a) Three phase 6/4 SRM nameplate

MEZ	EM Brno	TYPE SR 40N
3x 10V	28,5A	5000rpm

b) Measurement of phase resistance

	V(V)	I(A)	R_{ph}(Ω)
A	0,165257	4,020114	0,041108
	0,214368	5,184788	0,041346
B	0,23206	5,561871	0,041723
	0,189066	4,562403	0,04144
C	0,240724	6,120662	0,03933
	0,194844	4,976214	0,039155

2. SRM equivalent circuit parameters measurement

2.1. Measurement of phase resistance

In this SRM, the phase winding is created by two coils, which are connected in parallel. The rated current of SRM is high (see Table 1a.), so phase resistance is low. For phase resistance measurement, the Ohm's method is used. The circuit wiring is shown in Fig.1c. The

DC current and voltage have been measured by digital oscilloscope, because the common ammeters and voltmeters are not suitable. It is caused by low phase resistance. For each phase, many measurements have been made. The measured values of currents and voltages with calculated values of phase resistances are collected in Table 1b. The final measured average value of phase resistance is R_{ph}= 40,68 mΩ.

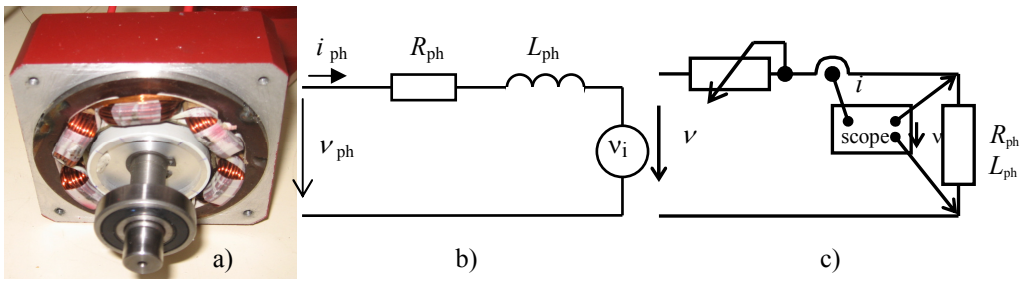

Fig. 1 a) Photo of investigated real SRM, b) Equivalent circuit of SRM, c) The measurement of phase resistance connection

2.2. Phase inductance measurement

As it is known from a theory of the SRM, the phase inductance L_{ph} depends on phase current and rotor position. Two basic rotor positions are defined: aligned rotor position, where the inductance is maximal L_{max} and unaligned rotor position, where the inductance is minimal L_{min} (see Fig. 2d.), [1], [2].

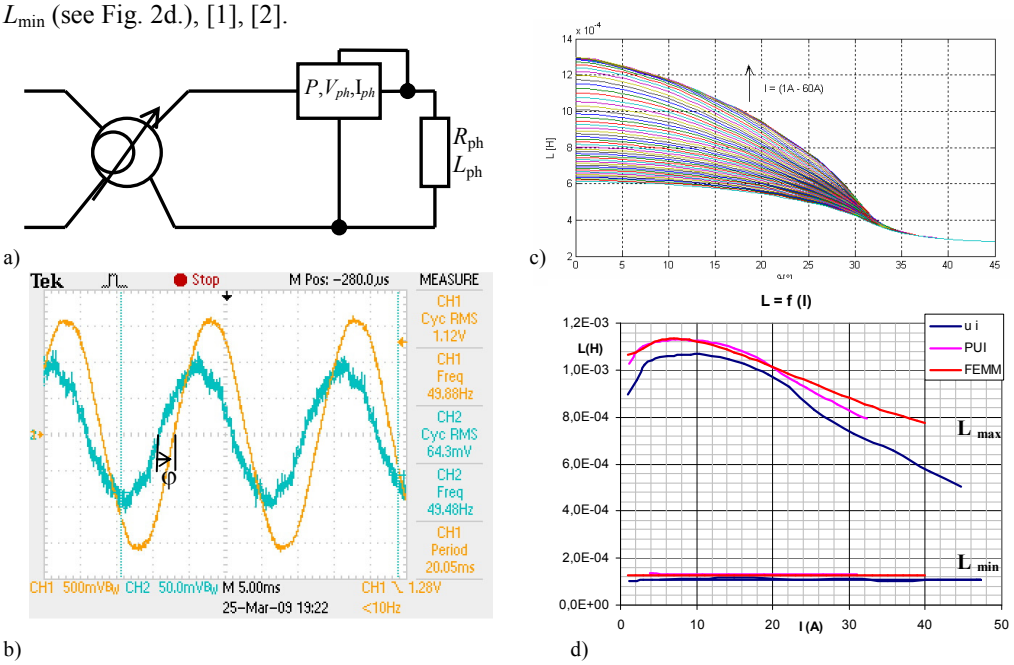

Fig. 2. a) Basic schemes for phase inductance measurement by wattmetric method, b) Phase current and voltage waveforms, c) FEM analysis of phase inductance versus rotor position for different phase current, d) Comparison of measurements PUI – wattmetric method, ui – AC supply and φ angle measurement and FEM calculation

In aligned position, the phase inductance depends strongly on the current and there occurs a high saturation because, of a short air gap. In unaligned position the air gap is very high and phase inductance in this position is independent on the current.

There are many methods for inductance measurement, but not all are suitable for SRM phase inductance from some points of view: a) accuracy of method – method of three ammeters, where very accurate and comparable resistance with phase resistance is needed, b) from point of view of time consumption - DC decay test or DC arise test [2], because for each rotor position and each phase current a new measurement and evaluation is needed. These methods are suitable only for comparison with results of other methods. In this paper, two methods are used: 1) wattmetric method (see basic scheme in the Fig.2a and 2) AC supply and φ angle measurement. They are compared and verified by means of FEM.

1. Wattmetric method: This method is used in accordance with circuit in Fig.2a. Only one phase has been supplied with AC variable source. With one phase wattmeter, the power, voltage and current have been measured for different phase current. The rotor was kept in aligned and unaligned position. The phase inductance is calculated from following equation:

$$L = \frac{V_{ph}}{\omega I_{ph}} \sqrt{1 - \left(\frac{P}{V_{ph} I_{ph}} \right)^2} \tag{1}$$

where ω is angular speed of supply voltage. The results are shown in Fig. 2d for aligned and unaligned rotor position and these results are marked as PUI.

2. AC supply and φ angle measurement: This method is based on one phase voltage and current measurement from AC source. The voltage and current are kept constant and also the rotor position is constant at a defined rotor position (aligned, unaligned or some a particular position). Then, the voltage and current waveforms are stored by digital scope and power factor is measured. The scope waveforms of voltage and current are shown in Fig.2b (the current is yellow and voltage is blue). The phase inductance can be calculated from following equation:

$$L = \frac{V_{phRMS}}{\omega I_{phRMS}} \sin(\varphi) \tag{2}$$

where φ is angle between voltage and current. The results obtained from this method are shown also in Fig. 2d and there are marked as ui. In the Fig.2d there can be seen, that the results are in very good coincidence. These methods are compared with FEM analysis.

2.3. Phase inductance FEM calculation

On the beginning, the geometry of SRM is created with definition of all points, lines, curves and circles of the SRM cross section area. After materials, boundary conditions are defined, the mesh grid is created. During FEM analysis only one phase is energized. The static phase inductance versus rotor position for different current is calculated from following equation:

$$L = \frac{\int A \cdot JdV}{i^2} \tag{3}$$

where A is magnetic vector potential, J is current density and V is volume. The values calculated by FEM are shown in Fig.2d for aligned and also for unaligned rotor position and they are marked as FEMM. For greater details of FEM analysis see [5].

3. Conclusion

An equivalent circuit parameters investigation is very important task to be able to investigate the behavior of the SRM. As it can be seen from results of measurements and FEM analysis, the achieved L values are in very good coincidence and they can be used in the process of torque ripple minimization also the FEM could be used in design process and the results are reliable.

4. Acknowledgement

This work was supported by Science and Technology Assistance Agency of Slovak Republic under the contract No. APVT-20-39602.

References

[1] MILLER, T. J. E. *Switched Reluctance Motors and their Control*, MAGNA PHYSICS, 1992

[2] HRABOVCOVA, V., RAFAJDUS, P., FRANKO M., HUDÁK, P. *Meranie a modelovanie elektrických strojov*. EDIS, 2008.

[3] RAFAJDUS, P., ŠUŠOTA, M., HRABOVCOVÁ, V. *Investigation of torque ripple in switched reluctance motor*. ISEM 2006.

[4] KRISHNAN, R. *Switched reluctance motor drives,* CRC Press, 2001

[5] ŠUŠOTA, M., RAFAJDUS, P. *Parameters investigation of switched reluctance motor*. LVEM 2008

Transcom 2009, 22-24 June 2009
University of Žilina, Žilina, Slovak Republic

Suggestion Methodology of Classification Luminaries Outside Lighting

*Petr Závada, *Karel Sokanský, *Tomáš Novák
VŠB – TU Ostrava, Katedra elektroenergetiky, 17. listopadu 15, 708 33 Ostrava,
http://fei1.vsb.cz/kat451/, {petr.zavada, karel.sokansky, tomas.novak1}@vsb.cz

Abstract-This article deal with rush methodology classification luminaire for lighting communication above all in cities and on surrounding communications. Further is here described method of metering luminance of luminaire through the use of luminance channel analyzer LMK mobile advanced.

Keywords: Road lighting, luminaire, luminance, uniformity.

1. Introduction

Main imposition of outside lighting is reservation possibilities moving and working on communications and outside quarters at night o'clock. Outside lighting is suggesting for different using:

- workplace outside lighting,
- lighting in transport (walking, motor, rail, naval and air),
- security lighting for protection persons and property in public areas,
- outside lighting for sports areas,
- outsider lighting for architectural building.

To main requirement light- technical suggestion of illuminative systems outside areas belongs to choice luminous sources and luminaries, size illuminance and brightness, illuminance uniformity and brightness, degree constraint glare, geometric parameters of illuminating system (suspension height luminary, distance of luminous points) and technical-economic estimation suggestion illuminating system.

2. Methodology of compare luminaries

This methodology is designed for comparison different luminaries outside lighting (especially for lighting communication in town parts and populated regions) on equal terms (the same luminous source and geometric configuration).

2.1. Description of methodology

Methodologies appear from directive requirement for lighting road area which are mentioned in norm CSN EN 13201-1÷4. The part of norm (4) defines on the basis photometric needs classes of lighting for lighting road way.

For this methodology classification luminaries was chosen part of class lighting ME/ MEW(4) by needs of company Ostravské komunikace , a.s. This class are relates on driver motor vehicles moving after traffic roads middle as far as high allowed speed especially in town parts.

2.2. Metering of surface road iluminance with brightness analyzer

To comparison were choice seven luminaries from five companies- Hellux - NWS 131 150W KO, Thorn 150W RIVIERA1, Siteco 150W 552, Schréder 150W SAFIR2 and 150W ATOS2, Elstav 150W MAGNOLIA and 150W LUNOIDE.

Metering of luminaries:

Metering was performed brightness analyzer LMK mobile advanced. A component of analyzer is as well software on processing pictures taking with brightness analyzer.

On the figure 1 is see, that the brightness analyzer isn't in distance values 60 m from edgings computational field, as indicated in norm(5), but only 30 m. So as to the metering was correct is necessary conserve angle of scan between brightness analyzer and computational field so that is also lowered high of brightness analyzer above surface road on half value on 0,75 m.

On the figure 2 are mentioned distance between single computational points and edge computational field and geometric ordering metering station.

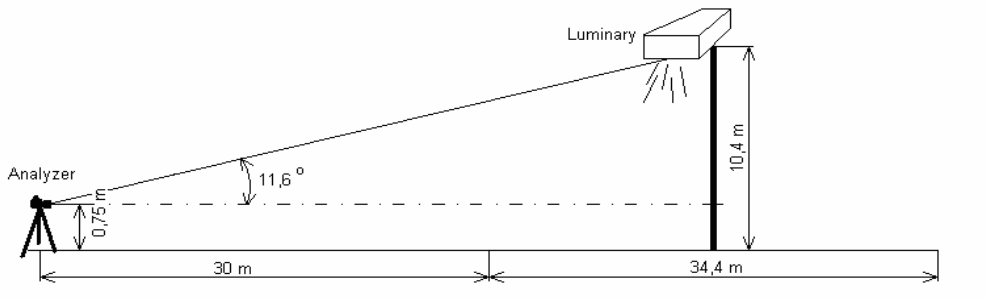

Fig. 1. Outline of metering station.

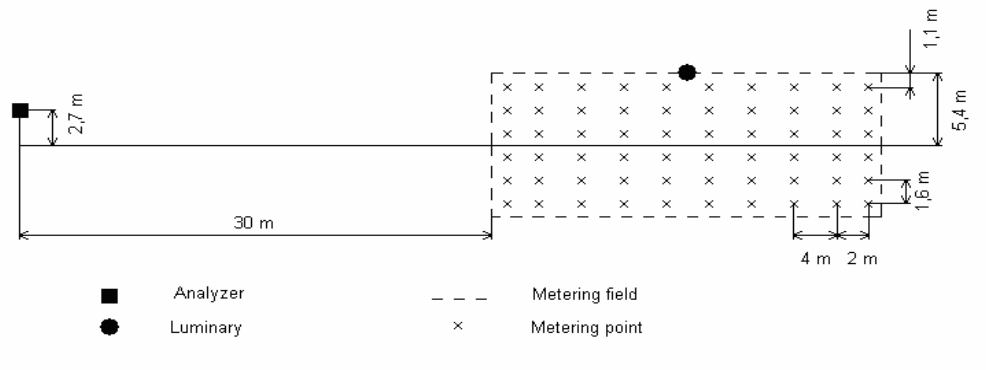

Fig. 2. Ground plan of metering station.

From reading values of brightness from points of calculation field single luminary were to be calculated values average brightness, overall uniformity of brightness and longitudinal uniformity of brightness in first and second lane intimated roadway (Fig. 2).These values are mentioned in table 4 and from these values are created graph on figure 3. From these graph is except described changes brightness and uniformity of brightness it is see, that the if is the highest values average brightness is overall and longitudinal uniformity of brightness very low - level in comparison with others score luminaries.

		$\overline{L}$ (cd/m2)	$U_0 = \frac{L_{min}}{L_{av}}$	$U_l = \frac{L_{min}}{L_{max}}$	**Meet class requirements for metering field and luminary(4)**
Hellux - NWS 131 150W KO	1. lane	1.02	0.24	0.16	-
	2. lane	0.74	0.33	0.16	-
Thorn 150W RIVIERA1	1. lane	0.31	0.30	0.18	-
	2. lane	0.30	0.39	0.24	-
Siteco 150W 552	1. lane	0.64	0.56	0.48	ME5,MEW5
	2. lane	0.50	0.49	0.31	MEW5
Schréder 150W SAFIR2	1. lane	0.42	0.54	0.39	ME6
	2. lane	0.27	0.52	0.27	-
Schréder 150W ATOS2	1. lane	0.50	0.40	0.29	MEW5
	2. lane	0.32	0.52	0.27	-
Elstav 150W MAGNOLIA	1. lane	0.79	0.17	0.11	-
	2. lane	0.31	0.33	0.12	-
Elstav 150W LUNOIDE	1. lane	0.38	0.50	0.38	ME6
	2. lane	0.33	0.55	0.32	-

Tab. 4. Calculated valuables of metering luminaries.

Where:

- $\overline{L}$ - the smallest averange road surface luminance (cd/m^2)
- U_0 – the smallest overall uniformity of luminance (-)
- U_l – the smallets longitudal uniformity of liminance (-)

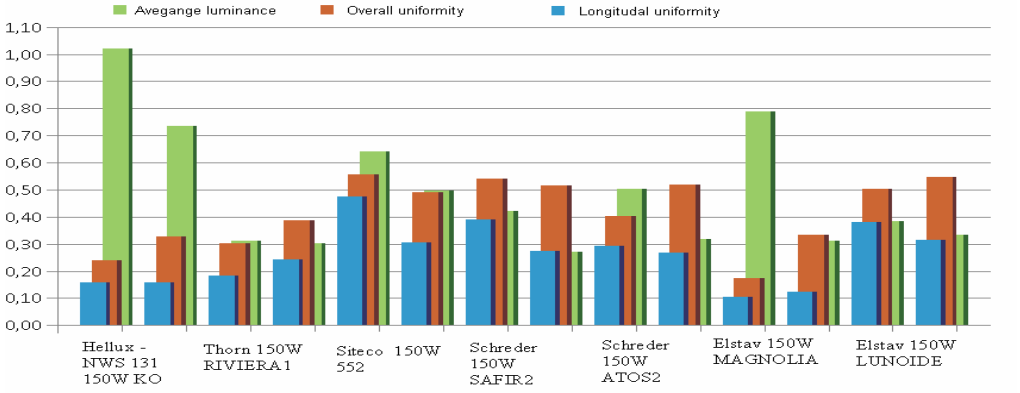

Fig.3. Comparison of metering brightness on communication for different luminaries.

The biggest average brightness is reaching the luminary named Hellux – NWS 131, where it was measured 1.02 cd/m^2 at first lane and 0,74 cd/m^2 in the second lane. The second maximum value of average brightness has luminary named Elstav 150W MAGNOLIA where was measured 0.79 cd/m^2 in first lane and 0.31 cd/m^2 in the second lane. This luminary has the worst values of overall and longitudinal uniformity of brightness. The best overall uniformity of brightness in combination with high average brightness notching luminary Siteco 150W 552. Value overall uniformity off this luminary in metering areas notching 0.56. Luminaries Elstav 150W LUNOIDE and Schreder 150W SAFIR2 reach similar values of overall and longitudinal uniformity, but their average brightness is about 0.2 cd/m^2 lower.

On figure 4 is visible brightness map of luminary Siteco 552, where we can see almost uniform brightness all over flat metering field.

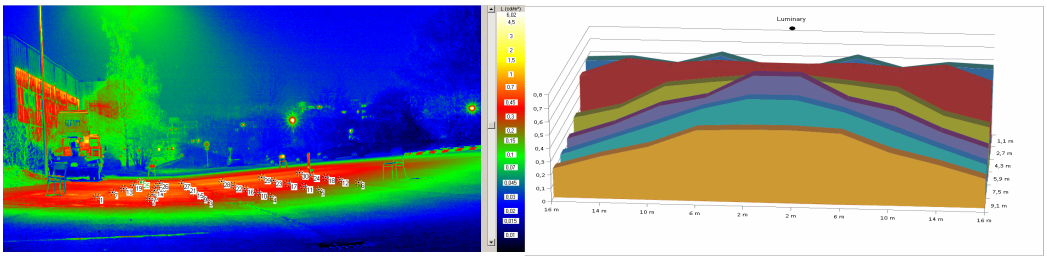

Brightness map Graph of brightness distribution

Fig. 4. Brightness map and graph of brughtness distribution of luminary Siteco 150W 552.

Graph sizes of brightness in single metering points of luminary Siteco 150W 552 is on figure 4, where are see values in single rows. Difference between the highest and the lowest brightness is only 0.6 cd/m2, while the worst luminary reaching difference as far as 1.2 cd/m2 (Fig. 6).

To compare luminary Siteco 150W 552 was chosen luminary with the worst overall uniformity of brightness – Elstav MAGNOLIA, whose brightness map is on figure 5 and graph of values brightness in metering points is on figure 5.

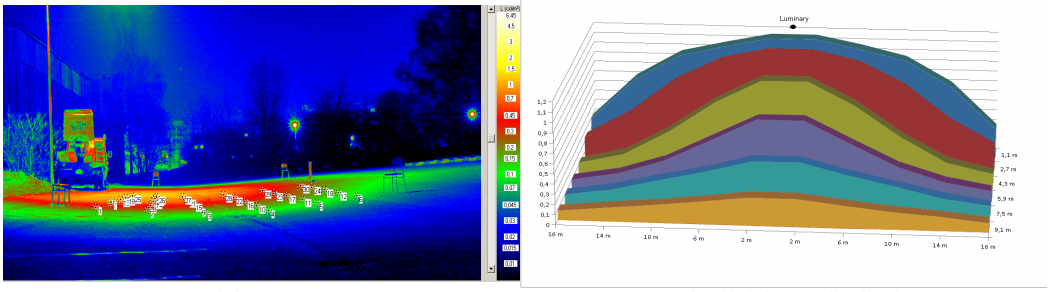

Brightness map Graph of brightness distribution

Fig. 5 Brightness map and graph of brightness distribution of luminary Elstav MAGNOLIA.

Brightness map of luminary Hellux – NWS 131 is on figure 6 with the worst overall and longitudinal uniformity of brightness.

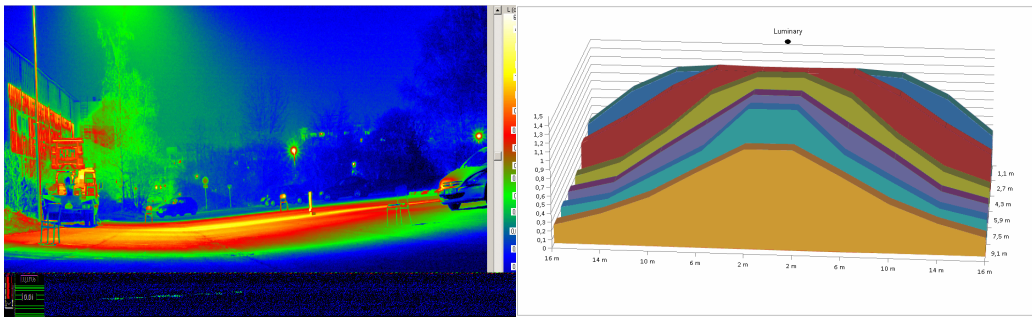

Brightness map Graph of brightness distribution

Fig. 6. Brightness map graph of brightness distribution of luminary Hellux NWS 131.

This luminary reaching the highest average brightness about 1.4 cd/m^2 and the lowest 0.2 cd/m^2, how is see on figure 6.

2.3. Luminaries evaluation

In agreement with norms CSN EN 13201- 1 and CSN EN 13201- 2 meet requirements defined class of road lighting according with tables 1 and 2 luminaries Siteco 150W 552, Schreder 150W SAFIR2, Schreder 150W ATOS2 and Elstav 150W LUNOIDE (standardly is evaluated metering field between two luminary of metering communication). Individual executed trust classes in lanes are introduced in table 4.

Because luminary was plumbed separately are values in end points lower, because there isn't dues brightness from next - door luminaries. It is possible reasonable suppose, if the luminaries will be located in road illuminating system , so will be heighten their average brightness and longitudinal and overall uniformity. From result of measurement brightness for suspension high and class of road A1 shows luminary Siteco 150W 552 as optimal for use lighting town communication Spacing it is possible increase until drop average brightness below required limit. For class ME4b it is possible reach for described communication disperse luminous seats as far as 48 m with this luminary.

3. Conclusion

Methodology is designed for simple comparison luminaries and findings suitable their application for concrete communication. This methodology we can use also for comparison interior (comparable) luminary and find their acceptable application.

According to norm CSN EN 13201- 4 for metering communication must be luminance analyzer able limit total angle metering cone on 2 arc minutes in vertical flat and 20 arc minutes in horizontal flat. By using luminance analyzer LMK2000 mobile advanced is caught up all metering field by the help of one's photos with resolution 3456 x 2304, where's size of horizontal and vertical angle one's pixel 26 arc seconds. According to norm are then size metering cone 4 x 46 pixels.

On the photo provided by the help of luminance analyzer is writing value of brightness of each pixel and then it is possible in applied software chooses position, size and form single metering objects. Software will analyze average brightness this object, which is contribution order advantage (we can meter average brightness in whole metering area, or in particular point) and next possibilities in different metering.

References

[1] Sokanský, K. - *Měření a posouzení světelně-technických, konstrukčních a ekonomických parametrů svítidel, Závěrečná zpráva – 2. a 3. část*

[2] TechnoTeam Bildverarbeitung GmbH – *Operating instructions for mobile luminance meansuring system LMK mobile advanced*, 2006

[3] ČSN EN 13201-1 Osvětlování pozemních komunikací- Část 1: Výběr tříd komunikací

[4] ČSN EN 13201-2 Osvětlování pozemních komunikací- Část 2: Výkonnostní požadavky

[5] ČSN EN 13201-3 Osvětlování pozemních komunikací- Část 3: Výpočet výkonnostních parametrů

[6] ČSN EN 13201-4 Osvětlování pozemních komunikací- Část 4: Metody měření výkonnostních parametrů

Transcom 2009, 22-24 June 2009
University of Žilina, Žilina, Slovak Republic

The Utilization of Software Tools for The Electronic Circuits Simulation by The Safety Analysis

[*]Ján Zelenka
[*]University of Žilina, Faculty of electrical engineering, Department of control and information systems, Univerzitna 1, 01026 Žilina, Slovakia, jan.zelenka@fel.uniza.sk

Abstract. This article refers to the utilization of software tools intended for a simulation of electronic circuits function by the analysis of circuit safety attributes. By the example of the disconnecter circuit, the influence of the disconnecter parameters dispersion to the safety will be ilustrated.

Keywords: safety, inherent fail-safety, safety integrity level.

1. Introduction

By the circuit design of safety critical systems we have to assure that designed circuits achieve required functions and the performance of these functions would be in accordance to the requirement of safety. The modelling of the failure consequences to the system safety we can execute:

- qualitative methods;
- quantitative methods;
- the combination of qualitative and quantitative methods.

The qualitative methods of the failure consequences analysis are centred on the analysis of particular types of random failures or on the influence of operating stage on the system safety. By the realization of such circuits we crash at the problems, to accrue from the safety requirement related to the application area. For example, the strict requirements (now valid norm EN50129) for establishment of the failure consequences to the system safety give birth to it, that establishment of the SIL4 for the electronic circuit realized on the basis of inherent fail-safety (realized by semiconductor elements without using of the special relay) is complicated. It is for the reason, that we must meditate with the current change of the several circuit elements parameters by the failure consequences analysis of electronic circuit to safety. Analysis of the failure consequences or the changing of the circuit elements parameters to safety we can execute:

- simulation of circuit function;
- mathematical modeling of circuit function;
- measuring on the real circuit.

The quantitative methods allow to count the possibility of dangerous state occurrence, which can happen as the result of failure occurrence. These methods are supported by software instruments centred on the modelling of RAMS system parameters [1]. The influence of the parameters dispersion to the safety will be illustrated on the disconnecter circuit.

2. Description of the disconnecter circuit function

The most used way of the failure negation and reach of the safety state in failure detection is a disconnection of the system from the control process or separation of the failure part of system (in the case *M* from *N* systems) from the other (functional) part of system. In the publication [2], there is described the circuit function whith enable to disconnect (or separate) the failure part of control system (below only disconnecter) by the state diagram.

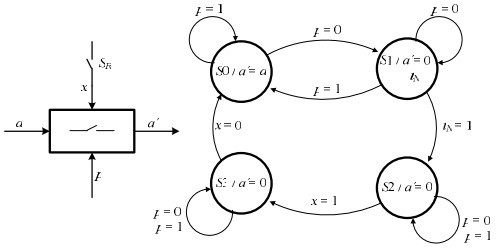

Fig. 1. The state diagram of the disconnecter.

The state *S*0 of the state diagram (Fig. 1.) is the basic state of disconnecter. If the failure signal *p* is negative (*p*=1), then the signal on the disconnecter output is the same as the signal on the disconnecter input (*a*=*a´*). In the case of the positive failure signal (*p*=0), the disconecter crosses to the state *S*1. The disconnecter output will have the interdictory meaning (*a´*=0) and the disconnecter starts to measure the disconnecter insensibility time t_N. If the failure signal becomes extinct (*p*=1) during measuring the disconnecter insensibility time t_N, then the disconnecter crosses to the state *S*0 and reset the timer. If the failure signal (*p*=0) takes longer to the disconnecter insensibility time t_N, then the disconnecter crosses to the state *S*2 and the disconnecter output will have the interdictory meaning (*a´*=0). From the state *S*2 the disconnecter can cross to the basic state *S*0 only controlled way (for example, by pressing S_R (*x*=1) and next releasing S_R (*x*=0)). For the value of the disconnecter insensibility time t_N has to be fulfilled next condition:

$$t_N \leq t_0 , \tag{1}$$

where t_0 is the maximal allowable time. We tolerate the potential dangerous behavior of system during this time t_0. In the case of the high demands in the safety integrity level SIL, it is strenuous to realize the dicsonnecter circuit (circuit realized on the basis of inherent fail-safety), which function is described in the Fig.1. For the inherent or reactive fail-safety technique is characteristic the single channel dicsonnecter solution on the discrete elements-based. In practice are used mainly the solution realized on the based of relay with special safety attributes and in the isolated cases are used the solution realized on the based of the contactlees elements. One solution of the inherent fail-safety circuit solution of the disconnecter circuit is shown in Fig. 2a (circuit solution is taken from [2]).

a)

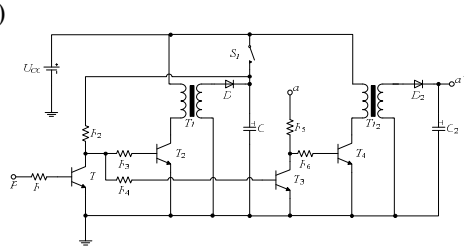

b)

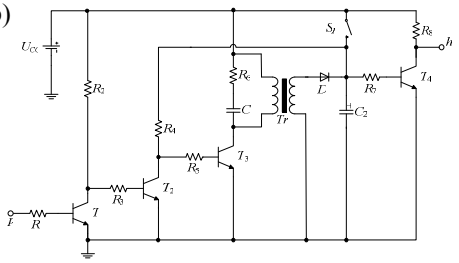

Fig. 2. The disconnecter principle with dynamic activity.

3. The analysis of disconnecter safety attributes

The disconnecter task at ensure the fail-safe attribute of safety critical control system is important, in many cases it is indispensable. The disconnecter safety depends on the influence of disconnecter element failures or stability of disconnecter elements on the insensibility time value t_N (during this time is toleranced signal absence on the disconnecter input p). This time determines tolerated potential dangerous behavior of the system, which is disconnect by the disconnecter circuit. The occurrence probability of dangerous state of system P_N depending of absence dynamic signal on the disconnecter input p is given by a curve, which is visible in the Fig. 3. If the value of time t_N is longer, then the probability of dangerous state P_N and the availability of system will be growing. Reduction of the time t_N has positive influence on safety, but negative influence on availability of the system. We have to choose the insensibility time t_N so that the safety requirements will be executed in case of the worst operating conditions (maximal value of driving voltage, maximal temperature of operating environment,…) and disadvantageous parameters dispersion of using circuit elements too. The maximum allowable value of dangerous failure probability is referred to as P_{NA} in the Fig. 3.

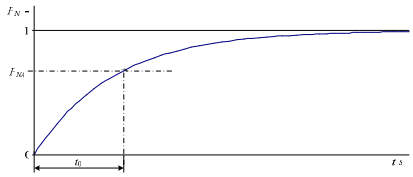

Fig. 3. Graphical dependency of the dangerous failure probability on time.

For example, in the case when the failure occurrence has an exponential distribution, then we can the dangerous failure probability P_N describe by equation (2).

$$P_N = \left(1 - e^{-\lambda_N t}\right), \tag{2}$$

where λ_N is the dangerous failure rate. If the maximum time of toleranced signal absence on the disconnecter input p we refer to as t_0, then the condition of disconnecter safety (1) we can express by:

$$t_N \le t_0 \le -\frac{\ln\left(1 - P_{NA}\right)}{\lambda_N}. \tag{3}$$

In the analysis of influence of the element parameters in disconnecter circuit on insensibility time t_N (depends on value of the time constant of capacitor C_2 discharging circuit), the disconnecter state can evaluate on the base of signal on the output h (Fig. 2b). If the voltage value on the output h is low (value of voltage is equal pinchoff voltage U_{SK} cca. 0,2V), then the disconnecter is in the state on. If the voltage value on the output h is equal driving voltage U_{CC}, then the disconnecter is in the state off.

Comment: Circuit with the transistor T_4 is added by reason of circuit analysis. By the practice usage the failure of transistor T_4 (cut off K-E) leads to the dangerous state (on the output h is low voltage value, even if the input p is perpetually without the dynamic signal).

On the simulation of circuit activity shown in the Fig. 2b, I use the Micro-Cap Evaluation software (v9.0.5.0), which was chosen on the base of requirements noted in publication [3]. Results of the insensibility time t_N obtained by calculation (Fig. 4a), simulation and measuring on the real circuit are reffered in Tab. 1. The influence of the particular circuit elements parameters dispersion (e.g. variation of capacitor capacity C_2, resistor resistance R_4) to insensibility time t_N is showed in the Fig. 5, by the different value of driving voltage U_{CC}.

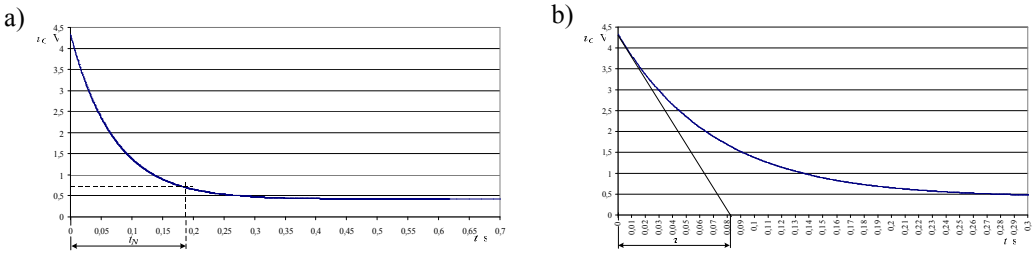

Fig. 4. Graphical dependency of discharge of capacitor C_2 on time.

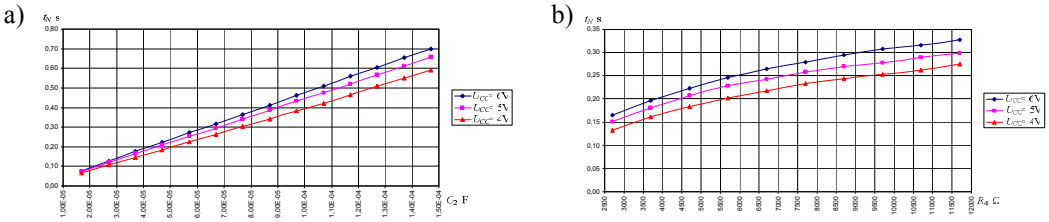

Fig. 5. Graphical dependency of insensibility time t_N on capacitor capacity C_2 and resistor resistance R_4.

Deducted value of time t_N occurs in the linear part of curve $u_C(t)$. A small change on the axis of voltage $u_C(t)$ results in a bigger inexactitude by the determination of time value. For these reasons the tangent line to capacitor C_2 discharge curve was crafted. The results of the time constant τ obtained by calculation (Fig. 4b), simulation and measuring on the real circuit are reffered in Tab. 1.

	calculation	measuring on the real circuit	simulation
τ	82 ms	93,33 ms	82,423 ms
t_N	187,8 ms	241,67 ms	207, 388 ms

Tab. 1. Obtained results.

4. Conclusion

By the safety analysis of the circuit realized on the basis of inherent fail-safety, it is convenient to use the software tools for the influence of the particular circuit elements parameters dispersion evaluation. The results obtained by these software tools are comparable to the calculated or measured values (see Tab. 1). We can experiment with the model of circuit like with the real object by computer simulation, but without emergency state risk without the need of real object existence and especially at lower costs.

Acknowledgement

This work has been supported by the scientific grant agency VEGA, grant No. VEGA-1/0040/08 *"Mathematic-graphical modeling of safety attributes of safety-critical control systems"*.

References

[1] ZELENKA, J.: *Modeling and simulation analysis of electronic safety-related circuit*, In: Zborník konferencie TRANSCOM 2007, Žilina 2007, ISBN 978-80-8070-693-7

[2] ZAHRADNÍK, J. - RÁSTOČNÝ, K. - KUNHART, M.: *Bezpečnosť železničných zabezpečovacích systémov*. Vydavateľstvo EDIS ŽU. Žilina 2004. ISBN 80-8070-296-9

[3] ZELENKA, J. Reakcia bezpečnostne kriticého riadiaceho systému na poruchu, Písomná časť dizertačnej skúšky, Žilina 2007.

Transcom 2009, 22-24 June 2009
University of Žilina, Žilina, Slovak Republic

Models of Single Relaxation Processes in Biological Tissues Influenced by Electromagnetic Field

Juraj Zrník
University of Žilina, Faculty of Electrical Engineering, Department of Measurement and Applied Electrical Engineering, Univerzitná 1, 01026 Žilina, Slovakia, {zrnik}@fel.uniza.sk

Abstract. The article deals with the theoretical modeling of the frequency dependence of the complex permittivity in dielectrics at the macroscopic level. Numerical solution of single Debye model and Cole-Cole model for various distribution parameters shows their applicability for biological materials with single relaxation processes investigation.

Keywords: dielectric properties, biological tissue, Debye model, Cole-Cole model, single relaxation

1. Introduction

The knowledge of material parameters at RF and microwave frequencies is important in many applications. Complex permittivity of biological materials investigation and measurements enable to understand the interaction of electromagnetic energy with biological tissues up to millimeter wave frequencies. Some of this interest stems from the potential health hazards due to the advent of wireless communications, therapeutic applications of microwaves, and microwave imaging. The therapeutic, dosimetric, or other applications require knowledge of dielectric properties of the biological tissues. From the electromagnetic engineering point of view, studying the bulk dielectric properties remains the most direct way of characterizing any substance. With the knowledge of dielectric properties as they appear in Maxwell's equation, the absorption of energy and the field distribution which are the results of the solution to a boundary value problem can be obtained. The observations made at the macroscopic level can greatly contribute to an understanding of the microscopic phenomena.

Any changes in tissue physiology produce changes in the tissue electrical properties. This principle has been used to identify or monitor the presence of various illnesses, such as cancer, or conditions such as body fluid shift, blood flow, cardiac output, and muscular dystrophy. Tumors generally have higher water content than normal cells because of cellular necrosis but also irregular and fenestrated vascularization and also differences may exist in the membrane structure [1].

2. Theory of frequency dependence of dielectric materials

If the permittivity varies in time-varying electromagnetic field as a function of frequency, it must be a complex function. From a macroscopic view, in electromagnetic problems dielectric properties of materials are quantified by their bulk complex permittivity $\bar{\varepsilon}$ which is represented by

$$\bar{\varepsilon} = \varepsilon_0 \left(\varepsilon' - \mathrm{j}\varepsilon''\right) = \varepsilon_0 \left(\varepsilon' - \frac{\mathrm{j}\sigma}{\omega \varepsilon_0} \right) = \varepsilon_0 \varepsilon' \left(1 - \mathrm{j} \tan \delta\right), \tag{1}$$

where ε_0 is the vacuum permittivity, σ is the conductivity, and $\tan \delta = \frac{\varepsilon''}{\varepsilon'}$ is the loss tangent. The real part of complex permittivity is relative permittivity and determines the amount of energy stored per unit volume in material for a given applied electromagnetic field. The imaginary part of complex permittivity is a loss factor and represents the energy loss in a material.

The frequency response of the first-order system is obtained from the Laplace transformation, which provides the relationship known as a single relaxation Debye-type response, which corresponds to simple model for a real material, such as biological tissue which responds to the parallel combination of capacitor and resistor

$$\bar{\varepsilon} = \varepsilon_\infty + \frac{\varepsilon_\mathrm{s} - \varepsilon_\infty}{1 + \mathrm{j}\omega\tau}, \tag{2}$$

where the time constant (relaxation time) $\tau = \frac{1}{RC}$ corresponds to a relaxation frequency $f_\mathrm{r} = \frac{1}{2\pi\tau}$, which is the half way between its low and high frequency values, the limiting values of permittivity, ε_∞ and ε_s, are known as static and infinite permittivity, respectively. In (3) is ionic conductivity ignored. Heterogeneous material such as biological tissue does not exhibit single time constant relaxation behavior and several dispersions are observed. If the relaxation times are not well separated, the material will exhibit a broad dispersion encompassing all the relaxation times. In this case the multiple Debye expression is written

$$\bar{\varepsilon} = \varepsilon_\infty + \left(\varepsilon_\mathrm{s} - \varepsilon_\infty\right) \int_0^\infty \frac{p(\tau)\mathrm{d}\tau}{1 + \mathrm{j}\omega\tau}, \tag{3}$$

where $p(\tau)$ is distribution function of relaxation time. The choice of distribution function should depend on the cause of the multiple dispersions in biological material.

Numerous empirical distribution functions or models have been proposed to model the experimental data without elaboration of the underlying mechanisms. One of the most commonly used models, a modified version of the Debye expression is Cole-Cole model, in which is used the approximation of complex relative permittivity by appropriate analytical function

$$\bar{\varepsilon} = \varepsilon_\infty + \frac{\varepsilon_\mathrm{s} - \varepsilon_\infty}{1 + \left(\mathrm{j}\omega\tau\right)^{1-a}}, \tag{4}$$

where a is a distribution parameter in the range $1 > a \geq 0$; for $a = 0$, the model reverts to the Debye equation. The Cole-Cole model is generally used in the analysis of the dielectric properties of biological materials.

The behavior of biological tissues at RF and microwave frequencies is largely determined by the electro-chemical behavior of cells and its cellular structure as well as the intra-cellular fluid in which cells are suspended and the internal cellular materials, including the nucleus.

It is observed, that low water content tissues like bone, fat, lung and skin have a lower permittivity values while high water content tissues like blood, brain, and totally internal organs possess higher permittivity. The dielectric spectrum of the biological components Tab. 1 is characterized by three main regions α, β, and γ at low, medium and high frequencies and

other minor dielectric dispersions are reported as δ dielectric dispersion, Tab. 2. The relative permittivity and conductivity change in these dispersion regions significantly with frequency.

For small and relatively simple molecular structures (e.g. water) there is often only a single relaxation processes. In contrast, for polymers and biological tissues, the dielectric dispersion can consist of several components associated with small side chain movements and the whole macromolecular movement.

Biological components	Relaxation mechanism
electrolytes	γ
amino acids	δ + γ
proteins	β + δ + γ
nucleic acids	α + β + δ + γ
cells (free of protein)	β + γ
charged cells	α + β + γ
cells with excitable membranes	α + β + γ

Tab. 1. Relaxation mechanisms in biological components.

Relaxation mechanism	Frequency range [Hz]
α	$1 - 10^4$
β	$10^4 - 10^8$
γ	$10^8 - 10^9$
δ	2.10^{10}

Tab. 2. Frequency range of relaxation mechanisms in biological materials.

3. Numerical results

The data provided by dielectric materials measurements and complex permittivity calculation can be presented in different ways. One classical representation is in plotting the real and imaginary part of the permittivity as a function of frequency. One representation is the plot of imaginary part of complex permittivity against real part of complex permittivity.

A Debye model plot (2) of dependence of normalized relative permittivity and imaginary part of complex permittivity on normalized frequency $f_n = \omega\tau$ calculated for pure water is in Fig. 1a). The graphical interpretation of Fig.1a) in complex plane, so called Cole-Cole diagram, is in Fig. 2b), in which the centre of semicircle is in the middle of ε' axis. The main impact on the dielectric processes in investigated materials has frequencies in the region of dielectric dispersion, where the relative permittivity decreases [1].

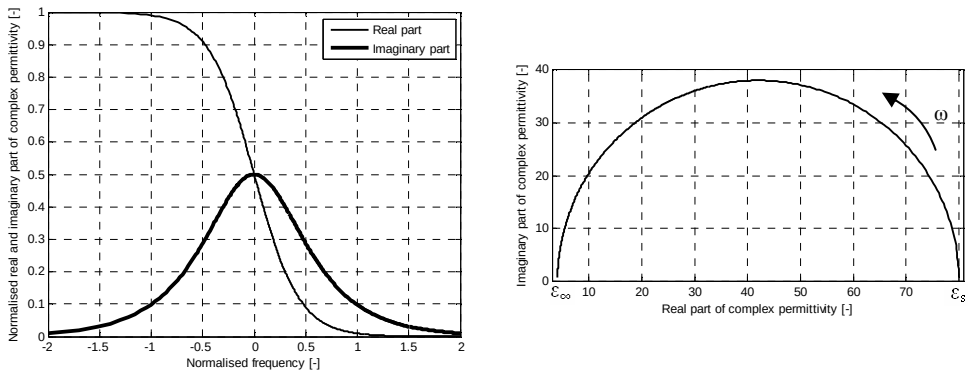

a) b)

Fig. 1. a) The frequency dependence of normalized ε' and ε'', b) Cole-Cole plot for Debye dielectric – water.

Fig. 2 displays the influence of distribution parameter α on the shape of curve calculated for Cole-Cole model (4) for biological material characterized with relaxation frequency $f_r = 1\text{GHz}$. We have chosen distribution parameter α from the interval $a \in$ <0;0.5> in which

the distribution parameter functions in mostly cases of biological tissues. In the case $a = 0$ the Cole-Cole plot corresponds to the Debye equation.

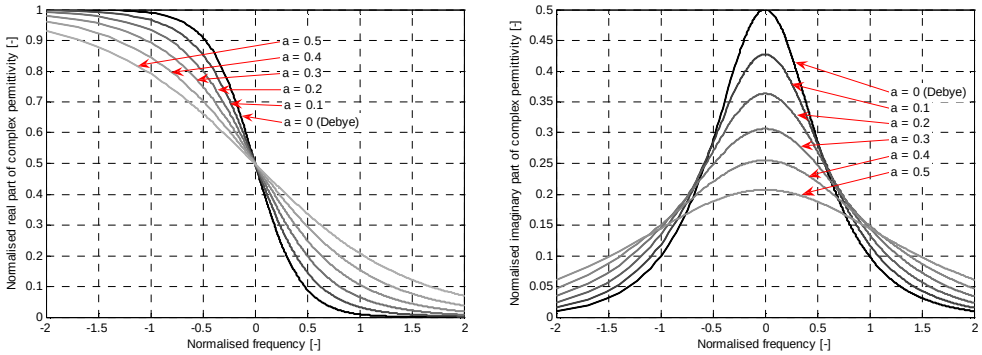

a) b)

Fig. 2. The frequency dependence of normalized a) ε' and b) ε'' for various values of distribution parameter *a*.

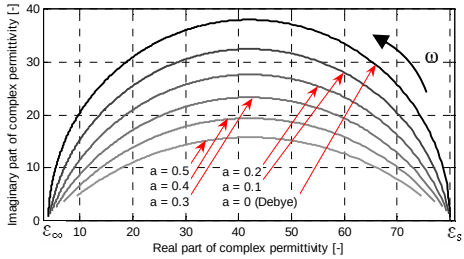

Fig. 3. Cole-Cole plot for various values of *a*.

The influence of distribution parameter α on the centre of semicircle position is given in Fig. 3. It can be seen that the centre of the semicircle corresponds to the distribution parameter and is shifted under the horizontal axis with *a* increasing. It can be seen that distribution parameter characterizes the width of relaxation spectra of investigated material [1]. The shown explanations of complex permittivity, which represents polarizing effects in dielectrics, do not consider the temperature changes [1].

4. Conclusion

The knowledge of biological tissues dielectric properties has been one of the keys to increasing our understanding of their structure and function in normal and pathological state The numerical results of complex permittivity for different distribution parameters show that from the shape of curves for complex permittivity there can be possible to obtain information about characteristic parameter for materials with single dispersion. The use of impedance spectroscopy [1-2] electrical characterization is a novel approach to comprehend underlying operative phenomena in a number of material systems, including biological tissues. The next work will be directed to more complex evaluation of dielectric parameters of investigated material with accent on relaxation mechanisms corresponding with real biological materials.

Acknowledgement

This work has been supported by grant VEGA No. 1/0761/08 of the Slovak Min. of Educ.

References

[1] FAKTOROVÁ, D. *Microwave Characterisation of Frequency an Temperature Dependence of Beef Bone Dielectric Properties Using Waveguide Measurement System,* Conference Measurement 2009, in press.

[2] PETHIG, R: *Dielectric and Electronic Properties of Biological Materials,* John Wiley & Sons, New York, 1979, p. 23-147.

Transcom 2009, 22-24 June 2009
University of Žilina, Žilina, Slovak Republic

The Economic Aspects of Wind-power Plants

[*]Martin Vysloužil, [*]Zdeněk Hradílek
[*] VŠB-TU Ostrava, FEI, Department of Electric Power Engineering 17. listopadu 15,
708 33 Ostrava - Poruba, Czech Republic, {martin.vyslouzil, zdenek.hradilek}@vsb.cz

Abstract. Nowadays the renewable resources continue to be more important in the Czech Republic especially thanks to tendency reach of 8 % share of total production of electricity power which the Czech Republic sing on the European Union. This article contains an analysis of price from the wind-power plant and a comparison with the other renewable resources. There is an indication of the impact of wind power plants on the reserves.

Keywords: wind-power plants, economy of operation, backup of output

1. Introduction

The rotary motion of our planet and influence of the solar radiation induce a regular air flow over the see and land. The technically usable potential of the wind power is estimated 26 000 TWh per year [1].

Fig. 1. The picture of the wind-power plants.

Wind power is one of the fast expanding power systems which is coming to the market. Production of wind power plants has been growing up very fast. Wind power station capacity is growing up every year by approx. 1000 MW. The biggest share of the growth in production has Nederland, Germany and the Great Britain. The European Union has made decision to reach power of 100 GW by the year 2030. The biggest share should be focused on the lands with costal places.

Wind power could deliver up to 50 % of electricity to several countries, which are situated in the location with favorable wind conditions. About a half of installed wind power plants on the world are located in the North Sea coast of Germany and Denmark. The offshore wind farms in the North Sea have a big potential for the entire Europe [1,2].

Although wind power requires new transference networks and new power regulations. The most difficult situation is during storm when all generators can be shut down by the wind speed over 25 m/s. There are requirements on the regulation and reserve of the power in the

wind power plants. The reserve requirements grow fast if the share of wind power is more than 20 %.

Hugh power systems can be controlled by extra reserve build up of other supports determined for new power control. Power reserves can include water-power plants, gas or oil aggregates and gas turbines. The installation of wind power plants can additionally require highest investments in the transmission network from the coast to inland consumers.

In this branch the Czech Republic is at the beginning of the development. Wind power plants work on decade of locations and their power is about 75kW – 3 MW.

In the Czech Republic an average wind speed is over 4 m/s in the high of 10 m and over 5,3 m/s in the high of 30 m. The friendliest locations are in the high over 700 m. The most frequent locations are on Českomoravská vrchovina and on the frontier zone. By the estimates it is possible to build approx. 350 power wind plants by the delivery of 170 MW in a location Krušné hory [1,2].

2. To the possibility of application of the renewable energy sources is the support of the state necessary.

The price of energy made from the renewable sources must be as the low as because of the possibility of compete with other sources of energy. This is affected by the capital costs, the operating costs, the method of funding, the quantity of made energy and other effects.

The Energetic Regulation Office (ERO) determines the minimal redemption prices of the electrical power.

According to the statistics of European Union the present world's boom of the wind-power engineering reduced costs of production of one kilowatt-hour from 15-20 eurocent in 80´ of the last century to today's 6-8 eurocent. For example the new composite materials used by production of sheets for the turbines with a high delivery (over 1 MW), the improvement of the operation and control systems and especially the partial solution to the critical problem of air vessel efficiency at very weak or too strong wind, contributed to it.

The modern wind-power plants are equipped with two- or three-bladed airscrews with average of 80-100 m. They reach the rated power of around 2 – 3 MW by the wind speeds of around 13 m/sec, so-called the starting wind speed is 3 m/sec [9].

The total building-up costs of one wind power plant can range from 35 to 40 millions CCZ per the generating capacity megawatt of output in dependence on the total number of machines, on the range of adjustments of side cuts, on the distance and the type of construction of the electric connection. The price of generating capacity of megawatt moves about 45 millions CCZ in the coal plant, about 70 millions CCZ in the atomic-power plant. The building up of photovoltaic plant is the most expansive, for 110 millions/MW.

The redemption price (2,34 CCZ/kWh) is set to assure to investors the recovery of investment to 15 years. The concrete recovery of investment in defined investment costs is affected firstly by the annual average wind speed in the locality and the used technology too.

With the development of this technology the price of wind electricity quickly declines. The production costs of one kilowatt-hour of wind declined to one fifth during the last 20 years. This trend continues. By the help of one wind power plant of the type Vestas V90 – 3,0 MW it is possible to produce in 20 years of it´s serviceability about 37 times so much energy how much it was used not only by the production, by the operation and by the liquidation.

The limit of the recovery of investment of the project to 15 years (in the specific costs of investment from 37 to 40 thousands CCZ/kW) is presented by the position when the machines

produce at the level of the equivalent of the operation with the full output of 1800 hours per year. The doped projects often produce markedly less.[2, 5, 6, 7, 8, 9].

Country	Output (MW)
Czech Republic	116
Belgium	287
Bulgaria	70
Denmark	3125
Estonia	58
Finland	100
France	2454
Ireland	805
Italy	2726
Cyprus	0
Lithuania	50
Latvia	27
Luxemburg	35
Hungary	65
Malta	0

Country	Output (MW)
Germany	22247
Netherlands	1746
Poland	276
Portugal	2150
Austria	981,5
Rumania	8
Greece	871
Slovakia	5
Slovenia	0
Spain	15145
Sweden	788
England	2389
Sum EU-12	**675**
Sum EU-15	**55860**
Sum EU-27	**56535**

Tab. 1. The generating capacity of wind power plants of the EU-country (2007), [9]**.**

3. The price of the energy in the Czech Republic [6]

3.1. The redemption prices of the electrical energy from the wind-power plant

From the decision of the Energetic Regulation Office (ERO) emerges that the redemption prices of the electrical energy from the new wind-power plant built in the 2009 amounts for the year 2009 2,34 CCZ/kWh. For the earlier built plants the redemption prices increase by the inflation in the next year:

2,55 CCZ/kWh for the plants built in the 2008,
2,62 CCZ/kWh for the plants built in the 2007,
2,67 CCZ/kWh for the plants built in the 2006,
2,93 CCZ/kWh for the plants built in the 2005,
3,07 CCZ/kWh for the plants built in the 2004 and
3,41 CCZ/kWh for the plants built by the 2004.

3.2. The comparison of prices of electrical energy of the renewable resources, which are put into the operation in the 2009, is [6]

- photovoltaic 12,89 CCZ/kWh,
- geothermal energy 4,50 CCZ/kWh,
- biogas station 3,55 – 4,12 CCZ/kWh,
- small water-power plants 2,70 CCZ/kWh,
- burning of biomass 2,48 – 4,49 CCZ/kWh,
- wind-power stations 2,34 CCZ/kWh.

3.3. The shares of the separate components of price for supply of electricity for households in the 2007 without VAT [4]

ERO has a limited possibility of regulation of the final price in the market for consumer approx (30 – 45 %).

- electricity inclusive business margin 52,22 %
- distribution of electricity 37,73 %
- systems services ČEPS, Inc. * 5,32 %
- transfer of electricity 2,98 %
- renewable resources and combinedheat and power 1,24 %
- decentralizations produce 0,34 %
- market operator 0,17 %

* ČEPS, Inc. is the transmission system operator in the Czech republic.

4. The impact of wind power plants on the reserves

For most of the time the conventional sources (for example nuclear power plant) produce electrical energy by the output approximating with a installed capacity of a existent source. In case of a disturbance or a planned outage they stop to provide electric energy at all. There are other rules of a production of electric energy by a wind-power installation. Volume of produced electric energy depends on the wind speed at the place where a wind-power plant location is. Contrary of the conventional source is an achievement of a installed capacity is an extraordinary event (a wind-power plant reaches this stadium for c. 1 % of its runtime, a coal-fired power plant or a nuclear-power plant reaches this stage for c. 85 % of their runtime). In all the operating time the production of wind-power plant energy is practically heavily fluctuating (till tens of percents of an installed capacity) in order of a few hours. In addition this variability is unpredictable on a long-term basis (c. more than 24 hours). Mentioned, strong irregularity and unpredictability in supplies of energy by the wind-power plants impact on a function of a power network and then of a holding of the reserves and their pumping. Building up of the wind-power plants should affect following three types of reserves [3]:

- a secondary power control,
- a tertiary power control,
- a dispatching reserve.

Exactly presented three types of auxiliary services have the best properties to a substitution of an operation of the wind-power plants.

Due to the wind-power stations ČEPS, Inc. are planning a total increase of the reserves by a 20 % of their installed capacity. This rate results from the preliminary models by ČEPS, Inc. The valuation shall be corrected pursuant to practical experiences in operation of the wind-power plants [2].

Following relation is applied on the basis of calculations realized by EGU Brno (Power Institute) for ČEPS, Inc. for determination of a system reserve (it is an output of the auxiliary services which are necessary for provision of a run of the system owing to operation of wind-power plants).

$$P_{Pps} = round(k_{PpsVTE} \cdot P_{instVTE})$$

where is: P_{Pps} – an increase of auxiliary services;
k_{PpsVTE} – a coefficient of an increase of a capacity for a system reserve for the year 2006 = 0,22;
$P_{instVTE}$ – an installed capacity in wind-power plant.
Signification „round“means that computed value is rounded.

Diversification to individual types of system reserves are following:
30 % to a secondary regulation reserve,
35 % to a tertiary regulation reserve, and
35 % to a dispatching reserve [10].

5. Conclusion

The price of energy made from the renewable sources must be as the low as because of the possibility of compete with other sources of energy. This is affected by the capital costs, the operating costs, the method of funding, the quantity of made energy and other effects. The redemption price should be set to assure to investors the recovery of investment to 15 years.

Acknowledgement

The paper was prepared the frame of research with the project GACR 02/09/1842.

References

[1] VUORINEN, A. *Planning of Optima Power Systéme*. 309 s. ISBN 978-952-1741-0
[2] MASTNÝ, P. *Ekonomika provozu obnovitelných zdrojů energie*. Sborník: Electric Power Engineering 2006.
[3] RYVOLOVÁ, I. *Ekonomické souvislosti využívání větrné energie v ČR* 34 s.
[4] Sborník: *Aktuální otázky a vybrané problémy řízení elektrizační soustavy*. EGU Praha energineering, a.s., 2007
[5] http://www.ewea.org
[6] http://www.eru.cz
[7] http://www.ewea.org
[8] http://www.csve.cz
[9] http://www.vetrneelektrarny.bestweb.cz/info/csve/ve_moznosti_csve.pdf
[10] ŠKORPIL, J., MERTLOVÁ, J., WILLMANN, B. *Obnovitelné zdroje a jejich začlenování do energetických systémů*. 50 s. ISBN 978-80-7043-733-9